**US Army Corps
of Engineers**
Waterways Experiment
Station

Improving the Traction Prediction Capabilities in the NATO Reference Mobility Model (NRMM)

by   Jody D. Priddy

19991005 188

DTIC QUALITY INSPECTED 4

The contents of this report are not to be used for advertising, publication, or promotional purposes. Citation of trade names does not constitute an official endorsement or approval of the use of such commercial products.
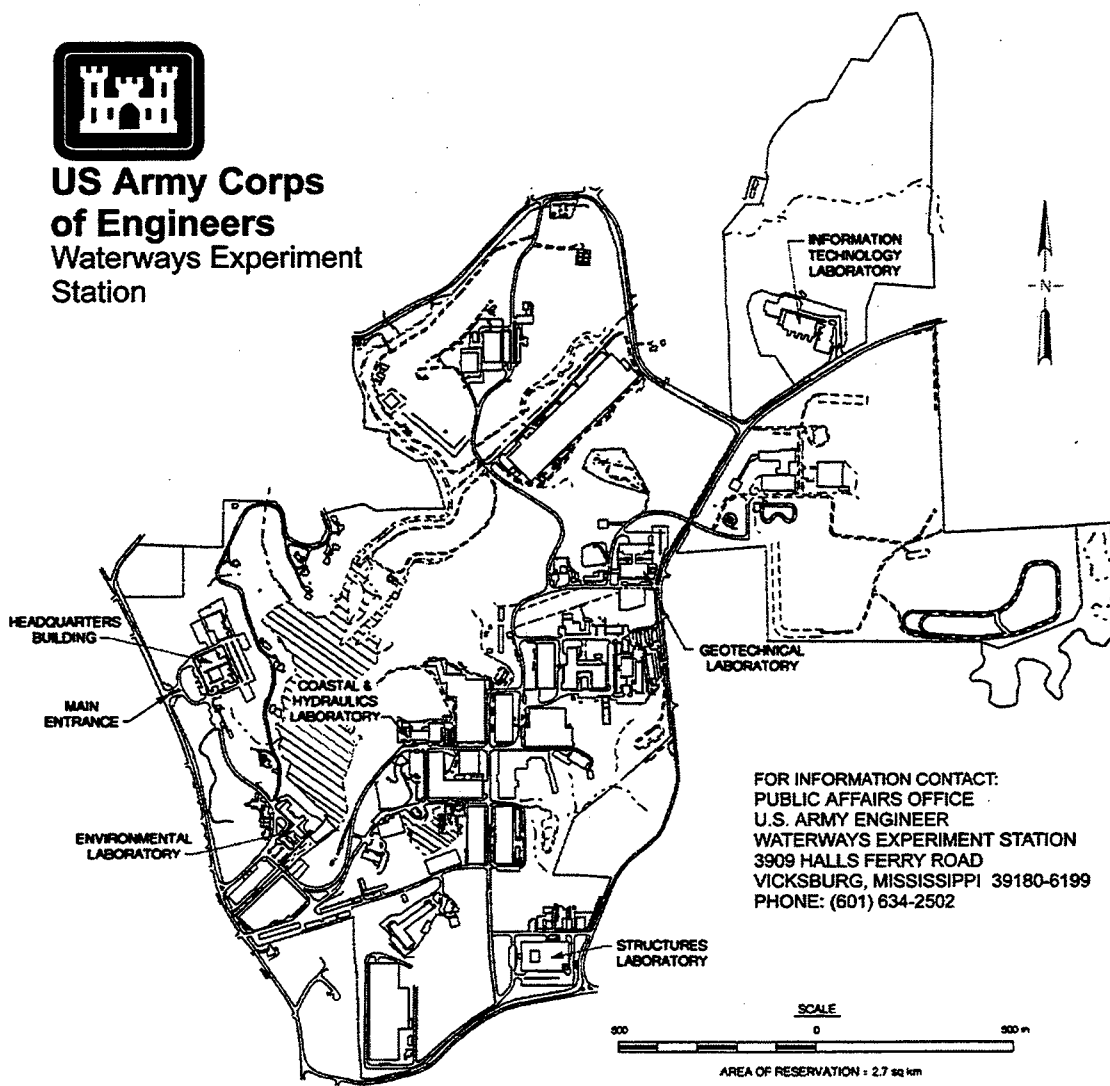
The findings of this report are not to be construed as an official Department of the Army position, unless so designated by other authorized documents.

US Army Corps
of Engineers
Waterways Experiment
Station

INFORMATION
TECHNOLOGY
LABORATORY

- N -

HEADQUARTERS
BUILDING

GEOTECHNICAL
LABORATORY

COASTAL &
HYDRAULICS
LABORATORY

MAIN
ENTRANCE

FOR INFORMATION CONTACT:
PUBLIC AFFAIRS OFFICE
U.S. ARMY ENGINEER
WATERWAYS EXPERIMENT STATION
3909 HALLS FERRY ROAD
VICKSBURG, MISSISSIPPI 39180-6199
PHONE: (601) 634-2502

ENVIRONMENTAL
LABORATORY

STRUCTURES
LABORATORY

SCALE

500   0   500 m

AREA OF RESERVATION = 2.7 sq km

TABLE OF CONTENTS

LIST OF TABLES

LIST OF FIGURES

PREFACE

The research reported herein is being published under RDTE Work Unit Number AT40-MW-534, entitled "Real-Time Mobility Model for Models and Simulations." This work unit was a part of the "Advanced Mobility Modeling" AT40-146W work package.

The research was conducted and the report was prepared by Mr. Jody Durell Priddy, Mobility Systems Division (MSD), Geotechnical Laboratory (GL), U.S. Army Engineer Waterways Experiment Station (WES), Vicksburg, MS, a complex of five laboratories of the U.S. Army Engineer Research and Development Center (ERDC). Critical latitude and support were provided during this research by MSD personnel, especially Messrs. M. Wendell Gray and Randolph A. Jones. Dr. Dean R. Freitag and Messrs. Newell K. Murphy, Jr. and Barton G. Schreiner, former WES employees who were heavily involved in mobility research, provided constructive review and comments.

This report was prepared in partial fulfillment of the requirements for the degree of Master of Science in Civil Engineering from Mississippi State University (MSU). Permission to reprint this copyrighted work as a technical report has been granted by the author, Mr. Priddy. Sincere thanks are given to the thesis committee members, namely, Dr. Oswald Rendon-Herrero, Committee Chairman, MSU, Dr. William E. Willoughby, acting Chief, MSD, and Dr. James W. Epps, MSU. Dr. William F. Marcuson III was Director, GL.

Commander of ERDC during the research and publication of this report was COL Robin R. Cababa, EN. This report was published at the WES complex of ERDC.

ACRONYMS

TACOM   Tank-automotive and Armaments Command (United States)

WES   Waterways Experiment Station (United States)

DERA   Defense Evaluation and Research Agency (United Kingdom)

NRMM   NATO Reference Mobility Model

NATO   North Atlantic Treaty Organization

USCS   Unified Soil Classification System

NOMENCLATURE

A_{XZ} projected stress area in the XZ plane

A_{YZ} projected stress area in the YZ plane

b average tire section width (inflated; unloaded)

CF clearance factor (part of MI)

CI cone index

$CP1$ average contact pressure parameter no. 1

$CP2$ average contact pressure parameter no. 2

CPF contact pressure factor (part of MI)

d average tire outside diameter (inflated; unloaded)

D drawbar force

DCF deflection correction factor

$\dfrac{D}{W}_{20}$ drawbar coefficient at 20 percent slip

$\dfrac{D^{"Max"}}{W}_{20}$ NRMM prediction for drawbar coefficient at 20 percent slip and "maximum" soil strength (from slip versus drawbar relationship)

$\dfrac{D^{"Max"}}{W}_{100}$ NRMM prediction for drawbar coefficient at 100 percent slip and "maximum" soil strength (from slip versus drawbar relationship)

$\dfrac{D^{"Max"}}{W}_{Slip}$ NRMM prediction for drawbar coefficient at particular slip and "maximum" soil strength (from slip versus drawbar relationship)

$\dfrac{D^{RCI}}{W}_{20}$ NRMM prediction for drawbar coefficient at 20 percent slip and particular soil strength (from drawbar versus soil strength relationship)

$\dfrac{D^{RCI}}{W}_{100}$ NRMM prediction for drawbar coefficient at 100 percent slip and particular soil strength (from drawbar versus soil strength relationship)

e_N eccentricity of the normal force at the tire/soil interface

e_R eccentricity of the motion resistance force at the tire/soil interface

e_T eccentricity of the tractive force at the tire/soil interface

EF engine factor (part of MI)

GF grouser factor (part of MI)

GVW gross vehicle weight

h average tire section height (inflated; unloaded)

h_c vehicle minimum clearance height

L_{CA} length of the effective contact area

L_z additional effective contact length due to sinkage

L_δ effective contact length resulting from hard-surface deflection

LC long chord length

m total number of axles on a vehicle

M middle ordinate length

MI mobility index

MMP mean maximum pressure

MMP_L Larminie's MMP

MMP_M Maclaurin's MMP

MMP_R Rowland's MMP

n average number of tires per axle for a vehicle

N normal force at tire/soil interface

N_{3b} new numeric variant 3b for VCI_1

$N_{c(F)}$ Freitag's numeric for wheels in clay soils

$N_{c(F)}^{VCI}$ Freitag's numeric for wheels in clay soils cast in a VCI form

$N_{c(S)}$ Smith's numeric for wheels in clay soils

$N_{c(T)}$ Turnage's numeric for wheels in clay soils

N_{D1} new numeric variant 1 for drawbar

N_{D4} new numeric variant 4 for drawbar

N_{D8} new numeric variant 8 for drawbar

N_{D16} new numeric variant 16 for drawbar

N_M Maclaurin's numeric for drawbar of wheels in clay soils

PWR engine gross power-to-weight ratio

Q torque applied to the wheel

R motion resistance force at tire/soil interface

R^2 coefficient of determination

RCI rating cone index

RCI_X excess rating cone index

S_e standard error

T tractive force at tire/soil interface

TCF tire construction factor

TEF traction element factor (part of MI)

TF transmission factor (part of MI)

VCI_1 one-pass vehicle cone index

VCI_{50} fifty-pass vehicle cone index

w average axle loading

W_{CA} width of the effective contact area

W_W wheel load

WF weight factor (part of MI)

WI work index

WLF wheel load factor (part of MI)

z sinkage

δ hard-surface tire deflection

σ normal stress

σ_X normal stress component in the X direction

σ_Y normal stress component in the Y direction

τ shear stress

τ_X shear stress component in the X direction

τ_Y shear stress component in the Y direction

$\varnothing$ circle diameter

CHAPTER I

INTRODUCTION

Background

A ground-based vehicle's ability to get from one place to another and perform work is controlled on the most fundamental level by its traction performance characteristics. A common method of assessing longitudinal traction performance is by conducting an experiment to measure the drawbar performance. Drawbar represents a vehicle's towing ability or its acceleration potential. The drawbar force (or towing force) can be directly measured during a controlled experiment whereas the tractive force cannot. However, the drawbar force is equal to the tractive force reduced by the motion resistance force[1]. Therefore, drawbar and motion resistance forces are typically the parameters of interest during traction experiments.

The NATO Reference Mobility Model (NRMM) was developed jointly by the United States Army Tank-automotive and Armaments Command (TACOM) and the United States Army Engineer Waterways Experiment Station (WES). NRMM was developed primarily to predict the maximum speed a vehicle can attain over various terrain conditions and environmental scenarios [Ahlvin and Haley 1992]. The baseline speed prediction generated by the

_____

[1] - A section containing definitions of specialized terms is provided beginning on page 7.

model is based on traction potential. In order to predict traction potential in off-road environments, the model uses relationships for predicting drawbar and motion resistance as functions of vehicle and soil characteristics.

One of the traction relationships in NRMM predicts the drawbar potential of wheeled vehicles operating on highly plastic clay soil (CH classification by USCS[2]) in a non-slippery state. The relationship is specifically applicable to all-drive wheeled vehicles with no traction assist devices (e.g., tire chains) operating on level terrain. The relationship was developed from the results of several traction studies which involved experiments with full-scale vehicles in a field environment (i.e., naturally occurring soil terrain). These experiments were conducted by WES during the 1960s through the 1980s.

The NRMM relationship uses the One-Pass Vehicle Cone Index (VCI_1) to predict drawbar potential. VCI_1 is the minimum soil strength necessary to support a vehicle for one pass with all of the vehicle's traction potential being expended just to maintain a slow, steady speed. Therefore, VCI_1 represents a soil strength at which a vehicle's drawbar potential is zero. The NRMM relationship makes use of another traction relationship that was developed specifically for predicting VCI_1. WES developed the VCI_1 relationship based on the results of soil trafficability studies with full-scale vehicles conducted during the 1940s through the 1960s, and WES has continuously refined the VCI_1 relationship over the years based on new information.

---

[2] - Sections describing specialized acronyms and nomenclature used throughout this document are provided on pages x through xiv.

The NRMM relationship predicts drawbar potential as a function of the soil strength above VCI_1 termed the excess soil strength (i.e., excess soil strength equals the soil strength minus VCI_1). Therefore, the NRMM relationship essentially predicts drawbar potential as a function of the soil strength only. This modeling approach, referred to as the VCI Approach, works fairly well because many wheeled vehicles have similar drawbar performance characteristics above their VCI_1 values even though their VCI_1 values can differ greatly. Although the approach works fairly well, it gives no consideration to the effects that important vehicle characteristics (e.g., tire diameter, tire deflection, etc.) can have on traction performance above VCI_1. The relationship would be much more beneficial in many NRMM applications if it included these effects.

As a direct consequence of this shortcoming in the VCI Approach, the drawbar relationship is separated into two prediction categories. One of the categories is for wheeled vehicles with contact pressure factors (CPF) greater than 4 psi, and the other is for wheeled vehicles with CPF less than 4 psi. The CPF is a parameter that is loosely related to the average contact pressure under a vehicle on a non-yielding surface. There are two separate categories because a few unusual vehicles tested by WES [Schreiner 1971] demonstrated significantly better drawbar performance than other vehicles WES had tested. The vehicles demonstrating better performance had CPF values less than 4 psi whereas all the other vehicles had values of 5 psi or higher. The form of the NRMM relationship could not account for the observed difference in performance, and hence two separate equations (or curve-fits) were developed based on the two CPF categories. However, it has never been substantially verified that differences in contact pressure caused the differences in drawbar performance.

WES has attempted to develop other methods of predicting drawbar potential that consider the effects of vehicle characteristics on traction performance. A large research effort was conducted during the 1960s and 1970s in which laboratory experiments were conducted with a single tire dynamometer in highly processed and controlled clay and sand soils. The primary goal of this research effort was to develop a single dimensionless parameter (termed a numeric) that could be used to predict the total traction performance of wheeled vehicles [Turnage 1995]. This approach, referred to as the Numeric Approach, was founded on a dimensional analysis of tire/soil interaction [Freitag 1965], and the VCI_1 relationship was not considered or used in the approach.

The Numeric Approach research generated a lot of information demonstrating effects that vehicle characteristics can have on total traction performance, but the primary goal was never achieved. One significant reason the laboratory testing was abandoned was because relationships developed from the single tire, laboratory data could not predict real vehicle performance in a field environment. One possible reason for this inability to predict real vehicle performance was that the processing and control of the laboratory soils probably altered them to such a high degree that they no longer had the trafficability characteristics of naturally occurring soils. Another possibility arises from the unnatural process in which the dynamometer carriage controlled the longitudinal displacement of the tire rather than the more realistic process of the tire/soil interaction controlling the longitudinal displacement of the carriage. There is no proof to substantiate either of these explanations.

In a recent study [Priddy 1995], digital databases were developed for use in a statistical analysis to determine the inherent variability in the NRMM traction relationships.

The development of the digital databases involved the research of about seventy studies in which traction experiments were conducted. It also involved a detailed exploration of the implemented use of the traction relationships in NRMM. The databases include most of the original data used in the development of the current NRMM relationships for vehicle traction on fine-grained soils plus some data from more recent (post 1980s) traction experiments. These digital databases provide a readily accessible source of traction performance data for real vehicles in a field environment. The databases also provide a new opportunity for investigating potential improvements to the traction algorithms in NRMM.

Traction forms the baseline limitation on speed, but it is not the only thing considered in NRMM. Other speed-limiting mobility issues are considered such as overriding or avoiding discrete obstacles and vegetation, climbing or descending slopes, limited visibility concerns, surface roughness effects on ride quality, and tire durability concerns due to large operating deflections, and these issues don't include the on-road issues that are addressed in the model. The strength of NRMM is that it can be used to evaluate the mobility of one or more vehicles based on all these mobility concerns using real terrain data from regions of consideration that may encompass a vast amount of area. Terrain databases are mapped for use with NRMM, and standards have been established for the types of terrain data that must be used. These standards were partly the result of practical considerations for the types of information that could effectively be obtained for vast areas of terrain.

Objective and Scope

The goal of this thesis was to demonstrate the feasibility of utilizing existing performance data to develop better traction relationships for NRMM. The approach used to explore the feasibility was to conduct a statistical modeling effort for the development of some new relationships. The modeling effort encompassed a systematic and extensive exploration of new and old ideas from both the VCI and Numeric Approaches along with some new modeling concepts.

In order to judge whether or not the feasibility existed, a set of decision criteria related to the quality of the new relationships was established. First, the relationships should be logical, have a theoretical foundation where possible, and be dimensionally correct. Second, they should provide a more sound understanding of the role that vehicle characteristics have in traction performance throughout the full range of soil strengths from VCI_1 up to maximum strengths. Last, they should describe (i.e., collapse into a predictable trend) the existing data as well or better than the current NRMM relationships.

The statistical modeling effort focused on two major types of traction relationships: (1) VCI_1 and (2) drawbar. Three types of traction data were explored: (1) VCI_1 data from experiments with real vehicles in a field environment, (2) drawbar data from experiments with real vehicles in a field environment, and (3) drawbar data from experiments with a single tire dynamometer in a laboratory environment. The data were limited to experiments with pneumatic tires in non-slippery, highly plastic clay soils (CH classification by USCS).

There are two sides of the vehicle/terrain interaction system that must be characterized in some fashion for any relationship designed to predict vehicle traction: (1) the terrain and

(2) the vehicle. This research concentrated on more definitively characterizing the vehicle (i.e., loading) side of the interaction system for tires in soil. A simple, yet extremely usable, method of characterizing the soil (i.e., terrain) side of the interaction system has been developed and standardized by WES. WES' method involves soil characterization by USCS soil type and rating cone index (RCI) (see definitions for details). This method produces prediction accuracy that is adequate for NRMM requirements and has thus been standardized as the soil characterization method for use with the model. Therefore, WES' standard method of terrain characterization was employed in this research.

Definitions

The following are definitions of specialized terms used throughout this document.

<u>Pneumatic Tire Terms (see Figure 1)</u>

Carcass. The portion of a tire outside the lip of the rim flange that is free to deflect.

Diameter (d). The outside diameter, not counting the tread height, of an inflated but unloaded tire.

Section height (h). The distance from the lip of the rim flange to the outer tire surface, not counting the tread height, of an inflated but unloaded tire.

Section width (b). The distance between the extreme points on the tire carcass area of an inflated but unloaded tire.

Deflection (δ). The distance between the outer surface of a loaded tire and the outer surface of an inflated but unloaded tire taken at the center of the carcass cross section on a non-yielding surface.

Tread height. The thickness of the aggressive features on the outer surface of a tire.

Aspect ratio. The ratio of section height over section width.

Vehicle Terms

All-drive. Indicates that all of the axles (i.e., tires) are powered.

Contact pressure factor (CPF). A factor that is loosely related to the average hard-surface contact pressure under a vehicle. It is one of eight factors used to calculate the Mobility Index.

Mobility Index (MI). A parameter that is related to the VCI performance of vehicles on fine-grained soils. It was developed in the United States.

Mean Maximum Pressure (MMP). A parameter that is related to the average ground contact pressure under a vehicle and is used to represent soft-soil performance potential. It was developed in the United Kingdom.

Gross vehicle weight (GVW). The total weight of a vehicle.

Soil Terms

Trafficability. The ability of terrain to support the passage of vehicles [Meyer et al. 1977].

Cone Index (CI). An index of soil shear strength obtained using a trafficability cone penetrometer standardized by WES.

Remold Index (RI). An index of the sensitivity of soil to strength losses under vehicular traffic obtained using remolding equipment standardized by WES.

Rating Cone Index (RCI). An index of soil shear strength that includes consideration of the sensitivity of soil to strength losses under vehicular traffic. It is defined as the product of cone index and remold index for the particular layer of soil. For example, the 6-12" RCI equals the 6-12" RI times the 6-12" CI.

Cone penetrometer (see Figure 2). An instrument consisting of a circular cylindrical shaft (usually 18 to 36 inches in length) with a 30-degree right circular cone mounted on one end and a calibrated load measuring device on the other end. For fine-grained soils, the shaft is 3/8 inch diameter steel (previously 5/8 inch aluminum) and the cone has a 0.5-square-inch base area. The output measurement (CI) is the average of pressure readings (typically in pounds per square inch) taken at specified depths of penetration of the base of the cone into the soil. The depths of penetration used in the measurement are usually those taken at the top, mid-height, and bottom of the critical

layer. The pressure readings are the result of the penetration force divided by the base area of the cone with a standard penetration rate of 72 inches per minute.

Remolding equipment (see Figure 2). Equipment consisting of a circular cylindrical tube mounted on a steel base and a drop hammer. The tube has 1-7/8 inch inside diameter. The drop hammer weighs 2-1/2 lbf and has 12 inches of drop travel. In use, soil samples approximately 6 inches in height are inserted into the tube using a trafficability (or Hvorslev) sampler. For fine-grained soils, cone index measurements are taken in the center of the sample before and after 100 blows of the drop hammer. The cone index measurements are based on readings taken in the sample at depths of 0, 1, 2, 3, and 4 inches. The output measurement (RI) is the ratio of the cone index measurement after 100 blows over the cone index measurement before 100 blows.

Trafficability (or Hvorslev) sampler (see Figure 2). A piston-type sampling device that is used to obtain an undisturbed sample in soft soils. It has a circular cylindrical tube with 1-7/8 inch inside diameter that is sharpened on the open end. The piston within the tube retracts during penetration into the soil such that a partial vacuum is maintained above the sample preserving the soil's in situ structure.

Critical layer. A layer of soil lying below the natural terrain surface that exerts the greatest influence on trafficability. The depth of the critical layer is dependent upon vehicle characteristics and the nature of the cone index (CI) profile with depth. A 6 inch layer of soil is typically used, but sometimes a 12 inch layer of soil is used. It is

typically the 3-to-9 inch layer for light wheeled vehicles (wheel loads of 2,000 lbf and less) and the 6-to-12 inch layer for normal wheeled vehicles (wheel loads up to about 10,000 lbf).

Unified Soil Classification System (USCS). A system which identifies (classifies) soils according to their textural and plasticity qualities and to their grouping with respect to their performances as engineering construction materials [Meyer et al. 1977].

Vehicle/Terrain Interaction Terms

Traction. The process by which a ground-based vehicle develops tractive force and overcomes motion resistance to produce desired motion relative to the terrain.

Tractive force (T). The force developed at the vehicle/terrain interface by the traction elements as a result of applied torque from the power plant.

Motion resistance (R). Any force imposing resistance against desired motion. For element-level traction considerations, it is composed of rolling resistance forces only.

Rolling resistance. Motion resistance that arises from deformations in the terrain (external) and the traction elements (internal).

Traction element. Any element of a vehicle that is designed to provide support and/or traction for a vehicle traveling on a surface (e.g. tires, tracks, feet, screws, etc.) [Meyer et al. 1977].

Drawbar (D). The amount of sustained towing force a self-propelled vehicle can produce. It is the resultant of tractive force reduced by motion resistance.

Drawbar coefficient (D/W). Drawbar divided by gross vehicle weight.

Vehicle Cone Index (VCI). Minimum soil strength necessary for a vehicle to make a specified number of passes. Consideration is most often given to one pass (VCI_1) and fifty passes (VCI_{50}).

Sinkage (z). The depth to which the traction elements penetrate the terrain measured normal to the original, undisturbed surface.

Slip. An indication of how the speed of the traction elements differs from the forward speed of the vehicle. It is defined by the equation [Meyer et al. 1977]:

$$Slip = \left(\frac{r_R \omega - v}{r_R \omega} \right)$$

where: r_R = rolling radius
  ω = angular velocity of the wheel or number of revolutions per unit time divided by 2π for a track
  v = forward velocity of vehicle or wheel axle

Optimum slip. Slip at which maximum work index occurs.

Work Index (WI). A dimensionless number that represents the relative efficiency for a particular measure of drawbar. It is defined by the equation:

$$Work\ Index = \frac{D}{W} \left(1 - \frac{Slip(\%)}{100} \right)$$

Maximum pull slip. Slip at which maximum drawbar occurs.

Statistical Modeling Terms

Coefficient of determination (R^2). A measure of quality that indicates the amount of variation in the measurements (Y) that is accounted for by the relationship predictions ($\hat{Y}$). It is defined as the ratio of the explained variation in Y (i.e., the variation explained by $\hat{Y}$) over the total variation in Y, and it is usually expressed in percent. It can be calculated using the equation:

$$R^2 = 1 - \frac{\sum\limits_{i=1}^{n} \left(Y_i - \hat{Y}_i\right)^2}{\sum\limits_{i=1}^{n} \left(Y_i - \bar{Y}\right)^2}$$

where: i = increment counter for the observations
n = total number of observations
Y_i = measured value for i-th observation
$\hat{Y}_i$ = predicted value for i-th observation
$\bar{Y}$ = mean measurement for all observations

Degrees of freedom. A quantity related to quality that is equal to the total number of observations less the number of empirical constants.

Residual. The difference between measured (Y) and predicted ($\hat{Y}$) values for an individual observation.

Standard error (S_e). A measure of quality that estimates the standard deviation of the measurements relative to the equation describing the relationship. It represents the

amount of data scatter around the prediction equation. It can be calculated using the equation:

$$S_e = \sqrt{\frac{\sum_{i=1}^{n}\left(Y_i - \hat{Y}_i\right)^2}{n - k}}$$

where: i = increment counter for the observations
n = total number of observations
k = number of empirical constants in the prediction equations
Y_i = measured value for i-th observation
$\hat{Y}_i$ = predicted value for i-th observation

Adjusted coefficient of determination. A measure of quality that is identical to R^2 with the exception that it takes the degrees of freedom associated with the relationship into account. This measure of quality is more appropriate when comparing various relationships that have different degrees of freedom. It can be calculated using the equation:

$$Adj.\ R^2 = 1 - \frac{\sum_{i=1}^{n}\left(Y_i - \hat{Y}_i\right)^2}{\sum_{i=1}^{n}\left(Y_i - \bar{Y}\right)^2}\left(\frac{n - 1}{n - k}\right)$$

where: i = increment counter for the observations
n = total number of observations
k = number of empirical constants in the prediction equations
Y_i = measured value for i-th observation
$\hat{Y}_i$ = predicted value for i-th observation
$\bar{Y}$ = mean measurement for all observations
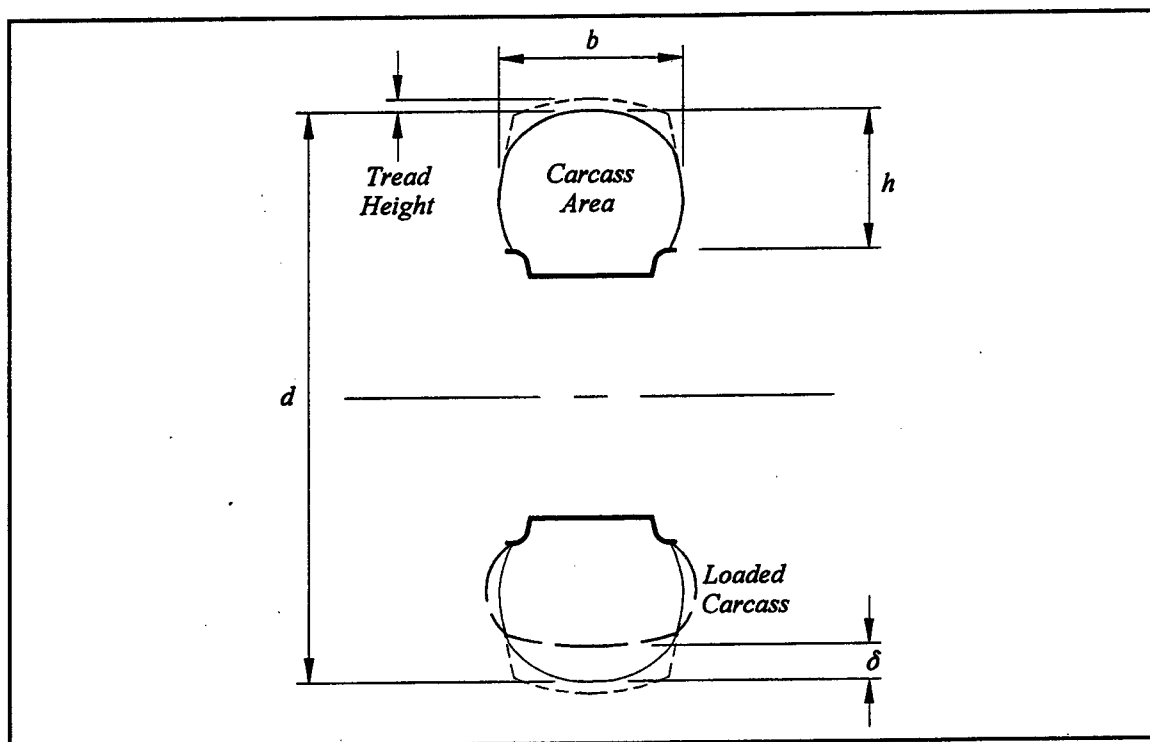
Figure 1. Principal shape variables for pneumatic tires
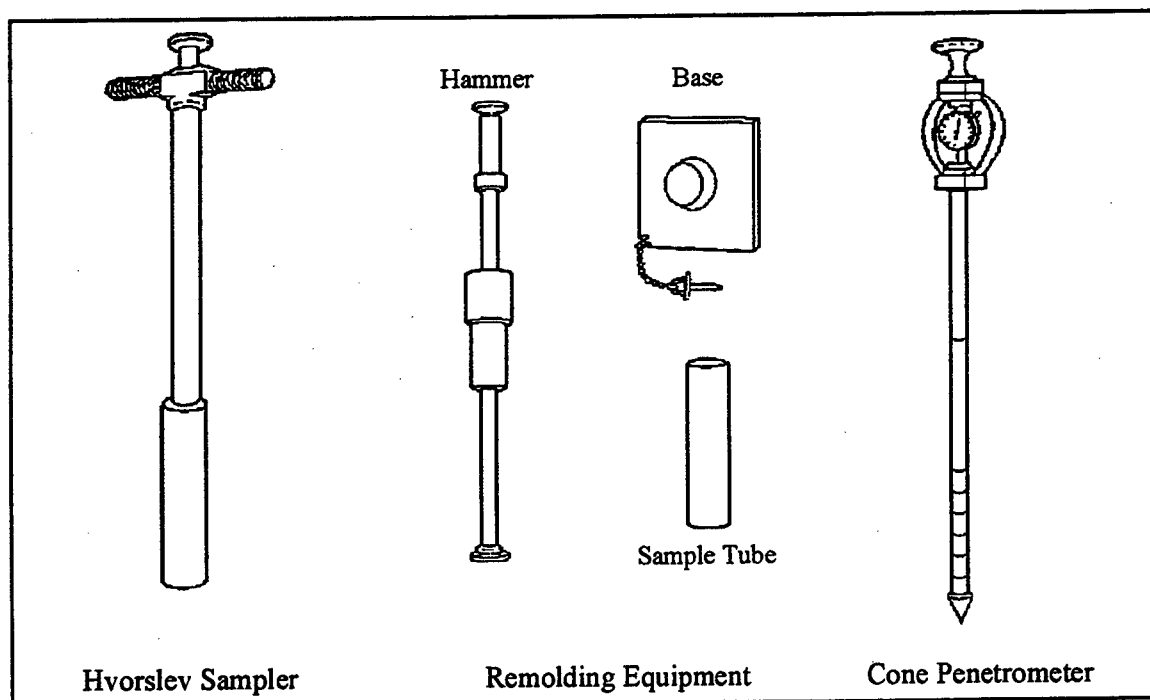
Figure 2. WES trafficability equipment

CHAPTER II

DATABASES

General Background Information

As described in the introduction, a recent study [Priddy 1995] produced a readily accessible source of traction data from experiments with real vehicles in a field environment. The digital databases generated during that study were used as the sole source of field performance data in this research. Only two of the major databases were required: the *Fine-Grained One-Pass Vehicle Cone Index* database, and the *Fine-Grained Drawbar at Nominal Slip* database. The vehicle characteristics associated with the performance data were not originally included in these databases. Therefore, the vehicle characteristics (primarily tire dimensions) were determined and added as part of this research. The vehicle characteristics were determined from the associated reports and from vehicle files maintained by WES

The wheeled portion of the *Fine-Grained One-Pass Vehicle Cone Index* database includes all of the wheeled vehicles tested by WES for which an estimate of the VCI_1 could be determined. Some of the data were from fifty-pass vehicle cone index (VCI_{50}) experiments and some had vehicles with non-powered traction elements (e.g. towed trailers). VCI_{50} is the minimum soil strength necessary to support a vehicle for fifty passes, and VCI_{50} experiments did not usually provide sufficient root multi-pass test data to determine VCI_1 with adequate

confidence for this study. Therefore, the observations originating from VCI_{50} experiments were reviewed, and those having low confidence estimates were not considered. The observations having non-powered traction elements were not considered either since the VCI_1 relationships are for all-drive vehicles only. NRMM has algorithms to handle vehicles with non-powered traction elements, but these algorithms employ other traction relationships (i.e., drawbar and motion resistance) in addition to the VCI_1 relationships. The final database used in the VCI_1 modeling included experiments that spanned a period of thirty years from the 1960s to the 1990s.

The wheeled portion of the *Fine-Grained Drawbar at Nominal Slip* database includes most wheeled vehicles tested by WES through the late 1980s and some vehicles from more recent experiments. The database includes drawbar performance data that are based on two critical slip zones: (1) 20 percent slip or optimum slip (typically 15 to 30 percent) and (2) 100 percent slip or maximum pull slip (typically 20 to 100 percent). Although the current NRMM drawbar relationships are based on 100 percent slip, the data from the 20 percent slip zone were used during the drawbar modeling. The data from the 100 percent slip zone were not used because the performance data were relatively limited and, more importantly, because there is always less quality control in drawbar testing at the 100 percent slip zone than at the 20 percent slip zone. The final field database used in the drawbar modeling included experiments that spanned a period of thirty years from the 1960s to the 1990s.

In order to explore the difference in drawbar performance measurements obtained by WES in field versus laboratory environments, some laboratory drawbar data were also explored. As will be shown in the discussion of the drawbar modeling (Chapter V), these data

also provided an enhancement to the drawbar modeling effort. The data selected for use were those reported by Freitag [1965] in his dimensional analysis of tire/soil interaction. This was the dimensional analysis research that laid the foundation for the Numeric Approach research effort described in the background portion of the introduction (Chapter I). The data contained experiments with four different treadless tires in soil bins containing clay soils that were essentially frictionless and saturated.

Descriptive Statistics

For relationships that are established using statistical modeling techniques, it is imperative that the limits of the experimental data be observed. Use of these relationships outside the experimental limits is always risky, especially if there is no underlying theoretical foundation. For this reason, tables were generated that show the total number and types of observations and the minimum, mean, and maximum values of the principal modeling variables. The relative magnitudes of variables are just as important in many cases as the absolute magnitudes. Therefore, the minimum, mean, and maximum values for several ratios of the principal variables were also included in the tables. This was especially important for tire deflection, a control variable usually specified (through recommended tire inflation pressures) as a percent of the tire section height for particular operating scenarios such as highway, cross-country, mud/sand/snow, or emergency.

Table 1 shows the descriptive statistics for the VCI_1 database. As shown, there were 79 total observations used in the VCI_1 modeling. About 40 percent of the observations had radial tires with the majority having bias ply tires, and there were two observations that had

dual tires on the rear. The gross vehicle weights ranged from less than 1,200 to over 86,000 pounds, and these loads were carried on anywhere from 2 to 5 axles translating into axle loadings of about 600 to 20,000 pounds. Tire diameters ranged from 17 to 63 inches with section widths ranging between 7 and 40 inches, and the tire shape ratio of width-over-diameter ranged from 0.25 to 0.95. The deflections expressed in percent of tire section height ranged from less than 10 percent to nearly 50 percent and were 25 percent on average. The measured VCI_1 values ranged from extremely low at 5 to fairly high at 40 and were 22 on average.

Table 1. General statistics for the VCI_1 database

Total Observations: 79	Radials: 31	Bias Ply: 48	Duals: 2	Singles: 77

	Vehicle Dimensions			Average Axle Dimensions						Meas. VCI_1 psi
	GVW lbf	m	h_c in.	w lbf	n	d in.	b in.	h in.	δ in.	
Min:	1190	2	9.0	595	2	17.4	7.1	4.5	0.37	5
Mean:	26038	3	13.2	7969	2	41.7	14.5	10.8	2.79	22
Max:	86255	5	22.0	20199	3.333	62.5	40.0	16.7	5.93	40

	$\dfrac{\delta}{h}$	$\dfrac{\delta}{d}$	$\dfrac{h}{b}$	$\dfrac{b}{d}$	$\dfrac{h}{d}$	$\dfrac{h_c}{d}$	$\dfrac{h_c}{h}$
Min:	0.060	0.016	0.298	0.248	0.223	0.216	0.857
Mean:	0.250	0.064	0.765	0.365	0.257	0.334	1.304
Max:	0.467	0.120	0.944	0.952	0.317	0.603	2.340

Table 2. General statistics for the field drawbar database

Total Observations: 84	Radials: 24	Bias Ply: 60	Duals: 0	Singles: 84

	Vehicle Dimensions		Average Axle Dimensions						Meas. RCI psi	Meas. $\dfrac{D}{W}_{20}$
	GVW lbf	m	w lbf	n	d in.	b in.	h in.	δ in.		
Min:	1900	2	950	2	22.5	8.5	6.2	0.93	9	0.04
Mean:	18785	3	5910	2	40.9	17.2	10.7	2.41	199	0.47
Max:	66000	5	16500	2	62.5	40.0	16.7	4.00	750	0.72

	$\dfrac{\delta}{h}$	$\dfrac{\delta}{d}$	$\dfrac{h}{b}$	$\dfrac{b}{d}$	$\dfrac{h}{d}$
Min:	0.130	0.033	0.300	0.257	0.230
Mean:	0.229	0.059	0.718	0.416	0.262
Max:	0.385	0.097	0.927	0.952	0.292

Table 2 shows the descriptive statistics for the field drawbar database. As shown, there were 84 total field observations used in the drawbar modeling. About 30 percent of the observations had radial tires with the vast majority having bias ply tires, and none of the observations had dual tires. The gross vehicle weights ranged from 1,900 to 66,000 pounds, and these loads were carried on anywhere from 2 to 5 axles translating into axle loadings of about 900 to 17,000 pounds. Tire diameters ranged from 22 to 63 inches with section widths ranging between 8 and 40 inches, and the tire shape ratio of width-over-diameter ranged from 0.26 to 0.95. The deflections expressed in percent of tire section height ranged from 13 percent to nearly 40 percent and were 23 percent on average. The measured drawbar

performance values expressed as a percent of gross vehicle weight at 20 percent slip ranged from near zero to 0.72. These drawbar values were obtained on CH soils that essentially spanned the entire spectrum of soil strengths varying from a very soft 9 to an extremely hard 750 RCI.

Table 3. General statistics for the laboratory drawbar database

Total Observations 119	Radials 0	Bias Ply 119

	Average Axle Dimensions						Meas. CI psi	Meas. $\dfrac{D}{W_{20}}$
	$\begin{array}{c}w\\ lbf\end{array}$	n	$\begin{array}{c}d\\ in.\end{array}$	$\begin{array}{c}b\\ in.\end{array}$	$\begin{array}{c}h\\ in.\end{array}$	$\begin{array}{c}\delta\\ in.\end{array}$		
Min:	100	1	14.1	4.2	3.1	0.26	14	-0.11
Mean:	472	1	25.4	5.9	4.6	1.16	39	0.43
Max:	892	1	28.3	8.3	6.4	2.24	67	1.51

	$\dfrac{\delta}{h}$	$\dfrac{\delta}{d}$	$\dfrac{h}{b}$	$\dfrac{b}{d}$	$\dfrac{h}{d}$
Min:	0.080	0.009	0.738	0.150	0.114
Mean:	0.254	0.046	0.771	0.239	0.184
Max:	0.450	0.079	0.803	0.298	0.226

Table 3 shows the descriptive statistics for the laboratory drawbar database. As shown, a total of 119 laboratory observations were explored in support of the drawbar modeling. There were no laboratory observations with radial tires. The tire loadings ranged from 100 to about 900 pounds. These tire loadings would hypothetically translate to realistic axle loadings of 200 to 1800 pounds which are much smaller than those associated with the

field (i.e., full-scale vehicle) observations. Tire diameters ranged from 14 to 28 inches with section widths ranging between 4 and 8 inches, and the tire shape ratio of width-over-diameter ranged from 0.15 to 0.30. The deflections expressed in percent of tire section height ranged from 8 percent to 45 percent and were 25 percent on average. The measured drawbar performance values expressed as a percent of tire loading at 20 percent slip ranged from below zero to an astounding 1.51 (this magnitude of drawbar has never been demonstrated with real vehicles). The soil strengths in the laboratory prepared CH soils ranged from 14 to 67 CI. These CI strengths were probably equivalent to RCI strengths for the laboratory soils since they were likely fully remolded during the high level of processing necessary to prepare the soil bins for testing. Therefore, these strengths can be directly compared to the RCI strengths from the field observations for comparing the strength ranges.

Another important concern when developing relationships with statistical modeling techniques is the distribution of values within the experimental range for the system variables. It is desirable to have values distributed throughout the experimental range rather than having a small number of clusters. In order to evaluate the distribution of values for the system variables in the three databases, dot plots were generated for selected variables.

Figure 3 shows the dot plots for the VCI_1 database, and it demonstrates that there were good distributions for all of the variables except for section width which had nearly all of the values in the lower half of the experimental range. Figure 4 shows the dot plots for the field drawbar database, and it demonstrates that although there were fair distributions for most of the variables, the values were more sparse than those in the VCI_1 database. Figure 5 shows the dot plots for the laboratory drawbar database, and it demonstrates that although
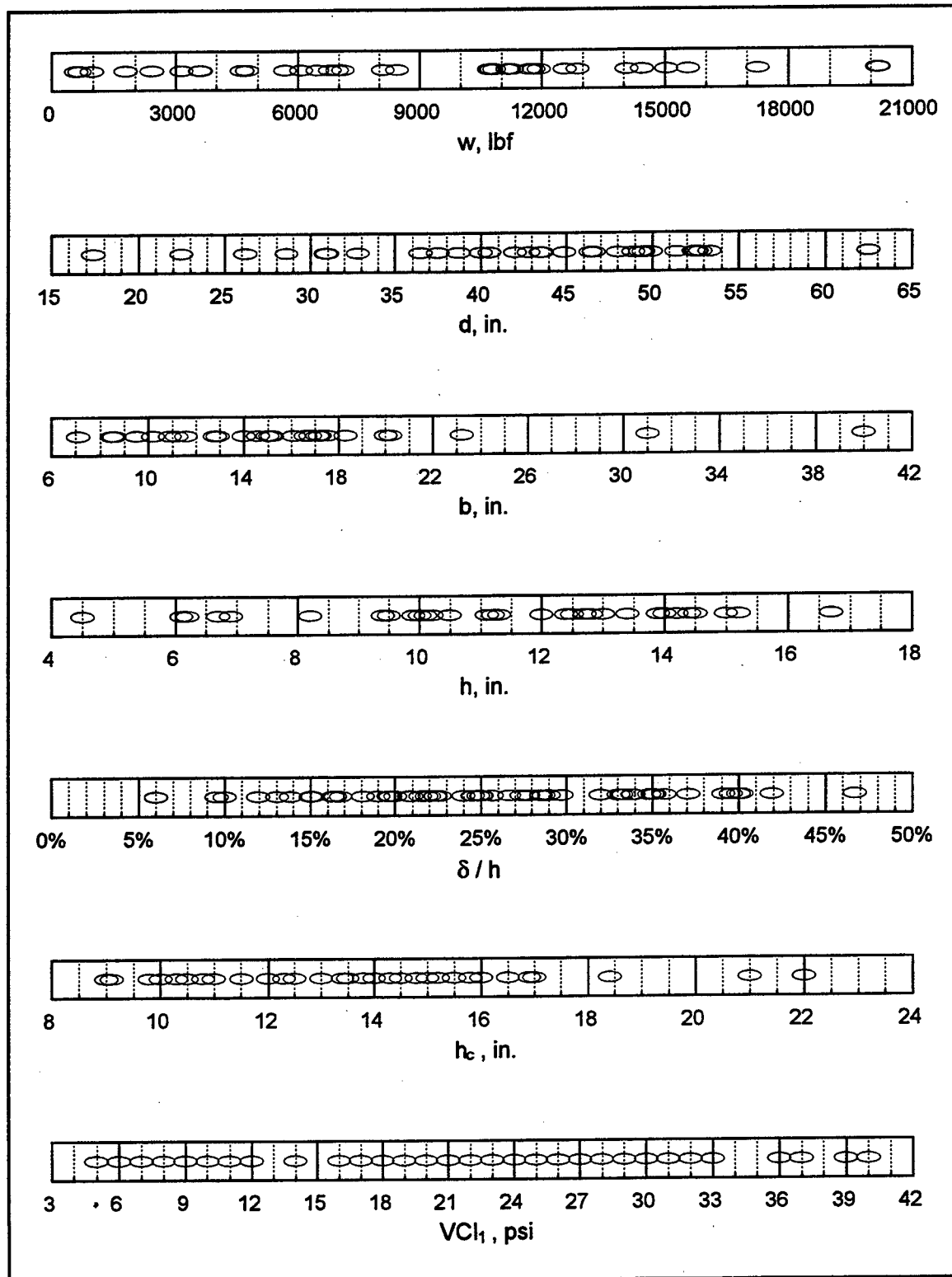
Figure 3. Distribution of selected system variables for the VCI$_1$ database
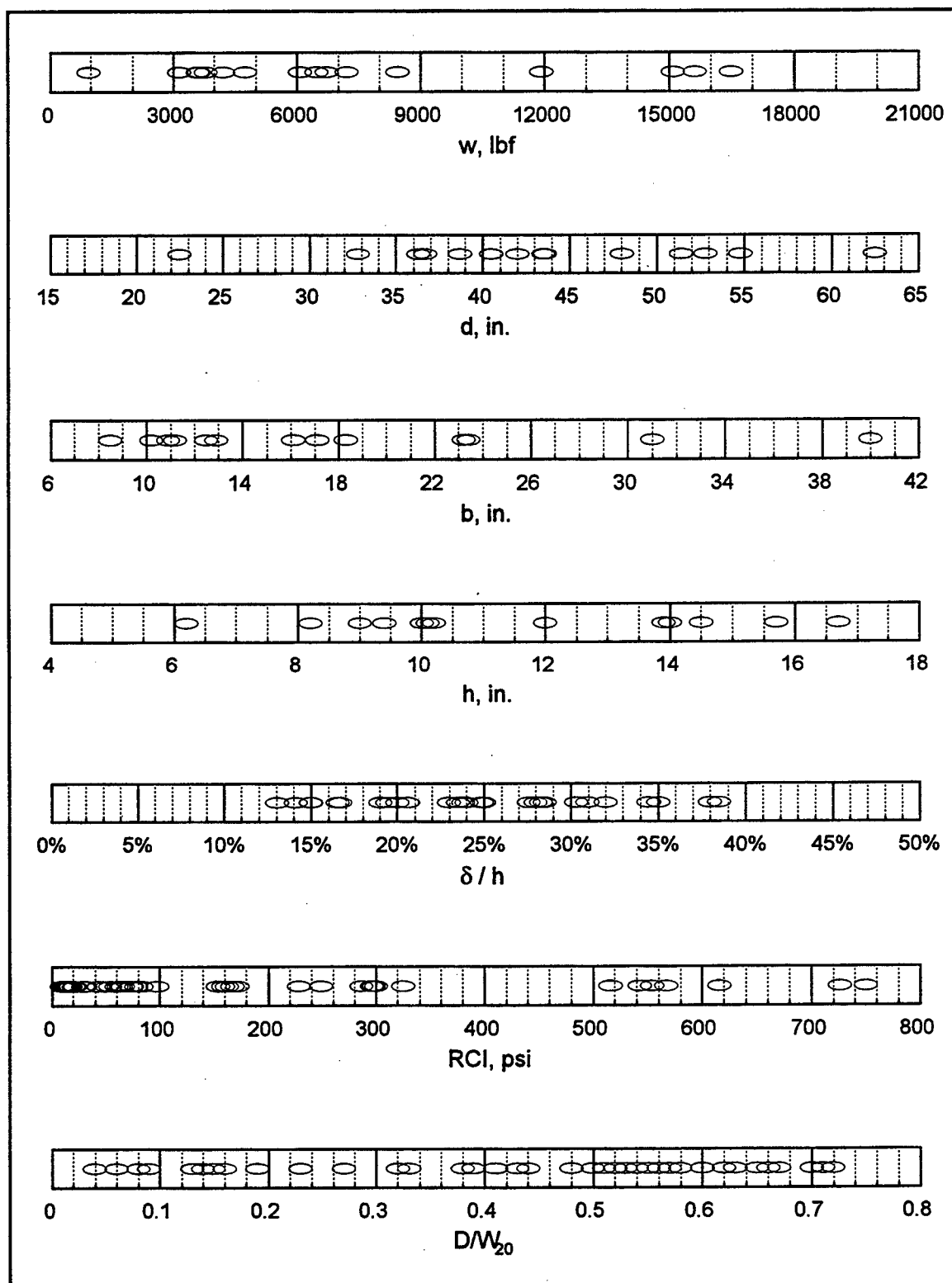
Figure 4. Distribution of selected system variables for the field drawbar database
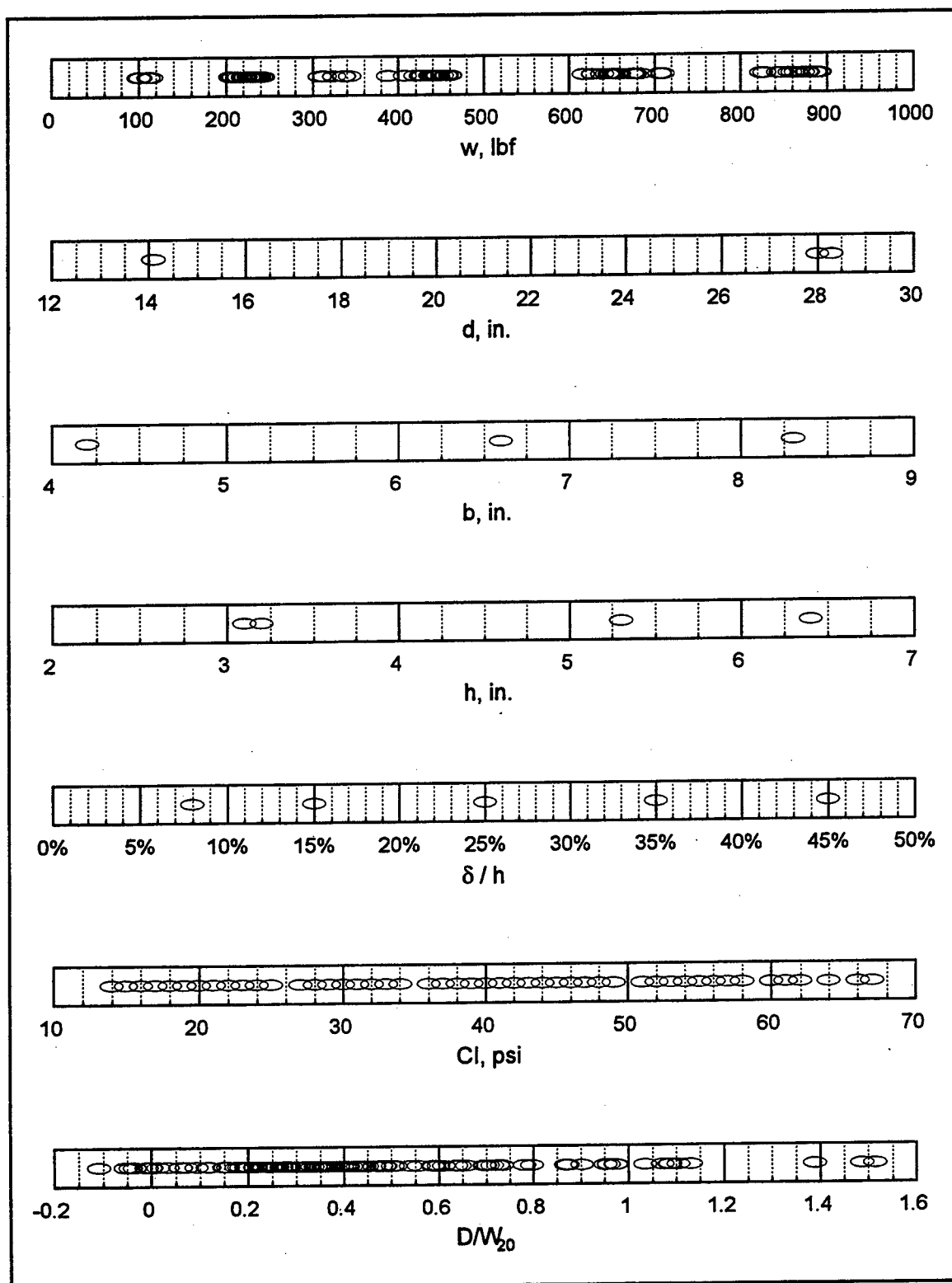
Figure 5. Distribution of selected system variables for the laboratory drawbar database

the tire diameter, section width, and section height variables were very limited relative to the field databases, the load, deflection, soil strength, and performance metric variables had good distributions.

Trends in Tire Shape

When statistical modeling techniques are used to develop relationships, it is imperative that interrelationships between the system variables be understood. In this research, the key task in the modeling effort was to find the best way of organizing the principal vehicle variables (i.e., w, d, b, h, and δ) into a loading parameter that had a strong correlation with the performance metrics. Therefore, interrelations between these variables were investigated. Tire load (i.e., W_w = w/n) and deflection are control variables for wheeled vehicles, but diameter, section width and section height are "fixed" variables for tires that could possibly follow trends based on standards in tire design, so the interrelations between these three were explored.

Figure 6 shows three x-y plots that illustrate the trends in tire shape for all three of the databases combined. Figure 6a shows that there was a strong linear relationship between diameter and section height for all of the tires in the three databases with the exception of one laboratory tire (4.00-20) whose section height was very small relative to its diameter. Figure 6b shows that there was a linear relationship between diameter and section width for most of the tires in the three databases, but several tires did fall far away from the normal trend. Figure 6c shows that there was also a linear relationship between section height and section width for most of the tires in the three databases. Several tires from field experiments fell far

away from the normal section height-to-section width trend, but all the tires from the laboratory experiments fell within the normal trend.

a. Diameter versus section height

b. Diameter versus section width

c. Section height versus section width

○ 1-Pass VCI Data △ Field Drawbar Data □ Lab Drawbar Data
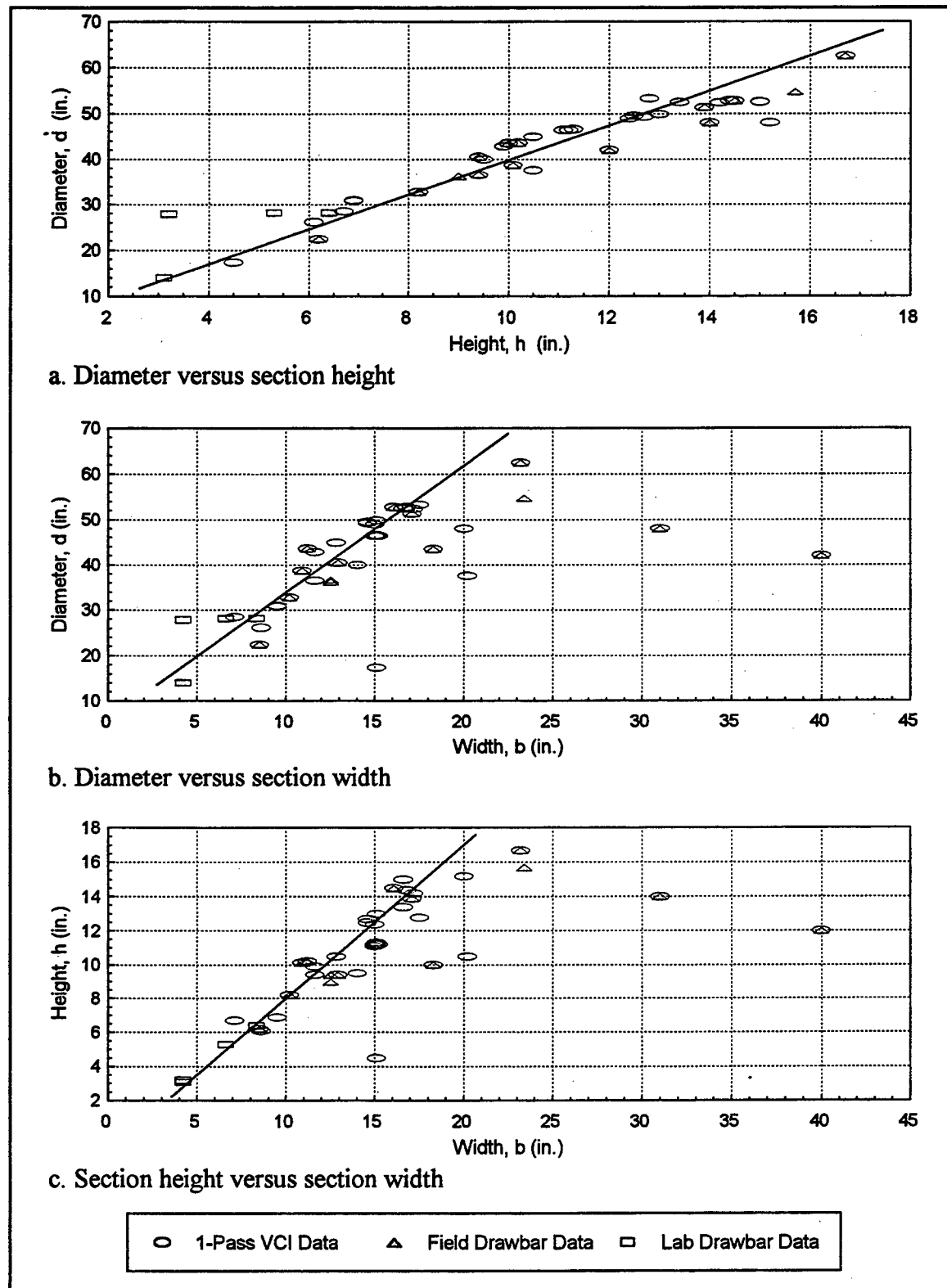
Figure 6. Tire shape trends

CHAPTER III

BASIC MODELING CONCEPTS

Simplified Tire/Soil Interaction

For a locomotive, there is the rail; for an airplane, there is the air; and for a wheeled vehicle, there is the road, unless of course, the road is not an option. Such is the case for wheeled vehicles designed for industries like military, mining, construction, agriculture, and so forth. For this breed of wheeled vehicle, which is designed primarily for off-road operation, there is the terrain as it is found in a natural state. The variability in composition and consistency of natural terrain is vast, and the mechanics that control the propulsion system of tires in this medium are immense in complexity. However, as with many other complex engineering problems, useful knowledge and understanding can be gained from a relatively simple evaluation of the system.

This research focuses on the interaction of tires in soil. A simple steady-state analysis of a tire interacting with soil can be used to evaluate the traction performance of wheeled vehicles. Figure 7 shows a powered tire with the loading forces, which are transferred from the axle to center of the wheel, and the reaction stresses, which are transferred from the soil to the tire along the interface. As shown in the figure, the reaction stresses can be aggregated into meaningful horizontal and vertical forces. All of the vertical stresses, normal (σ) and

shearing (τ), are converted into a normal reaction force (N), all of the horizontal normal stresses are converted into a motion resistance force (R), and all of the horizontal shearing stresses are converted into a tractive force (T).

$$N = \sum_{j=1}^{NC} [(\sigma_{Y_j} + \tau_{Y_j}) A_{XZ}]$$

$$R = \sum_{j=1}^{NC} [\sigma_{X_j} A_{YZ}]$$

$$T = \sum_{j=1}^{NC} [\tau_{X_j} A_{XZ}]$$
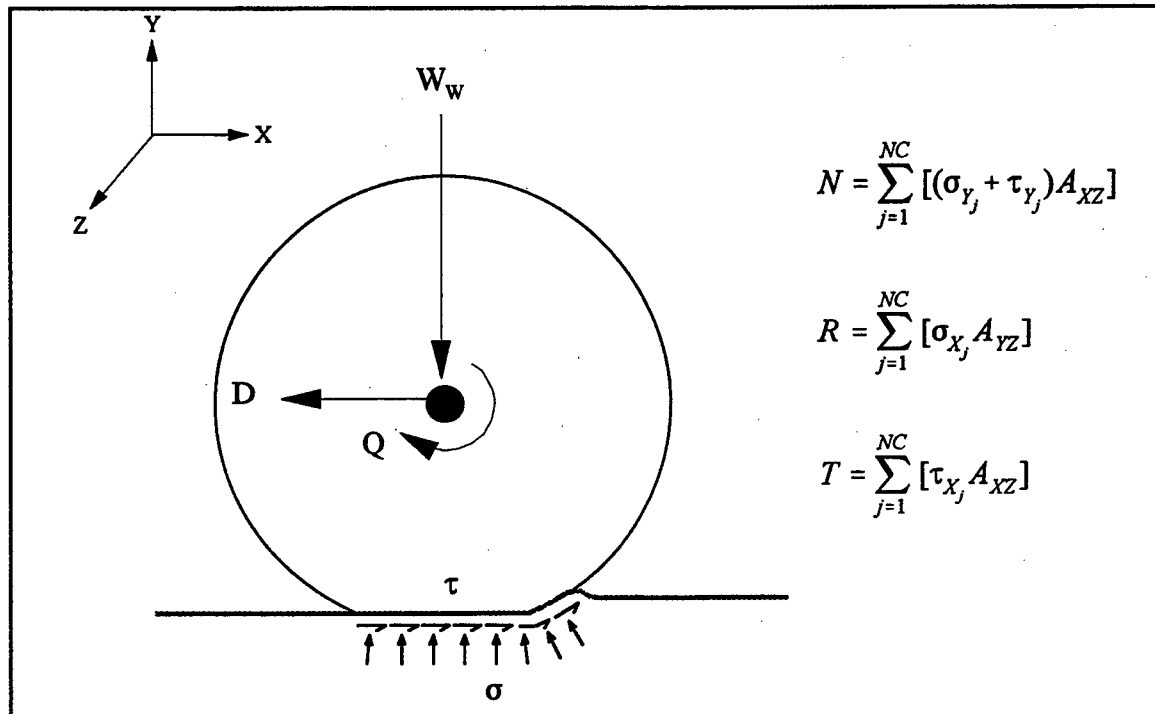
Figure 7. Simple stress analysis for tire/soil interaction

Figure 8 shows the same tire but with the reaction forces applied at the interface instead of the stresses. The reaction forces are located at unique points along the interface, and these points are designated by the force eccentricities. A steady-state analysis of the horizontal and vertical forces acting on the tire demonstrates that the normal force is equal to the weight on the wheel (W_w) and that the tractive force is equal to the sum of the motion resistance force and the drawbar force (D). This simple force analysis forms the fundamental logic used in NRMM by which drawbar and motion resistance relationships are used to

determine traction potential. The simple force analysis was presented herein to clarify why

drawbar and VCI$_1$ (i.e., zero drawbar) performance are major considerations in traction

modeling.
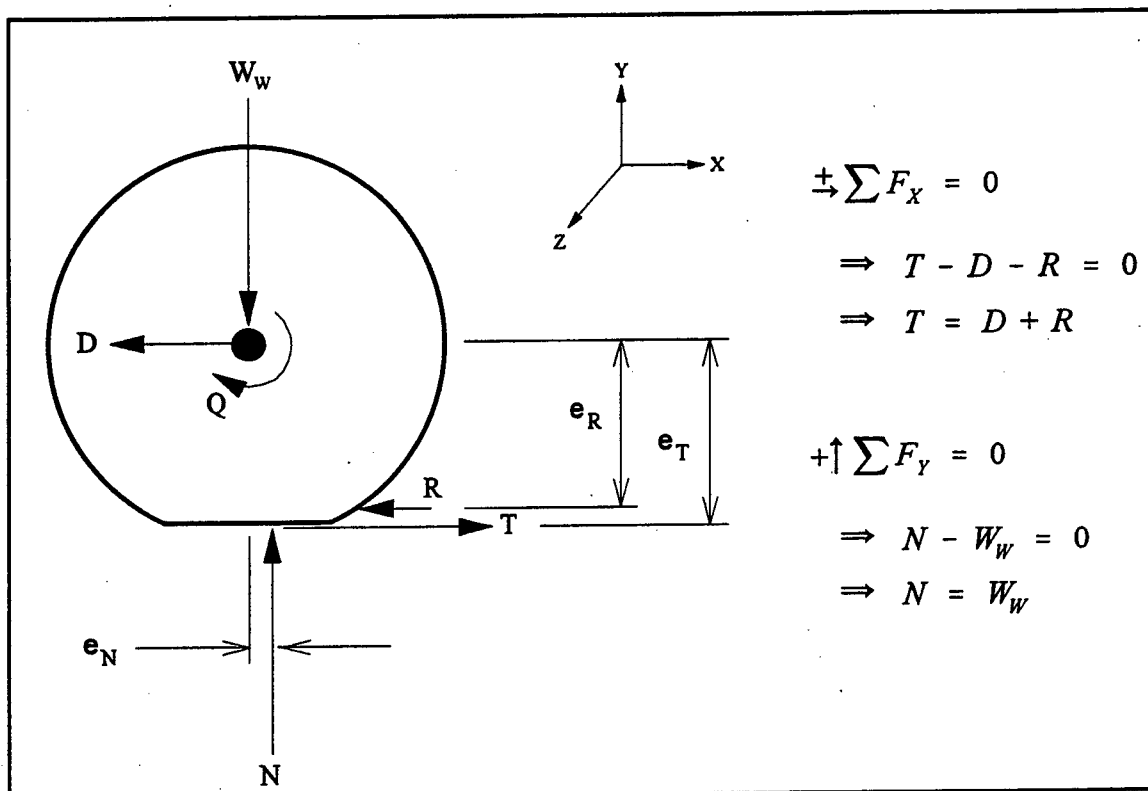
Figure 8. Steady-state force analysis for tire/soil interaction

Tire Deflection Effect

Tire deflection is a control variable for wheeled vehicles. The magnitude of tire

deflection is directly related to wheel loading and inflation pressure. Reduced inflation pres-

sure translates into increased deflection which results in an increased area of contact between

the tire and the ground. This increased contact area has a positive impact on traction per-

formance, especially in soft soils, but increased tire deflection also has a negative impact on

vehicle performance issues like rollover stability and tire durability. Therefore, operating deflections (i.e., tire inflation pressures) are recommended based on a consideration of the intended operating environment, design loading, and design speed such that an acceptable compromise is achieved between the positive and negative impacts on vehicle performance.

The principal manner in which deflection affects contact area is through an increase in the length of the contact area. The width is affected too, but the increase in width is small compared to the increase in length. Also, the increase in width occurs not at the tire tread but up along the side wall of the tire carcass. Thus, the effect of tire deflection on the area of contact at the tire/soil interface is almost entirely the result of increased contact length.

A mathematical expression was derived for estimating tire contact lengths and the effect that deflection has on those lengths. The assumption was made that tire contact length is analogous to the length of a long chord to a circle as illustrated in Figure 9. The figure shows that the length of a long chord to a circle (LC) can be calculated based on the diameter of the circle ($\varnothing$) and the middle ordinate height (M) using the equation $LC = 2\sqrt{\varnothing M - M^2}$. The long chord analogy can be used to estimate the hard-surface contact length (L_δ) by using the diameter of the tire for $\varnothing$ and the hard-surface deflection for M as shown below.

$$L_\delta = 2\sqrt{d\delta - \delta^2}$$

The long chord analogy was used throughout this research for estimating tire contact lengths which included projected bearing lengths resulting from sinkage in soft soils in addition to hard-surface contact lengths.

The figure shows a circle with diameter $\varnothing$. Equations:

$$c = \frac{\varnothing}{2} \quad , \quad a = \frac{\varnothing}{2} - M$$

$$b^2 = c^2 - a^2$$

$$\rightarrow \quad b = \sqrt{\left(\frac{\varnothing}{2}\right)^2 - \left(\frac{\varnothing}{2} - M\right)^2}$$

$$\rightarrow \quad b = \sqrt{\varnothing M - M^2}$$

$$LC = 2b$$

$$\rightarrow \quad LC = 2\sqrt{\varnothing M - M^2}$$
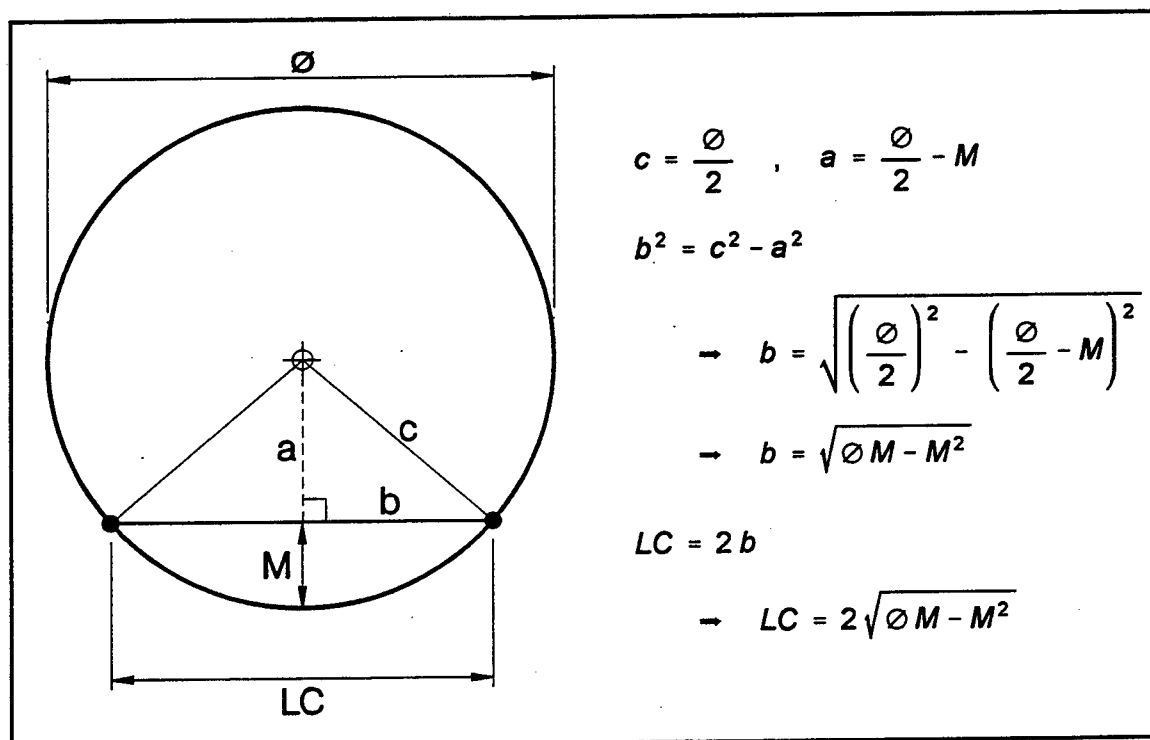
Figure 9. Long chord analogy for tire contact length estimates

The basic equation can be rewritten with LC and M expressed as fractions of the circle diameter as shown below.

$$\frac{LC}{\varnothing} = \sqrt{\frac{M}{\varnothing} - \left(\frac{M}{\varnothing}\right)^2}$$

With the expression in this form, the nature of variations in LC due to variations in M for a given diameter can be observed as shown in Figure 10. The figure shows that LC increases rapidly being 50 percent of the diameter when M is only 0.067 times the diameter, and LC reaches a maximum value equal to the diameter when M is 0.5 times the diameter. Figure 10 also illustrates that care must be taken when applying the long chord analogy if M has the potential to increase beyond 0.5 times the diameter. This realization becomes important when

using the long chord analogy to estimate projected bearing lengths for tires in soft soils where

large sinkage occurs.
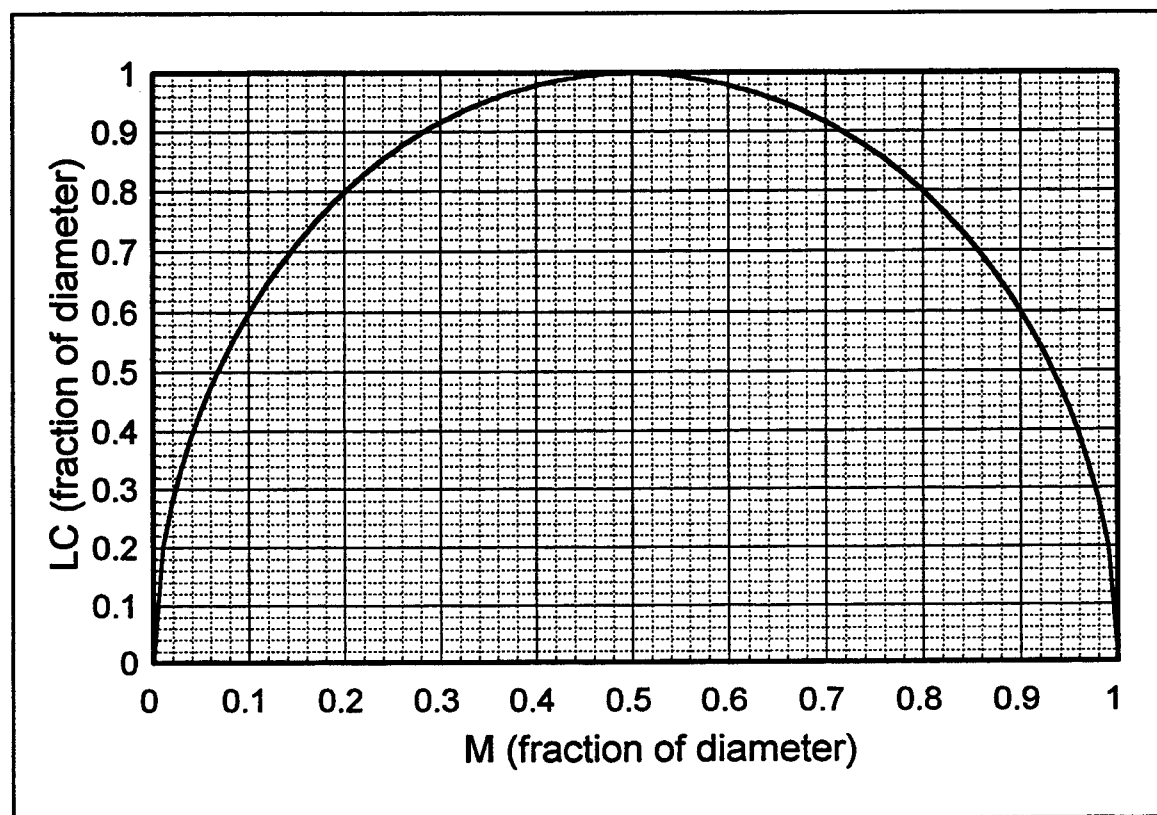
Figure 10. Long chord versus middle ordinate

Model Development Tools

Over one hundred statistical models were developed during this research. Some of

the models involved establishing a mathematical equation to describe the relationship between

a performance metric (VCI_1 or D/W_{20}) and one or more clearly defined system parameters.

Most of the models, however, involved establishing the form of the principal system

parameter in conjunction with establishing the mathematical equation that would describe the

relationship. The principal system parameters were mathematical terms that included some

combination of vehicle characteristics and/or soil strength. Depending on their origin, the principal system parameters may or may not have been dimensionally correct. Some of the principal system parameters were theoretically founded, some were theoretically founded with empirical improvements, and others were purely empirical being completely defined by the experimental data.

Statistical modeling techniques were used to develop the mathematical equations and the principal system parameters necessary to describe the traction relationships. Least squares linear regression was typically used to develop the mathematical equations, and curvilinear transformations were used when necessary, which was always the case in the drawbar modeling. Numerical optimization techniques were used to develop the principal system parameters. In some cases, numerical optimization techniques were also used to define the mathematical equations rather than using linear regression.

The numerical optimization techniques involved iterative trial and error routines. These routines systematically changed the value of constants (i.e., coefficients, additives, or exponents) within the principal system parameter in directions that minimized the standard error (S_e), or maximized the coefficient of determination (R^2), for the mathematical equation describing the relationship. It was necessary for the constants to be initialized with reasonable estimates first. Then the iterative trial and error routines would converge on better estimates for the constants by using intelligent mathematical algorithms. The algorithms that were used involved forward or central differencing for determining estimates of partial derivatives, a quasi-Newton or conjugate method for deciding whether to increase or decrease the constants, and a tangent or quadratic approach for obtaining the next estimates for the constants.

When linear regression was used to develop a mathematical equation and numerical optimization was used to define the principal system parameter, the two techniques were combined in a larger iterative process. Since numerical optimization is an iterative approach, the linear regression algorithms were included within the numerical optimization process. Each time the numerical optimization algorithms would increment the values of the constants within the principal system parameter, the linear regression algorithms would update the constants within the mathematical equation. This combined process resulted in quicker convergence to the optimum values of the empirical constants in the principal system parameters. Whether this combined iterative process or one of the individual statistical modeling tools (i.e., linear regression or numerical optimization) was used, computerized spreadsheet software was utilized to accomplish the complex and laborious task.

For clarification, a fictitious example is presented. Let there be a performance metric Y for which a means of prediction is desired. If Y is linearly related to system parameters X_1 and X_2, a least squares linear regression model, as shown below, could be used to develop a mathematical equation that would predict Y as a function of X_1 and X_2.

$$Y = \beta_0 + \beta_1 X_1 + \beta_2 X_2$$

The task of the linear regression would be to determine values for coefficients β_0, β_1, and β_2 that minimize the sum of the squared errors between the measured data and the predictions from the mathematical equation. An additional level of complexity is added if X_1 is an

undefined parameter such as that shown below where A, B, and C are system variables (such as tire diameter, soil strength, etc.) and p_1, c_1, and c_2 are undefined constants.

$$X_1 = \frac{A^{p_1} + c_1 B}{C + c_2}$$

For this second case, numerical optimization could be used in combination with linear regression as described in the preceding paragraph. The task of the numerical optimization would be to determine values of p_1, c_1, and c_2 that produce a stronger linear relationship between X_1 and Y, and the linear regression would continuously update the coefficients β_0, β_1, and β_2 during the iterative process. The numerical optimization process could also be used alone to determine all six of the empirical constants β_0, β_1, β_2, p_1, c_1, and c_2, but this approach was only used when linear regression was not applicable.

As stated, curvilinear transformations were always necessary in the drawbar modeling. They were necessary because trends observed in the drawbar relationships were not linear. Instead the trends were curvilinear with forms that were described well by a rectangular hyperbola. The general form of the rectangular hyperbola equation is shown below.

$$Y = \beta_0 + \frac{\beta_1}{X + \beta_2}$$

In order to determine the empirical constants β_0, β_1, and β_2, the curvilinear transformation shown below was applied.

$$X = b_0 + b_1 \frac{X}{Y} + b_2 \frac{1}{Y}$$

Least squares linear regression was used to determine b_0, b_1, and b_2, and then estimates for

β_0, β_1, and β_2 were determined using the equations below to translate the regression

constants from the transformed space into regression constants for the true space.

$$\beta_0 = b_1 \quad , \quad \beta_1 = b_2 + b_0 b_1 \quad , \quad \beta_2 = -b_0$$

This transformation process typically produces good estimates for β_0, β_1, and β_2. However,

it minimizes the sum of the squared residuals in the transformed space, not in the true space.

Therefore these estimates were used as initial estimates for numerical optimization, and

numerical optimization was used to determine new estimates for β_0, β_1, and β_2 that mini-

mized the sum of the squared residuals in the true space by minimizing S_e or maximizing R^2.

One other noteworthy item specific to the drawbar modeling is the manner in which

S_e was calculated. S_e is largely determined by the magnitude of the residuals. Since the

residuals are equal to the difference between the measured and predicted values, the predic-

tions will obviously influence S_e. The rectangular hyperbola equations were developed to

describe the drawbar relationships, but they were not used to predict the drawbar perform-

ance metric (Y) for all values of the system parameter (X). The equations were only used to

predict Y for observations that had X values greater than or equal to the X-intercept of the

equation. For observations that had X values less than the X-intercept of the equation, a

prediction of zero was used.

This approach of determining the predictions to be used in calculating S_e was used

for the following reasons. First, there physically is no such thing as negative drawbar for a

self-propelled, independent vehicle that is attempting to produce forward motion on level

terrain. Passive motion-resisting influences such as the soil do not push any harder on the

vehicle than the vehicle pushes on them. Therefore, if the maximum tractive force that the vehicle can generate is less than the maximum motion resistance force that the soil, etc. can generate, then the drawbar force (i.e., tractive force less motion resistance force) would be zero. Another reason arises from the nature of the rectangular hyperbola equation. The rectangular hyperbola equation has a vertical asymptote that is less than and usually very close to the X-intercept of the equation. The potential exists for some observations to have X values less than the value of the asymptote, and this situation usually produces extemely unrealistic predictions and hence greatly misleading estimates for S_e.

CHAPTER IV

VCI_1 MODELING

Overview

The VCI_1 modeling consisted of two major areas of focus. The first focus was on evaluating existing relationships or parameters that use cone penetrometer-based soil measurements and relatively simple vehicle characteristics to determine traction potential in soft soils. Four existing models were investigated which included the current NRMM relationship and three versions of Mean Maximum Pressure (MMP). The second focus was on the development of new relationships. Seven major types of new models were developed which included six different types of contact pressure models and a numeric-type model.

For most of the major types of new models that were developed, more than one variant was investigated. The term variant is used here to describe a slight variation on the same basic modeling theme. Slight variations include such things as: (1) using an empirical constant times hard-surface deflection to account for the possibility that tires deflect differently in soft soils than on a hard surface and (2) adding a tire construction variable as a secondary parameter to account for the possibility that radial and bias ply tires perform differently, even with similar size, loading, and deflection. Fifty-six variants of the contact pressure models and nine variants of the numeric-type model were developed. Additionally, five model

variants based on the standard NRMM relationship were investigated, the primary purpose being to optimize the current approach to the VCI$_1$ database.

For the sake of clarity and concision, all of the individual model variants are not addressed in the main text of this document. Only the four existing models and the best variants of the new development models are described. However, a listing of all the model variants explored and a table summarizing their quality are provided in Appendix B.

Existing Models

The standard NRMM relationship is based primarily on a parameter called the mobility index (MI). MI was initially developed based on the results of trafficability studies conducted by WES from 1945 through 1951 [1951], and was then upgraded to its current form based on additional trafficability studies conducted during the 1960s [Kennedy and Rush 1968]. MI was developed to predict VCI$_{50}$, but it was also adopted later as a parameter for predicting VCI$_1$. The MI parameter is actually an aggregation of eight smaller factors, each of which is based on some vehicle characteristic considered to influence vehicle mobility in soft soils. MI for wheeled vehicles is calculated as shown below.

$$MI = \left(\frac{(CPF)\,(WF)}{(TEF)\,(GF)} + WLF - CF \right)(EF)\,(TF)$$

The eight smaller factors are calculated as follows (see nomenclature for descriptions).

$$CPF = \frac{w}{0.5\,n\,d\,b} \qquad , \qquad TEF = \frac{10 + b}{100}$$

$$WLF = \frac{w}{2000} \qquad , \qquad CF = \frac{h_c}{10}$$

$$WF = c_{WF1}(w/1000) + c_{WF2}$$

$$where \begin{cases} w < 2,000 \ lbf & \Rightarrow & c_{WF1} = 0.553 & and & c_{WF2} = 0 \\ 2,000 \leq w < 13,500 \ lbf & \Rightarrow & c_{WF1} = 0.033 & and & c_{WF2} = 1.050 \\ 13,500 \leq w < 20,000 \ lbf & \Rightarrow & c_{WF1} = 0.142 & and & c_{WF2} = -0.420 \\ 20,000 \leq w & \Rightarrow & c_{WF1} = 0.278 & and & c_{WF2} = -3.115 \end{cases}$$

$$GF = 1 + 0.05 \, c_{GF} \quad where \quad c_{GF} = 1 \ if \ tire \ chains \ are \ used \ or \ 0 \ if \ not$$

$$EF = 1 + 0.05 \, c_{EF} \quad where \quad c_{EF} = 1 \ if \ PWR < 10 \ hp/ton \ or \ 0 \ if \ not$$

$$TF = 1 + 0.05 \, c_{TF} \quad where \quad c_{TF} = 1 \ if \ manual \ transmission \ or \ 0 \ if \ automatic$$

The data used during the development of MI involved tire deflections around 15 percent of the section height only; therefore, deflection was not considered in MI. When data were later obtained for tires with much higher deflections, the performance of MI as a predictor for VCI_1 greatly diminished. WES developed the deflection correction factor (DCF) to take the effect of tire deflection into account. DCF is calculated as shown below.

$$DCF = \left(\frac{0.15}{\delta/h}\right)^{0.25}$$

DCF actually acts to normalize VCI_1 to a 15 percent deflection magnitude and is applied as a multiplier to equations that were originally developed to predict VCI_1 as a function of MI alone. The standard NRMM equations for predicting VCI_1 as a function of MI and DCF are shown below [Ahlvin and Haley 1992].

$$VCI_1 = f(MI, DCF)$$

$$where \begin{cases} MI \leq 115 & \Rightarrow & VCI_1 = \left(11.48 + 0.2 \, MI - \dfrac{39.2}{MI + 3.74}\right) DCF \\ MI > 115 & \Rightarrow & VCI_1 = \left(4.1 \, MI^{0.446}\right) DCF \end{cases}$$
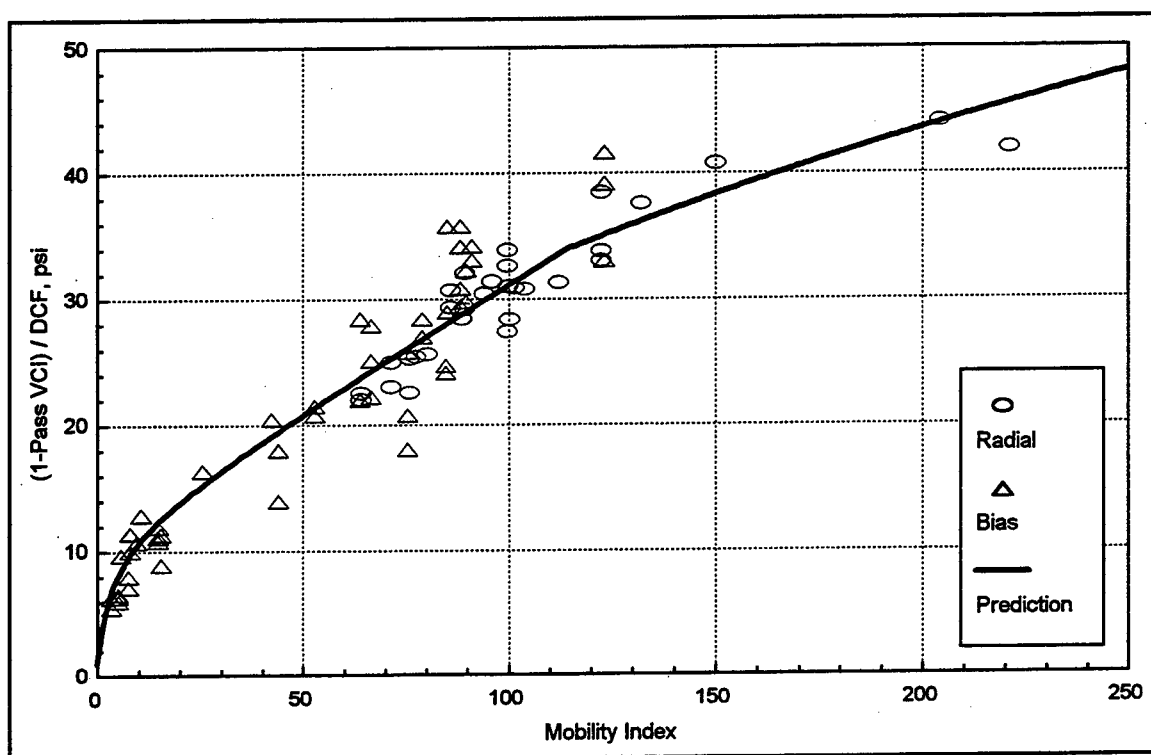
Figure 11. Standard NRMM relationship for VCI_1

MI and DCF were calculated for each of the observations in the VCI_1 database, and the data were plotted with the standard NRMM equations on a x-y plot as shown in Figure 11. Note that it was necessary to divide VCI_1 by DCF in order to generate the simple x-y plot. The figure shows that the data are described reasonably well by the standard NRMM relationship, but the relationship appears to be very unstable beyond an MI of about 100.

The standard NRMM relationship was developed using only part of the data contained in the VCI_1 database. New relationships developed using all of the data would have an immediate advantage over the NRMM relationship since their empirical constants would be optimized to the data. This situation meant that fair comparisons between the standard NRMM relationship and any of the other relationships evaluated during this research could

only be made if the NRMM relationship was optimized to the complete data set. Therefore, a modified version of the NRMM relationship was developed that optimized the empirical constants in MI, DCF, and the prediction equations (i.e., curve-fits).
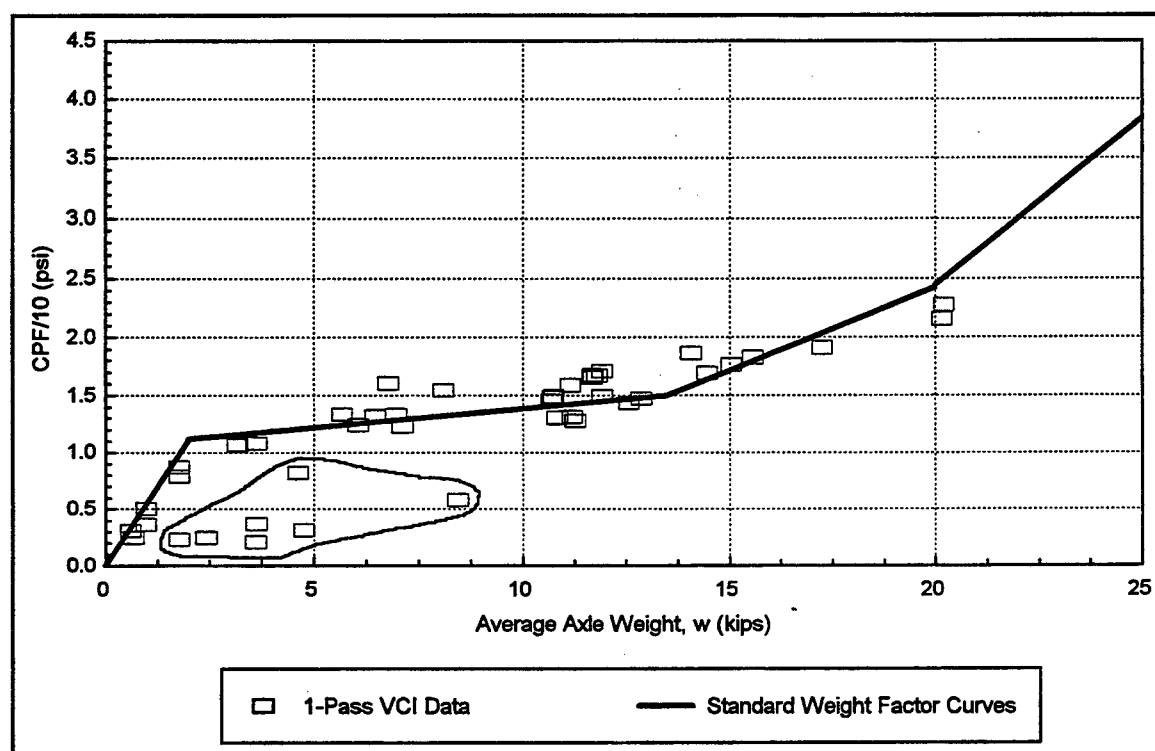
Figure 12. Apparent origin of the Weight Factor

Optimizing the NRMM relationship was a difficult task because of the large number of empirical constants and because the Weight Factor (WF), which is one of the smaller factors within MI, is a series of four curve-fits whose origin was not clear. A thorough dissection of MI using the measured data revealed a probable source for the origin of WF. Figure 12 shows a plot of CPF divided by 10 versus the average axle weight for all of the VCI_1 observations. The four WF curve-fits are also included in the plot, and the VCI_1 data,

with the exception of the circled outliers, follow trends very similar to the WF equations. This figure indicates that the linear equations defining WF were developed from trends in CPF versus average axle weight. Therefore, WF was optimized by using linear regression to develop new equations based on the observed trends in CPF/10 versus w (note that the circled outliers were ignored). These improved WF curves are shown in Figure 13.
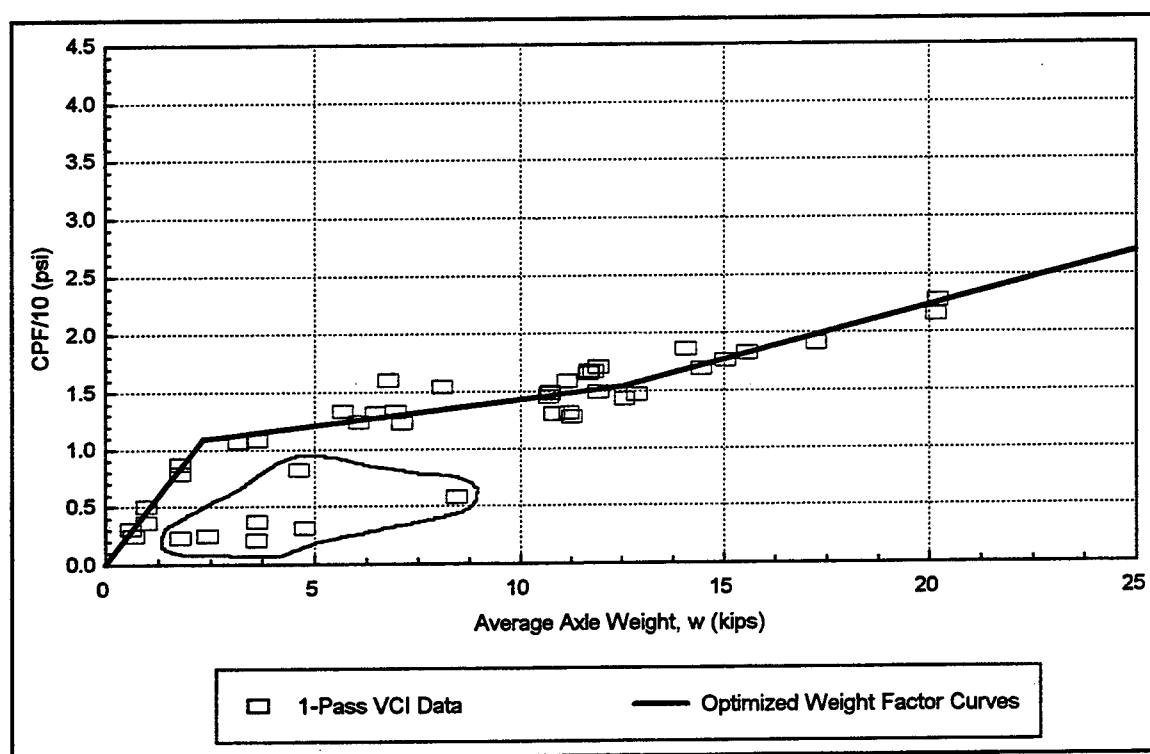
Figure 13. Optimized Weight Factor

Most of the remaining MI factors were also optimized. None of the observations were influenced by GF or EF since none had tire chains and all had horsepower-per-ton ratios of 10 or greater, and CPF is a theoretical parameter where $0.5d$ represents tire radius [Kennedy and Rush 1968]. Therefore, these three factors were not optimized. DCF and the

equations for predicting VCI_1 were optimized as well so that the final, improved NRMM relationship was fully optimized to the VCI_1 database. Numerical optimization techniques were used for the entire optimization process with the exception of the WF portion. The optimization changes made in the NRMM relationship are as follows.

$$MI' = \left(\frac{(CPF)(WF')}{(TEF')(GF)} + WLF' - CF' \right)(EF)(TF') \qquad DCF' = \left(\frac{0.15}{\delta/h} \right)^{0.30}$$

$$TEF' = \frac{8.3 + 1.13\,b}{100} \quad , \quad WLF' = \frac{w}{2000} \quad , \quad CF' = \frac{h_c}{6.9}$$

$$WF' = c_{WF1}\,(w/1000) + c_{WF2}$$

$$where \quad \begin{cases} w < 2{,}338\ lbf & \Rightarrow & c_{WF1} = 0.467 & and & c_{WF2} = 0 \\ 2{,}338 \le w < 12{,}564\ lbf & \Rightarrow & c_{WF1} = 0.044 & and & c_{WF2} = 0.988 \\ 12{,}564 \le w & \Rightarrow & c_{WF1} = 0.093 & and & c_{WF2} = 0.372 \end{cases}$$

$$TF' = 1 + 0.10\,c_{TF} \qquad where \quad c_{TF} = 1\ if\ manual\ transmission\ or\ 0\ if\ automatic$$

$$VCI_1 = f(MI', DCF')$$

$$where \quad \begin{cases} MI' \le 115 & \Rightarrow & VCI_1 = \left(10.2 + 0.222\,MI' - \dfrac{28.1}{MI' + 2.62} \right) DCF' \\[3mm] MI' > 115 & \Rightarrow & VCI_1 = \left(3.216\,MI'^{\,0.506} \right) DCF' \end{cases}$$

MI' and DCF' were calculated for each of the observations in the VCI_1 database, and the data were plotted with the optimized NRMM equations on a x-y plot as shown in Figure 14. Note that it was necessary to divide VCI_1 by DCF' in order to generate the simple x-y plot. The figure shows that the data are described reasonably well by the optimized NRMM relationship. There is little improvement in the visual appearance of the optimized relation over the standard. The most noticeable change is that the break in slope

between the two curve-fits at a mobility index of 115 is not nearly as drastic. It will be shown

in the last section of this chapter that significant improvement in quality was obtained.
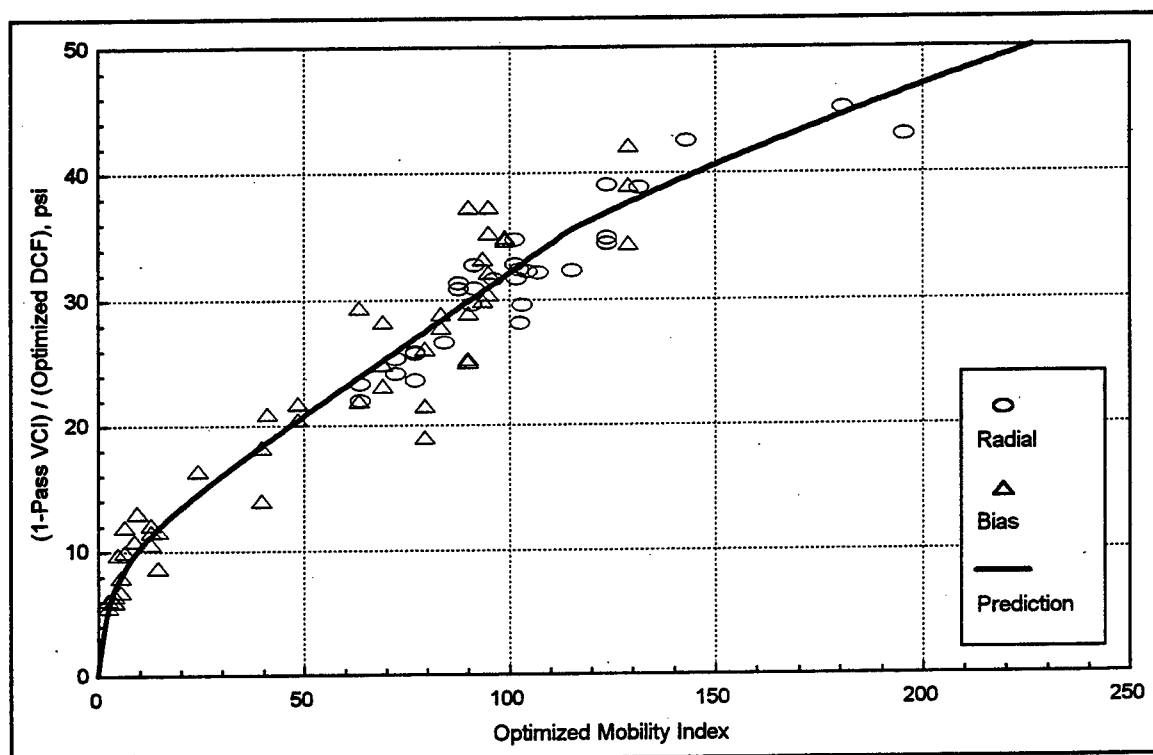
Figure 14. Optimized NRMM relationship for VCI_1

The other three existing models explored for VCI_1 are all versions of the Mean

Maximum Pressure (MMP) criterion for evaluating soft soil performance potential. Where

MI is the soft soil performance indicator developed by and for the United States military,

MMP is the soft soil performance indicator developed by and for the United Kingdom

military. The original MMP for wheeled vehicles was developed in the mid 1970s by D.

Rowland as a parameter for estimating mean ground pressures under tires that would be

directly comparable to the MMP he developed a few years earlier for tracked vehicles

[Larminie 1992]. Rowland developed MMP for wheels based in large part on the results of the Numeric Approach research performed by WES. MMP was actually a recast and slightly altered form of Freitag's Numeric for tires in clay soils.

MMP is used more as an indicator of vehicle performance potential. The trafficability research conducted by WES, which led to the development of the standard NRMM relationship, focused on developing a system of measuring soft-soil performance, and this culminated in the development of the VCI performance metric (i.e., minimum soil strength necessary to support the vehicle). The MI and DCF prediction parameters were developed for the sole purpose of predicting VCI. VCI was used as the basis for comparing (and specifying) the soft-soil performance since it allows direct comparison of different vehicles, regardless of the type of running-gear. MMP on the other hand, is essentially used as the performance metric where higher MMP values imply worse performance. Correlations apparently have been made between MMP and soft-soil performance data, but no sound relationship has ever been established to use MMP as a predictor for VCI_1. Therefore, relationships had to be developed to evaluate the three versions of MMP.

The first MMP model evaluated was based on Rowland's original version of MMP which was calculated as shown below.

$$MMP_R = \frac{0.97\,K\,GVW}{n\,m\,b^{0.85}\,d^{1.15}\,\sqrt{\delta/h}}$$

where for all-drive vehicles:

$m = 2 \Rightarrow K = 3.66$
$m = 3 \Rightarrow K = 3.90$
$m = 4 \Rightarrow K = 4.10$
$m = 5 \Rightarrow K = 4.32$

This formula is actually slightly different from the MMP formula found in the referenced publication. The true formula had the constant 2 in place of the average number of tires per axle (n), but two observations in the VCI_1 database that had dual tires on the rear (n=3.333) demonstrated that n was more appropriate. The VCI_1 data were plotted versus MMP_R, and a linear trend was apparent. Therefore, linear regression was used to develop a mathematical equation for predicting VCI_1 as a function of MMP_R. The resulting equation is shown below.

$$VCI_1 = 3.65 + 0.477 MMP_R$$

The equation is plotted with the measured data in Figure 15. The figure shows that the trend is very linear and that MMP_R describes the VCI_1 performance data well.
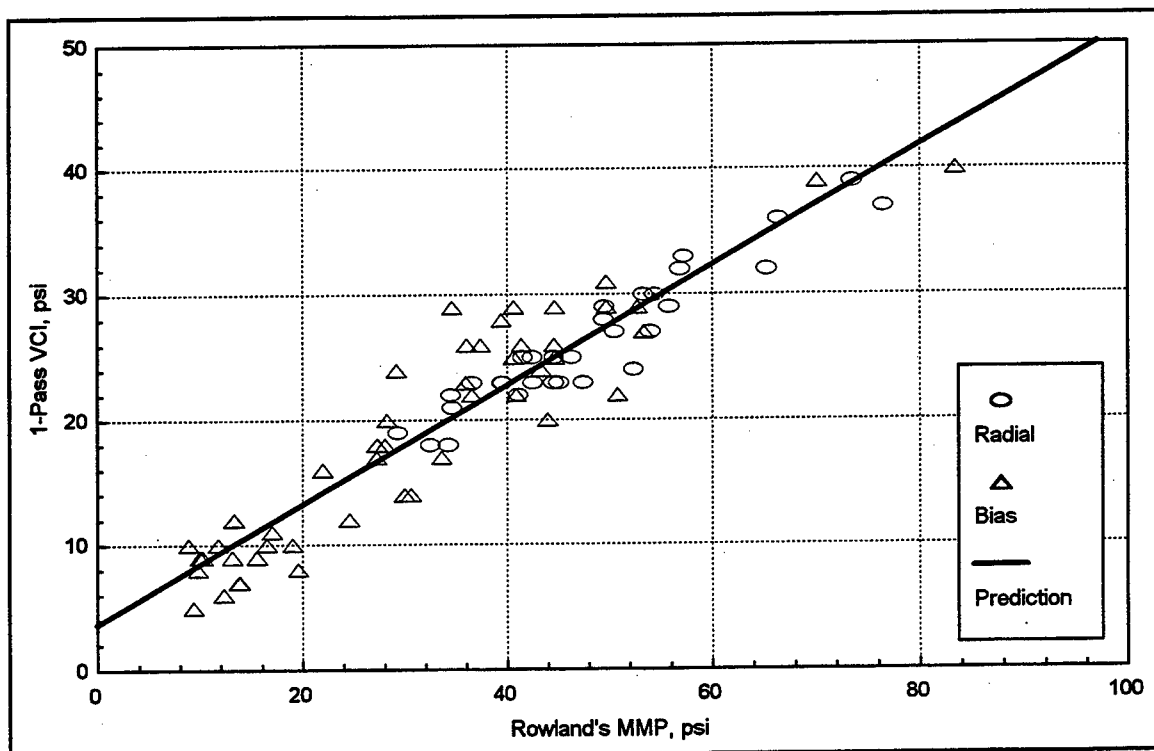
Figure 15. Relationship between Rowland's MMP and the VCI_1 data

The second MMP model was based on a slightly modified version of MMP that was proposed by Larminie [1992]. Larminie replaced the tire section height with diameter in the deflection ratio, and this change was proposed based on an evaluation of the effect that deflection has on tire contact length. He also adjusted the factor K to keep the modified MMP calculations in the same range of magnitudes as the original MMP formula since MMP is used directly for comparing vehicles. The MMP values for this model were calculated as shown below, where once again n was used instead of the constant 2 as described in the previous paragraph.

$$MMP_L = \frac{0.97\,K'\,GVW}{n\,m\,b^{0.85}\,d^{1.15}\,\sqrt{\delta/d}}$$

where for all-drive vehicles:

$$m = 2 \Rightarrow K' = 1.83$$
$$m = 3 \Rightarrow K' = 1.95$$
$$m = 4 \Rightarrow K' = 2.05$$
$$m = 5 \Rightarrow K' = 2.16$$

The VCI_1 data were plotted versus MMP_L, and once again a linear trend was apparent. Therefore, linear regression was used to develop a mathematical equation for predicting VCI_1 as a function of MMP_L. The resulting equation is shown below.

$$VCI_1 = 3.68 + 0.480\,MMP_L$$

The equation is plotted with the measured data in Figure 16. The figure shows that the trend is very linear and that MMP_L describes the VCI_1 performance data well. The figure also demonstrates that MMP_L describes the data in a fashion nearly identical to MMP_R.
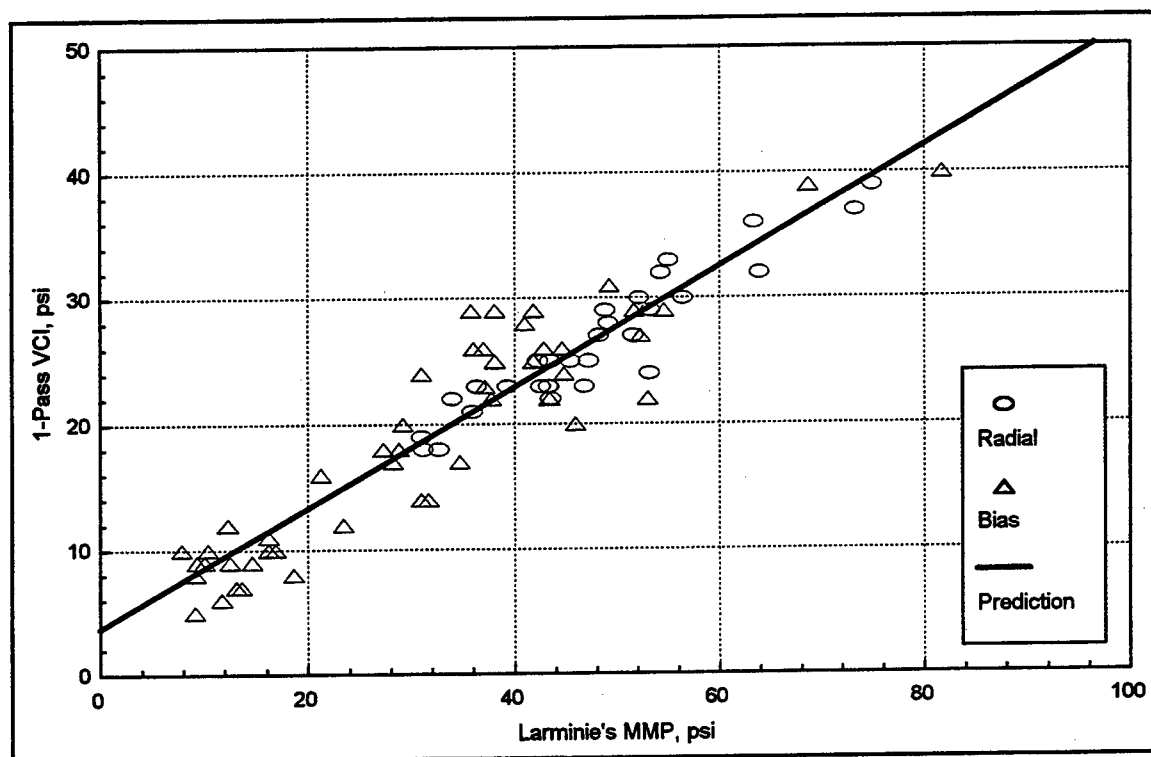
Figure 16. Relationship between Larminie's MMP and the VCI₁ data

The third version of MMP was based on the latest proposed version reported by

Maclaurin [1997]. Maclaurin proposed significant changes in the form and use of MMP. He

agreed with Larminie's recommendation that the diameter should be used instead of section

height in the deflection ratio, but he chose to mathematically combine the d from the δ/d ratio

with the other d in MMP such that the deflection ratio is no longer shown. He did not

recommend any changes be made to the K factor, instead recommending it be removed from

consideration. The proposed new MMP formula was derived from the results of recent

drawbar experiments conducted by the Defense Evaluation and Research Agency (DERA)

with a field deployable, computer controlled, single-wheel tire tester. The MMP values for

this model were calculated as shown below, where like the previous two versions, n was used

instead of the constant 2.

$$MMP_M = \frac{GVW}{n\,m\,b^{0.8}\,d^{0.8}\,\delta^{0.4}}$$

The VCI_1 data were plotted versus MMP_M, and once again a linear trend was apparent.

Therefore, linear regression was used to develop a mathematical equation for predicting VCI_1

as a function of MMP_M. The resulting equation is shown below.

$$VCI_1 = 2.53 + 1.35\,MMP_M$$

The equation is plotted with the measured data in Figure 17. The figure shows that the trend

is very linear and that MMP_M describes the VCI_1 performance data reasonably well.
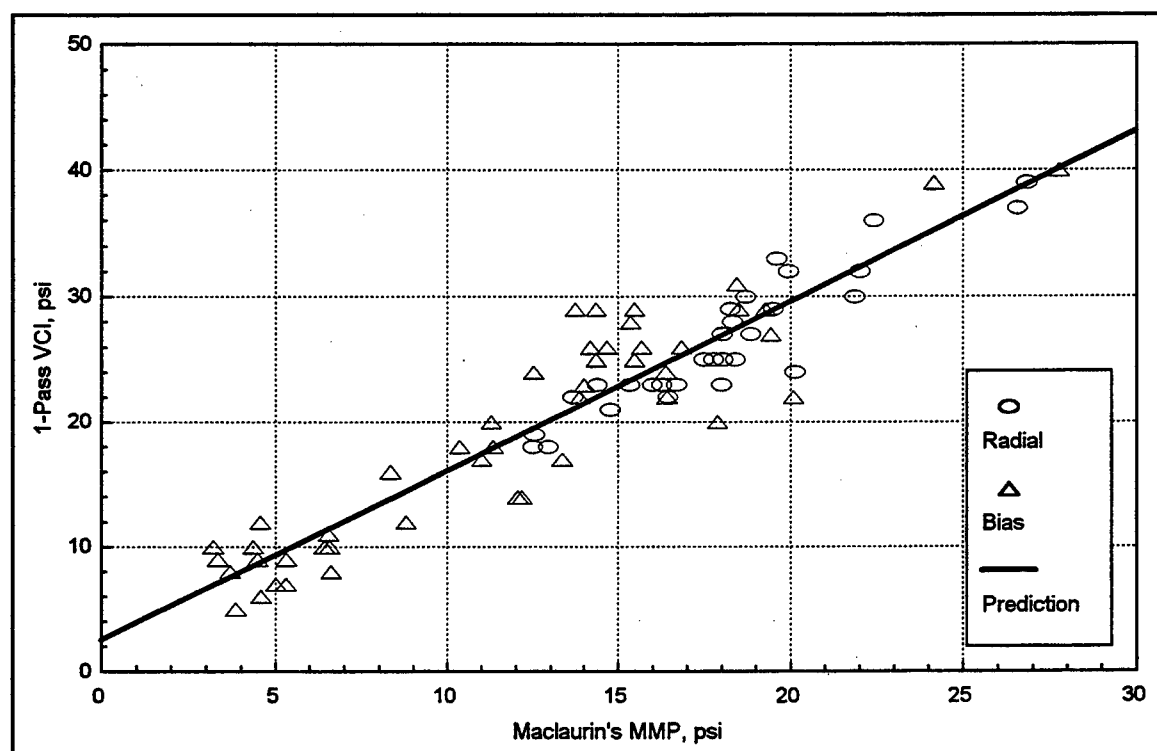
Figure 17. Relationship between Maclaurin's MMP and the VCI_1 data

As mentioned earlier, the original MMP was actually a recast and slightly altered form of Freitag's Numeric for tires in clay soils. Therefore, Freitag's Numeric ($N_{c(F)}$) was recast in a VCI form and evaluated as a predictor for VCI_1. This model was evaluated primarily to see how it compared with the three MMP models. Freitag's Numeric is calculated as shown.

$$N_{c(F)} = \frac{RCI\,n\,b\,d}{w}\left(\frac{\delta}{h}\right)^{1/2}$$

Recasting the numeric in a VCI form simply involved removing the soil strength (i.e., RCI), since predicting a soil strength was the new goal, and inverting the formula so that it would be in units of pressure. This was the same approach Rowland took in developing the original MMP. The recast form is shown below.

$$N_{c(F)}^{VCI} = \frac{w}{n\,b\,d\,\sqrt{\delta/h}}$$

The VCI_1 data were plotted versus $N_{c(F)}^{VCI}$ and, like the MMP models, the relationship was linear. Therefore, linear regression was used to develop a mathematical equation for predicting VCI_1, and the resulting equation is shown below.

$$VCI_1 = 2.99 + 1.58\,N_{c(F)}^{VCI}$$

The equation is plotted with the measured data in Figure 18. The figure shows that the trend is very linear and, just as expected, Freitag's Numeric describes the VCI_1 data well.
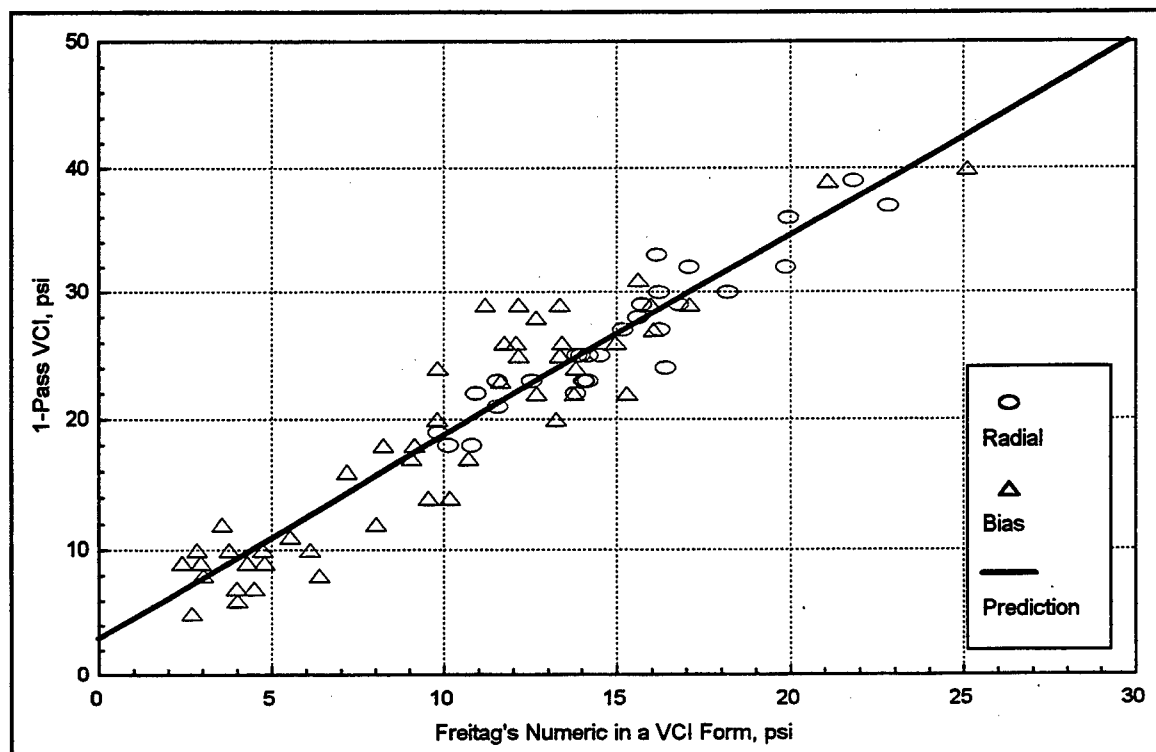
Figure 18. Relationship between Freitag's Numeric and the VCI_1 data

New Development Models

As stated, seven major types of new development models were explored. These included six different types of contact pressure models and a numeric-type model. Only two of the contact pressure models and the numeric-type model will be discussed, and only the best variants of those three will be presented. Before the individual models are addressed, clarification is provided on what is meant by 'contact pressure model' and 'numeric-type model' and explanations are given as to why these types of models were the focus in the VCI_1 modeling.

Contact pressure models are founded on the theory that bearing capacity is the controlling factor in soil response at VCI_1 and that the contact pressure imposed by the

vehicle on the soil drives the response. These models use logical, though possibly simplistic, derivations of average contact area (and hence pressure) at the vehicle/terrain interface. Different ideas and levels of complexity can be used in estimating average contact area, and hence several types of contact pressure models were explored. In actuality, the parameters developed for the contact pressure models during this research do not attempt to calculate the true contact area for tires in soil. Instead, they attempt to cast the principal tire dimensions into mathematical forms that give logical consideration to the influence of the tire dimensions on the true contact area. This approach should result in parameters that are highly correlated with the true contact area and, if the theory is correct, VCI_1 performance.

Numeric-type models are purely empirical with no pre-consideration of the controlling mechanism. Rather than using a logical derivation from a consideration of the influence that tire dimensions have on contact area, they allow the data to completely define the form of the principal parameter. They are loosely founded on the ideas of dimensional analysis and similitude. The approach with numeric-type models is to develop a single, simple parameter that casts the principal tire dimensions into a mathematical form which forces the units to work out correctly while producing the strongest possible correlation with the performance metric.

The focus for the new development models was placed on contact pressure and numeric-type models partly because of the potential that was demonstrated by the existing MMP formulas. The existing MMP formulas were developed using numeric-type models, and their intent was to predict contact pressure. Another reason these types of models were the focus arose from a consideration of what VCI_1 physically represents. VCI_1 is a zone of soil consistency where typical vehicles incur high sinkage and verge on dragging the

undercarriage, which makes it natural to infer that bearing capacity is the controlling factor in the soil response, greatly outweighing traction. It is probable that every researcher who has ever delved into trafficability research has intuitively thought that contact pressure was the dominant factor from the vehicle (i.e., loading) side of the VCI_1 problem.

The first new development model is a contact pressure model. It uses an average contact pressure parameter referred to as CP1 for the principal modeling parameter. CP1 is defined in general terms based on the width (W_{CA}) and length (L_{CA}) of the effective contact area under the tires as shown below.

$$CP1 = \frac{w}{n\,W_{CA}\,L_{CA}}$$

The basic logic behind CP1 is illustrated graphically in Figure 19. It was hypothesized that the effective contact width remains essentially constant and can be represented by the nominal section width of the tire. It was also hypothesized, as illustrated in Figure 19a, that each of the axles has an effective contact length (L_δ) under the tires that originates from hard-surface deflection and that the first axle, which is incurring the majority of the motion resistance, has additional contact length (L_z) along the front edge of the tires due to sinkage. These hypotheses resulted in CP1 being defined as shown below.

$$W_{CA} = b \quad and \quad L_{CA} = L_\delta + 1/m\,L_z$$

$$\Rightarrow \quad CP1 = \frac{w}{n\,b\,(L_\delta + 1/m\,L_z)}$$

a. Distribution of effective contact length along the axles of the vehicle

b. Geometry for the effective contact length under the tires
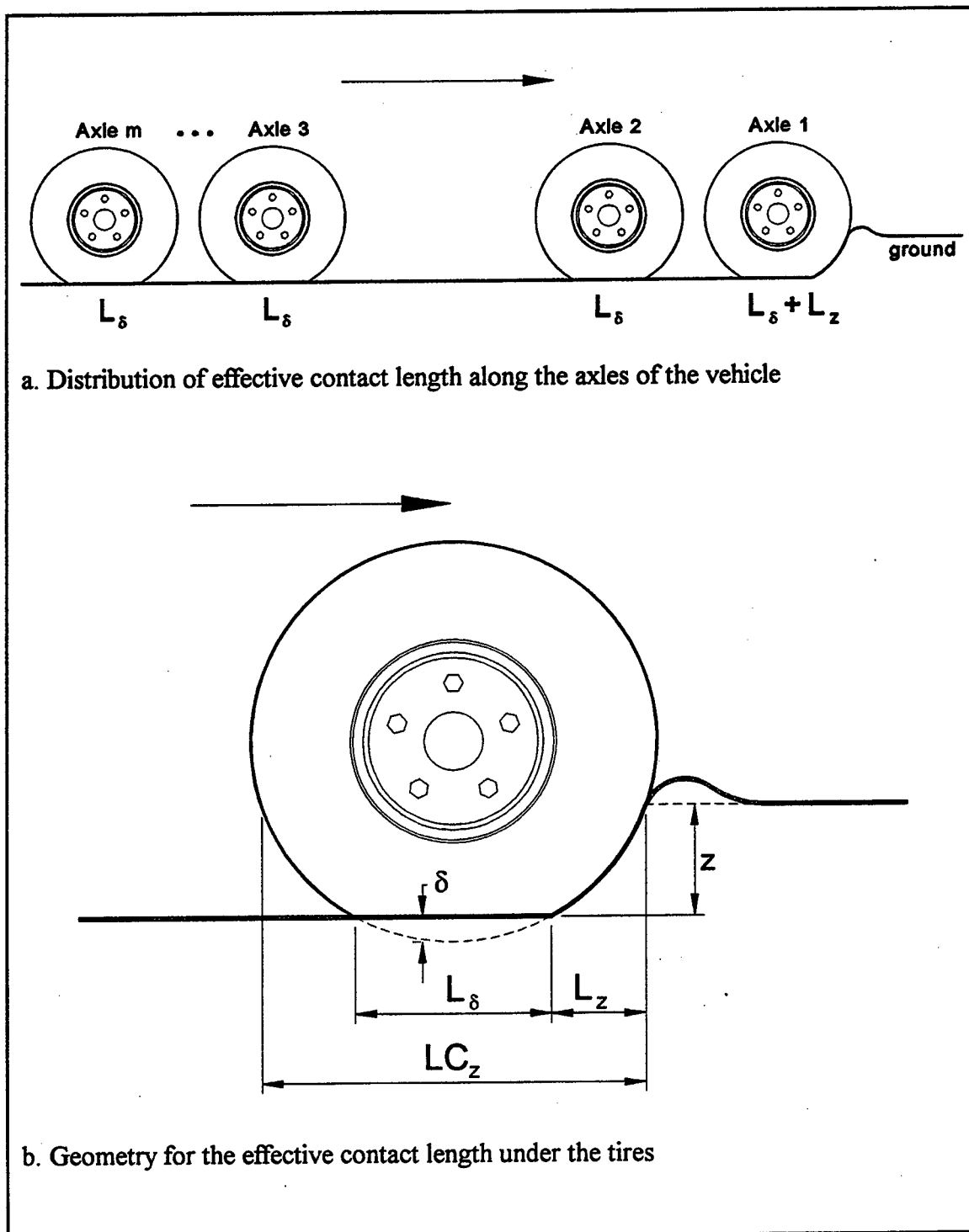
Figure 19. Basic logic behind the average contact pressure parameter CP1

Figure 19b shows the effective geometry used to mathematically describe the two contact lengths L_δ and L_z. Applying the long chord analogy resulted in the two contact lengths being defined as shown below.

$$LC = 2\sqrt{\varnothing M - \dot{M}^2}$$

$$L_\delta = LC_\delta \quad \Rightarrow \quad L_\delta = 2\sqrt{d\delta - \delta^2}$$

$$L_z = \tfrac{1}{2}\left[LC_z - L_\delta\right]$$

$$\Rightarrow \quad L_z = \tfrac{1}{2}LC_z - \sqrt{d\delta - \delta^2}$$

$$where \quad \begin{cases} z < \dfrac{d}{2} - \delta \quad \Rightarrow \quad LC_z = 2\sqrt{d(\delta + z) - (\delta + z)^2} \\[2ex] z \geq \dfrac{d}{2} - \delta \quad \Rightarrow \quad LC_z = d \end{cases}$$

Once the basic mathematical form of the CP1 parameter had been established, a x-y plot of VCI_1 versus CP1 was generated using the observations from the VCI_1 database, where clearance height (h_c) was used as the estimate for z. The plot showed that a linear relationship existed and that CP1 had good potential for describing VCI_1. Then an intensive effort was conducted in which empirical improvements for CP1 were explored through the development of model variants. Many different ideas were explored in the model variants which included using empirical multipliers within the CP1 parameter to modify the influence of the individual parts of the L_{CA} estimate, adding secondary parameters to the linear relationship between VCI_1 and CP1, using other estimates (besides h_c) for z, and others. A major source of ideas for the model variants came from the existing VCI_1 models described in the last section. This effort produced significant improvements to the relationship.

The best model variant used h_c as the estimate for z, had two empirical modifications within the CP1 parameter, and included a secondary parameter in the relationship. The first modification reduced the influence of L_z by multiplying a constant (c_1) times the $\frac{1}{2}LC_z$ part of the L_z calculation. The second modification involved an adjustment to the effective contact area by multiplying aspect ratio raised to a power (p_1) in the denominator of the CP1 formula. The secondary parameter included in the relationship was a simple tire construction factor (TCF) that accounted for the possibility of a difference in performance between radial and bias ply tires. The form of the best CP1 model variant is shown below.

$$VCI_1 = \beta_0 + \beta_1 CPI'_{19} + \beta_2 TCF$$

$$CPI'_{19} = \frac{w}{n b \left[2\sqrt{d\delta - \delta^2} + 1/m \left(c_1 \frac{1}{2} LC_z - \sqrt{d\delta - \delta^2} \right) \right] (h/b)^{p_1}}$$

$$\text{where} \quad h_c < \frac{d}{2} - \delta \quad \Rightarrow \quad LC_z = 2\sqrt{d(\delta + h_c) - (\delta + h_c)^2}$$

$$h_c \geq \frac{d}{2} - \delta \quad \Rightarrow \quad LC_z = d$$

$$TCF = c_{TCF} \quad \text{where} \quad c_{TCF} = 0 \text{ if radial or 1 if bias ply}$$

The combined linear regression and numerical optimization process was used to determine the empirical constants in the relationship. The process resulted in c_1 being 0.74 and p_1 being -0.47. The resulting final equations are shown below where c_1 has been combined with the $\frac{1}{2}$ in $\frac{1}{2}LC_z$ and the aspect ratio has been inverted for a positive exponent.

$$CPI'_{19} = \frac{w}{n b \left[2\sqrt{d\delta - \delta^2} + 1/m \left(0.37 LC_z - \sqrt{d\delta - \delta^2} \right) \right] (b/h)^{0.47}}$$

$$VCI_1 = 2.88 + 1.78 CPI'_{19} + 1.58 TCF$$

CPl'_{19} and *TCF* were calculated for each of the observations in the VCI$_1$ database, and the data were plotted with the equation describing the relationship on a x-y plot as shown in Figure 20. Note that it was necessary to subtract 1.58 *TCF* from VCI$_1$ in order to generate the simple x-y plot. The figure shows that the measured VCI$_1$ data are described very well by the best CP1 relationship.

Figure 20. Best CP1 relationship for VCI$_1$

The second new development model is also a contact pressure model. It uses an average contact pressure parameter referred to as CP2 for the principal modeling parameter.

CP2, like CP1, is defined in general terms based on the width (W_{CA}) and length (L_{CA}) of the effective contact area under the tires as shown below.

$$CP2 = \frac{w}{n\,W_{CA}\,L_{CA}}$$

The basic logic behind CP2 is illustrated graphically in Figure 21. It was hypothesized, once again, that the effective contact width remains essentially constant and can be represented by the nominal section width of the tire. It was also hypothesized, as illustrated in Figure 21a, that all of the axles have an effective contact length ($L_{\delta+c}$) under the tires that originates from hard-surface deflection plus an empirical correction variable (c). These hypotheses resulted in CP2 being defined as shown below.

$$W_{CA} = b \quad and \quad L_{CA} = L_{\delta+c}$$

$$\Rightarrow \quad CP2 = \frac{w}{n\,b\,L_{\delta+c}}$$

Figure 21b shows the effective geometry used to mathematically describe the contact length $L_{\delta+c}$. Applying the long chord analogy resulted in $L_{\delta+c}$ being defined as shown below.

$$LC = 2\sqrt{\varnothing M - M^2}$$

$$L_{\delta+c} = LC_{\delta+c} \quad \Rightarrow \quad L_{\delta+c} = 2\sqrt{d(\delta+c) - (\delta+c)^2}$$

Once the basic mathematical form of the CP2 parameter had been established, a couple of model variants were developed. The best variant used an empirical constant (c_1) times tire diameter as the estimate for c and used the best empirical adjustments that were found during the effort to empirically improve CP1. The empirical adjustments were: (1) aspect ratio raised to a power (p_1) which was used as an adjustment to the effective contact

a. Distribution of effective contact length along the axles of the vehicle

b. Geometry for the effective contact length under the tires
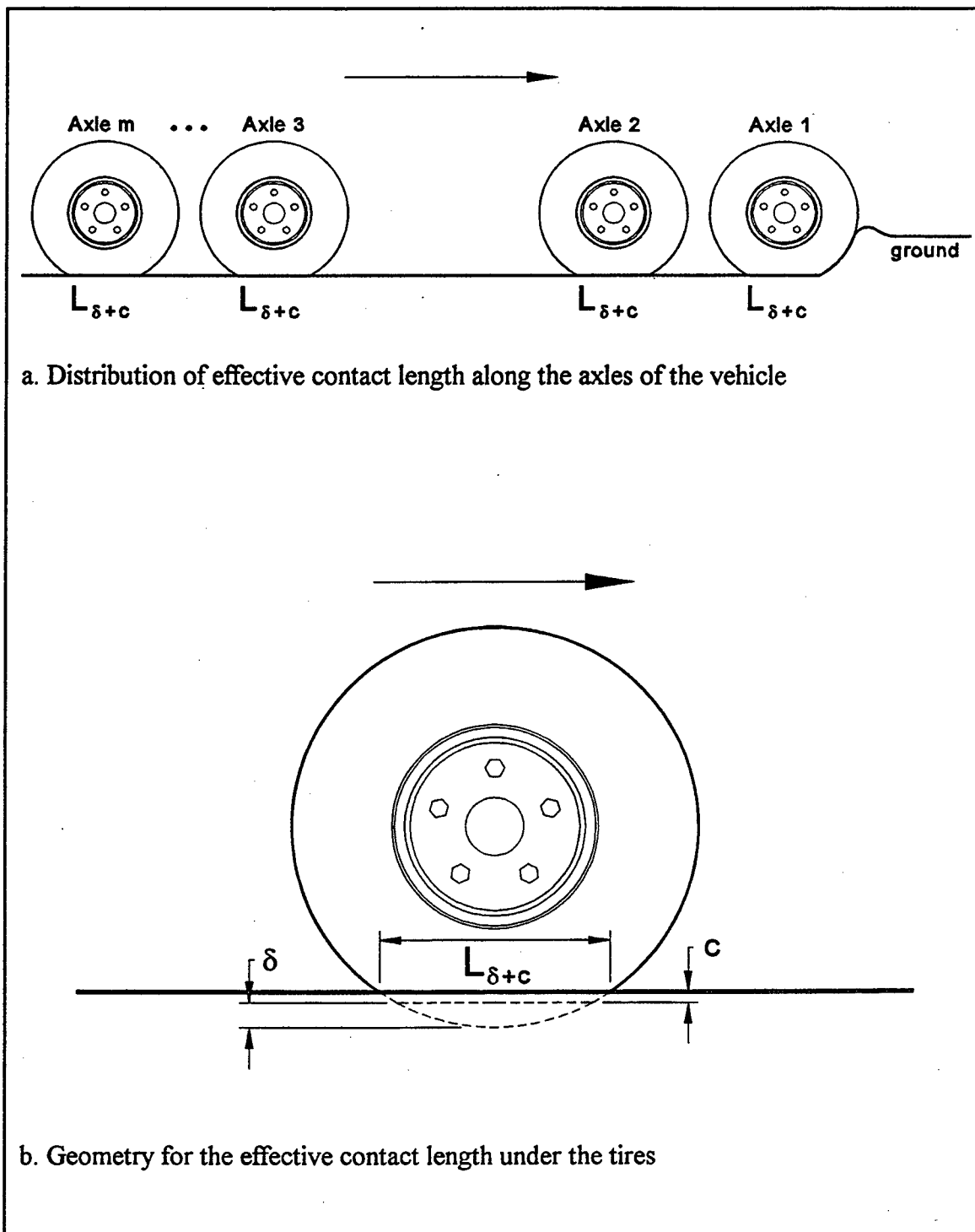
Figure 21. Basic logic behind the average contact pressure parameter CP2

area in the denominator of CP2 and (2) TCF which was used as a secondary parameter in the relationship between VCI_1 and CP2 to account for performance differences between radial and bias ply tires. The many other empirical adjustments that were evaluated for CP1 were not re-evaluated for CP2 because their influence on CP2 would have been very similar to their influence on CP1. The form of the final CP2 model variant is shown below.

$$VCI_1 = \beta_0 + \beta_1 CP2_1' + \beta_2 TCF$$

$$CP2_1' = \frac{w}{2\,n\,b\,\sqrt{d(\delta + c_1 d) - (\delta + c_1 d)^2}\,(h/b)^{P_1}}$$

$$TCF = c_{TCF} \quad \text{where } c_{TCF} = 0 \text{ if radial or } 1 \text{ if bias ply}$$

The combined linear regression and numerical optimization process was used to determine the empirical constants in the relationship. The process resulted in c_1 being 0.026 and p_1 being -0.52. The resulting final equations are shown below where the aspect ratio has been inverted for a positive exponent.

$$CP2_1' = \frac{w}{2\,n\,b\,\sqrt{d(\delta + 0.026\,d) - (\delta + 0.026\,d)^2}\,(b/h)^{0.52}}$$

$$VCI_1 = 1.95 + 2.03\,CP2_1' + 1.95\,TCF$$

$CP2_1'$ and TCF were calculated for each of the observations in the VCI_1 database, and the data were plotted with the equation describing the relationship on a x-y plot as shown in Figure 22. Note that it was necessary to subtract 1.95 TCF from VCI_1 in order to generate the simple x-y plot. The figure shows that the measured VCI_1 data are described very well by the best CP2 relationship.
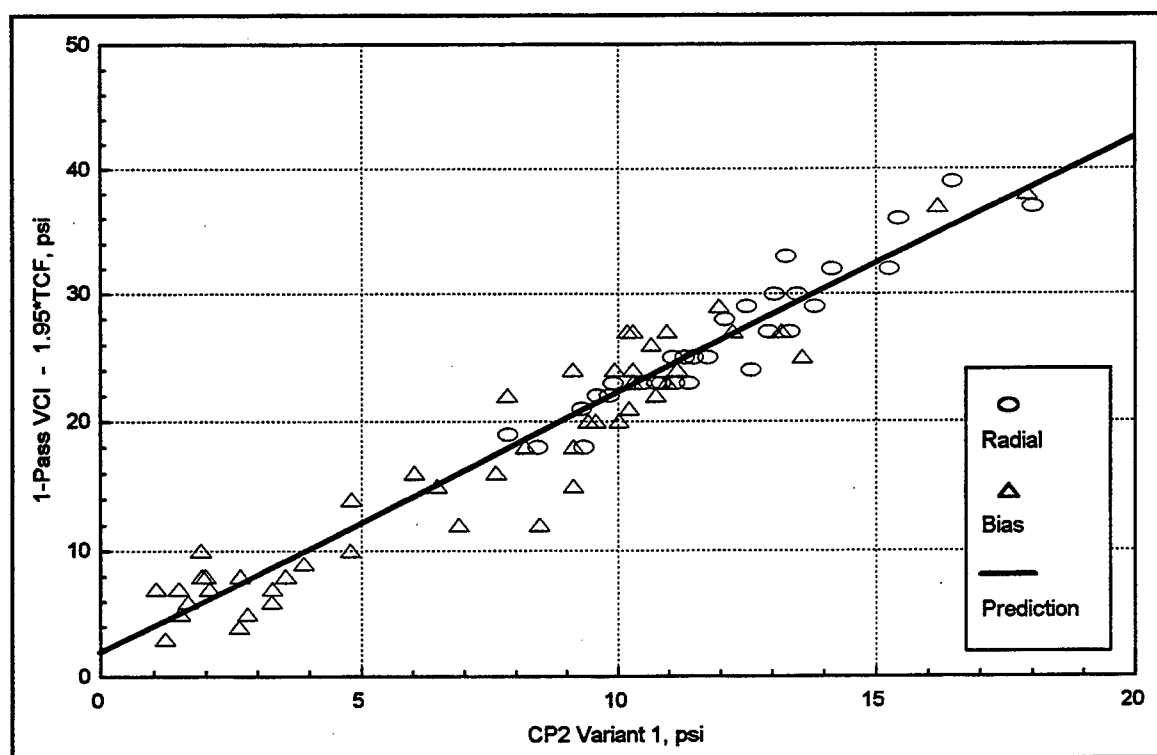
Figure 22. Best CP2 relationship for VCI₁

The last new development model is a numeric-type model. As previously stated, a numeric-type model allows the data to completely define the form of a simple, principal parameter (referred to as a numeric) under the constraint that the units must be correct. The VCI_1 performance metric has pressure units (i.e., force/length^2). Therefore, the numeric parameter was forced to also have pressure units. Several approaches were used for developing the numeric-type models, but only the approach used in developing the best numeric variant will be described.

In developing the best VCI_1 numeric variant, w/n was the obvious choice for including the force units. The approach taken to include the length^2 units was to use a product of b, d, and three dimensionless tire ratios where each ratio was raised to a power (p_1, p_2, and

p_3). The ratios chosen used d as the characteristic length in dimensionless ratios with each of b, h, and δ so that all four of the tire shape dimensions could be included in the final numeric. Three ratios (i.e., powers) were used because there were four length variables less one constraint. This modeling approach allowed the inclusion of b, d, h, and δ in the final numeric with each raised to its own numerically optimized power under the constraint that the summation of the four powers must equal two.

Once the basic mathematical form of the numeric was decided, a statistical model was used to develop the relationship between VCI_1 and the numeric. A linear equation was used due to the linear behavior demonstrated in the MMP models and the two average contact pressure models. Also, due to its demonstrated benefit in the average contact pressure models, TCF was used as a secondary parameter in the relationship to account for perform-ance differences between radial and bias ply tires. The form of the final numeric-type model is shown below.

$$VCI_1 = \beta_0 + \beta_1 N_{3b} + \beta_2 TCF$$

$$N_{3b} = \frac{w}{n\, b\, d\, (b/d)^{P_1}\, (d/h)^{P_2}\, (\delta/d)^{P_3}}$$

$$TCF = c_{TCF} \quad where \ c_{TCF} = 0 \ if \ radial \ or \ 1 \ if \ bias \ ply$$

The combined linear regression and numerical optimization process was used to determine the empirical constants in the relationship. The process resulted in p_1 being 0.42, p_2 being

0.66, and p_3 being 0.32. The resulting final equations are shown below where the numeric has been simplified by collapsing the ratios and collecting like terms.

$$N_{3b} = \frac{w\,h^{0.66}}{n\,b^{1.42}\,d^{0.92}\,\delta^{0.32}}$$

$$VCI_1 = 1.56 + 2.03\,N_{3b} + 2.03\,TCF$$

N_{3b} and TCF were calculated for each observation in the VCI_1 database, and the data were plotted with the equation describing the relationship on a x-y plot as shown in Figure 23. Note that it was necessary to subtract 2.03 TCF from VCI_1 in order to generate the simple x-y plot. The figure shows that the measured VCI_1 data are described very well by the best numeric relationship.
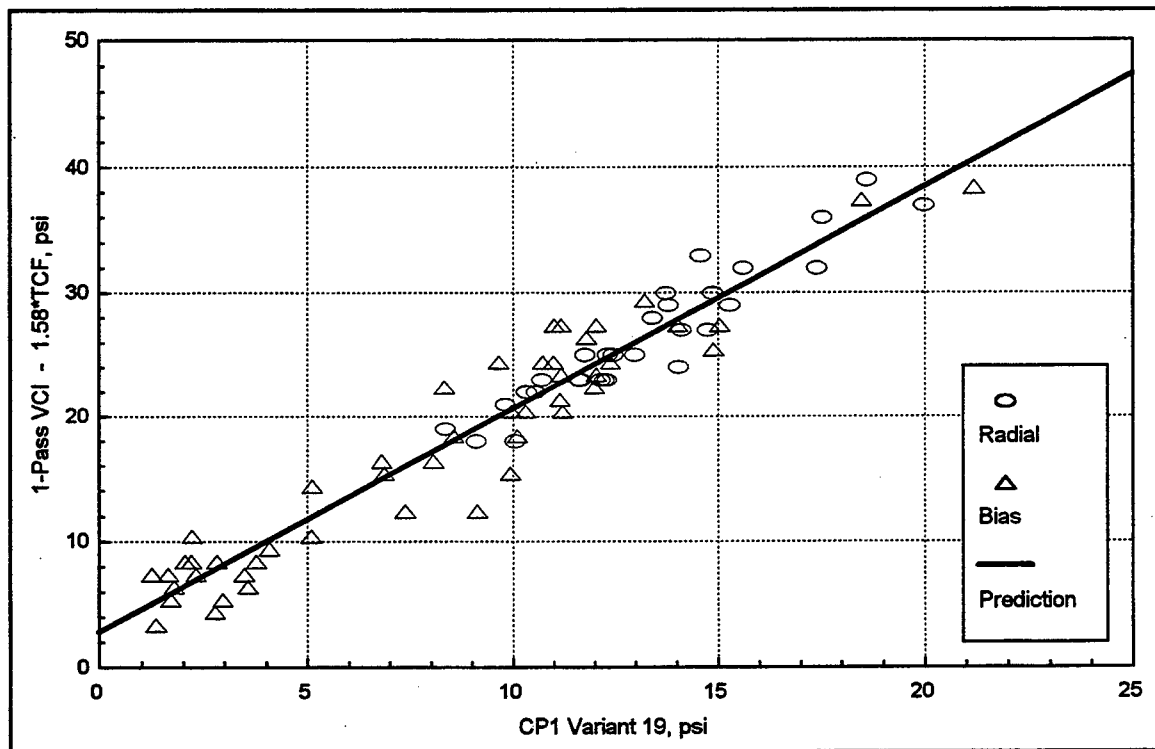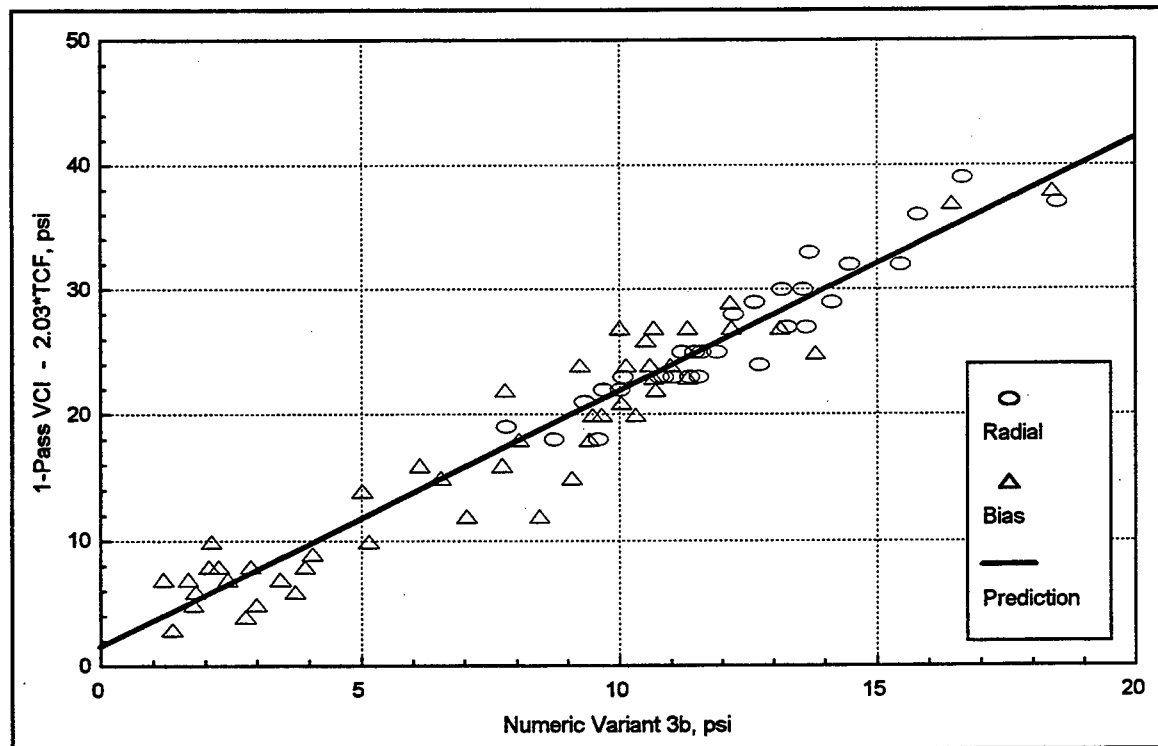

Figure 23. Best numeric relationship for VCI_1

Model Comparisons

Several existing and new VCI_1 relationships were presented in the preceding sections of this chapter, and a simple x-y plot of each relationship was shown. The x-y plots allowed a visual interpretation of the quality with which each relationship described the measured data, but higher accuracy methods of assessing quality were necessary to make sound comparisons between the relationships. For this purpose, the standard error (S_e) and adjusted coefficient of determination (Adj. R^2) measures of quality were used. These quality measures were determined during the development of each of the many model variants, and they were used as optimization targets in models that required numerical optimization as previously explained in Chapter III. Table 4 lists these measures along with their associated degrees of freedom for each of the relationships.

Several comparisons can be made using Table 4. First, the table demonstrates that the optimized NRMM relationship described the data significantly better (i.e., lower S_e and higher R^2) than the standard NRMM relationship[3]. The table also demonstrates that Rowland's original version of MMP described the data better than both Larminie's and Maclaurin's versions, but Freitag's numeric (from which MMP originated) described the data better than any of the three. In terms of the new relationships, the best CP2 relationship described the data slightly better than the best CP1 relationship, and the best numeric relationship ranked a close third. Most significantly, the table demonstrates that all three of

---

[3] - The degrees of freedom for the NRMM relationships were not the same for all of the observations because the weight factor equations had either one or two empirical constants and because the two equations describing the relationship between VCI_1/DCF and MI had either two or four empirical constants. This situation resulted in there being four possible values for the degrees of freedom associated with each individual observation.

the new relationships describe the data better than any of the existing relationships, with only the newly optimized NRMM relationship coming anywhere close to the quality of the new relationships. These results indicate that it is definitely feasible to develop new VCI_1 relationships that meet the decision criteria stated in the objectives for this research. The results also indicate that contact pressure under the vehicle is the driving factor in VCI_1 performance.

Table 4. Quality comparison for the VCI_1 modeling results

Relationship	Degrees of Freedom	Standard Error (psi)	Adjusted R-squared
Standard NRMM (MI&DCF)	70, 69, 68, or 67	2.68	90.3
Optimized NRMM	70, 69, 68, or 67	2.44	91.9
Rowland's MMP	73	2.91	88.5
Larminie's MMP	73	2.96	88.1
Maclaurin's MMP	74	3.01	87.7
Freitag's Numeric in a VCI_1 Form	76	2.82	89.2
Best CP1 Variant	74	2.39	92.2
Best CP2 Variant	74	2.37	92.4
Best Numeric Variant for VCI_1	73	2.40	92.2

One other major comparison was made from the results of the VCI_1 modeling. This comparison involved the best CP2 and numeric relationships. It was noted that the coefficients on $CP2_1'$ and N_{3b} were both equal to 2.03 and that the coefficient on TCF in both

relationships was essentially equal to two. This observation prompted a closer look at the similarities between $CP2_1'$ and N_{3b}. Table 5 shows a comparison between the exponents (or powers) in these two parameters, and it indicates that the two parameters are very similar in form. Figure 24 shows a x-y plot of N_{3b} versus $CP2_1'$, and it indicates that the two parameters are essentially identical in terms of their calculated magnitudes for each of the observations in the VCI_1 database.

Table 5. Comparison of exponents between best CP2 and Numeric relationships

Relationship	Exponents in Principal Parameter [a]			
	d	b	h	δ
Best CP2 Variant	1.00 [b]	1.52	0.52	0.50 [b]
Best Numeric Variant for VCI_1	0.92	1.42	0.66	0.32

[a] - d, b, and δ in the denominator; h in the numerator
[b] - approximate values

Two major conclusions can be drawn from this result. First, numeric-type relationships can be very useful in areas where little is understood about the controlling mechanism. Second, the measured VCI_1 data apparently cast N_{3b} into a form that is nearly identical to $CP2_1'$. Since N_{3b} had the flexibility to mold itself into the best possible form for describing the VCI_1 data, the fact that it molded itself into a form nearly identical to $CP2_1'$ provides even more confidence in the applicability of $CP2_1'$ for describing VCI_1 performance.
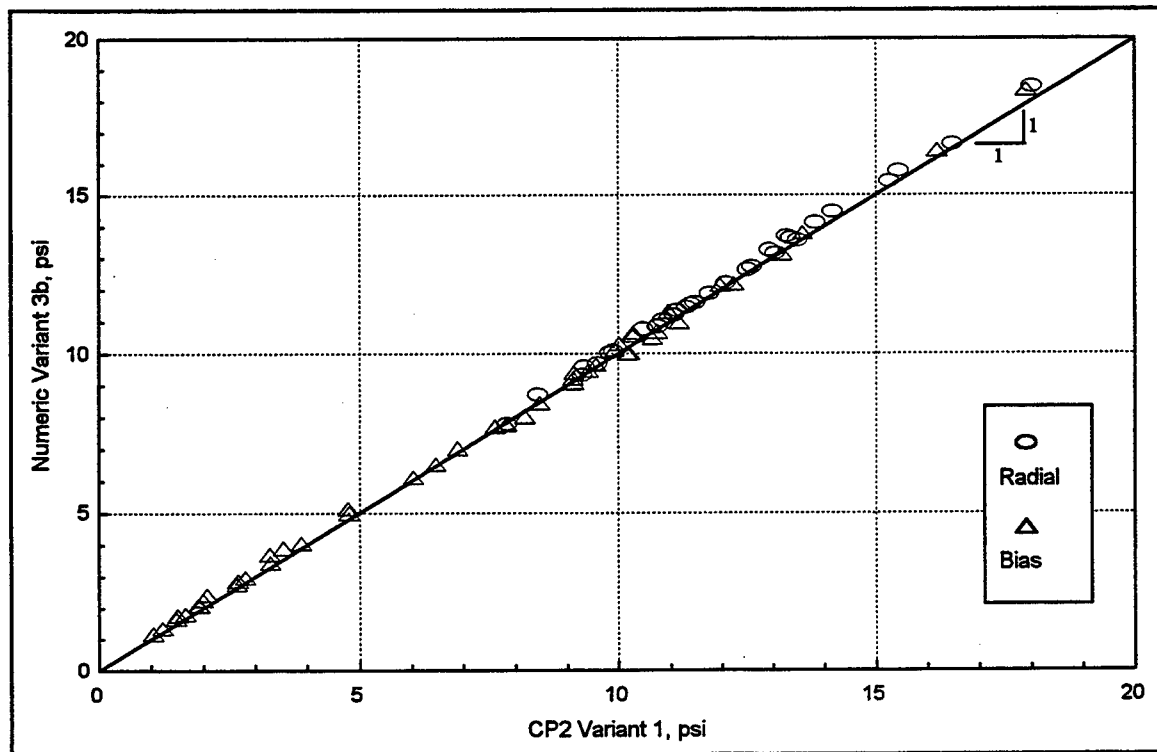
Figure 24. Similarity between best CP2 and Numeric parameters for VCI_1

CHAPTER V

DRAWBAR MODELING

Overview

The drawbar modeling consisted of two major areas of focus. The first focus was on evaluating existing relationships or parameters that use cone penetrometer-based soil measurements and relatively simple vehicle characteristics to determine drawbar performance potential in clay soils. Five existing models were investigated which included the current NRMM relationship and four existing drawbar numerics. The second focus was on the development of new relationships. Four major types of new models were developed which included a bearing ratio model, an excess bearing ratio model, an excess RCI ratio model, and a numeric-type model.

For all of the major types of new models that were developed, more than one variant was investigated. As in the VCI_1 modeling, the term variant is used here to describe a slight variation on the same basic modeling theme. Slight variations in the drawbar modeling included such things as: (1) using different estimates for contact pressure in the bearing ratio model and (2) using different combinations of four or less tire shape dimensions in the numeric-type model. Three variants of the bearing ratio model, four variants of the excess bearing ratio model, two variants of the excess RCI ratio model, and sixteen variants of the

numeric-type model were developed. Additionally, two model variants based on the standard NRMM relationship were investigated, the primary purpose being to optimize the current approach to the field drawbar database.

For the sake of clarity and concision, all of the individual model variants are not addressed. Only the five existing models and the best variants of the new development models are compared in the main text of this thesis. However, a listing of all the model variants explored and a table summarizing their quality are provided in Appendix C.

Existing Models

The standard NRMM relationship is based on a parameter called the excess soil strength (RCI_X). RCI_X was developed based on observations made by WES researchers during the 1960s [Priddy 1995]. During the early years of drawbar measurements, curves of drawbar versus soil strength (in RCI) were plotted for every vehicle configuration tested. Once several vehicle configurations had been tested over a fair range of soil strengths (usually VCI_1 to about 150 or 200 RCI), it was observed that drawbar versus RCI curves for vehicles with similar characteristics (e.g., wheeled or tracked) were very similar in shape and magnitude. This observation led to the realization that one prediction curve could be used to describe the performance of many vehicles with similar characteristics if the drawbar versus RCI curves for those vehicles were all plotted such that their zero drawbar points coincided. The zero drawbar points occur where the soil strength is equal to VCI_1, and relationships for predicting VCI_1 were already available. Therefore, the drawbar performance potential of many vehicles with widely varying VCI_1 values but similar basic characteristics could be

predicted using a single prediction curve by subtracting the predicted VCI_1 value for each vehicle from the actual RCI value as shown below.

$$RCI_X = RCI - VCI_1$$

As explained in Chapter I, the standard NRMM relationship for drawbar performance of wheeled vehicles on CH soils separates vehicles into two prediction categories: vehicles with CPF ≥ 4 psi and vehicles with CPF < 4 psi. The NRMM relationship was based on drawbar performance at 20 percent slip until the early 1990s, but it is now based on drawbar performance at 100 percent slip. This research concentrates on 20 percent slip performance for reasons explained in Chapter II. Therefore, the relationship shown below, which is based on standard NRMM logic explained by Priddy [1995], was used to translate the standard NRMM relationship from 100 percent slip to 20 percent slip performance magnitude.

$$\frac{D^{RCI}}{W}_{20} = \frac{D^{RCI}}{W}_{100} + \left(\frac{D^{"Max"}}{W}_{20} - \frac{D^{"Max"}}{W}_{100} \right)$$

The three drawbar coefficients on the right-hand side of the above equation can be determined from standard NRMM relationships, and the equations used to describe these relationships are shown below [Priddy 1995] (note that the new prediction curves proposed in the referenced report are now standard for NRMM).

$CPF \geq 4\,psi$	$CPF < 4\,psi$
$\dfrac{D^{RCI}}{W}_{100} = 0.7616 - \dfrac{6.322}{RCI_X + 7.614}$	$\dfrac{D^{RCI}}{W}_{100} = 0.7826 - \dfrac{5.804}{RCI_X + 6.799}$
$\dfrac{D^{"Max"}}{W}_{Slip} = 0.7764 - \dfrac{0.04858}{\frac{Slip(\%)}{100} + 0.06025}$	$\dfrac{D^{"Max"}}{W}_{Slip} = 0.7675 - \dfrac{0.03184}{\frac{Slip(\%)}{100} + 0.03508}$

The standard NRMM relationship translated to 20 percent slip performance magnitude, which resulted from consideration of the equations just mentioned, is shown below.

$$\frac{D^{RCI}}{W}_{20} = f(RCI_X)$$

$$where \begin{cases} CPF \geq 4\,psi \quad \Rightarrow \quad \frac{D^{RCI}}{W}_{20} = 0.621 - \frac{6.32}{RCI_X + 7.61} \\ \\ CPF < 4\,psi \quad \Rightarrow \quad \frac{D^{RCI}}{W}_{20} = 0.678 - \frac{5.80}{RCI_X + 6.80} \end{cases}$$

RCI_X was calculated for each of the observations in the field drawbar database. The best CP2 relationship, which was demonstrated in Chapter IV as the best overall relationship for VCI_1, was used to predict VCI_1 in the RCI_X calculations. The data were plotted with the standard NRMM equations (translated to 20 percent slip) on a x-y plot as shown in Figure 25. The figure shows that the data are described fairly well by the standard NRMM relationship, but there is a large amount of scatter and the data are not distributed very well throughout the RCI_X range, a lot of the data being clustered at about 270 RCI_X.

The standard NRMM relationship was developed using only part of the data in the field drawbar database. New relationships developed using all of the data would have an immediate advantage over the NRMM relationship since their empirical constants would be optimized to the data. Also, the relationship had to be translated from 100 percent slip to 20 percent slip performance magnitude as previously described. These facts meant that fair comparisons between the standard NRMM relationship and any of the other relationships evaluated during this research could only be made if the NRMM relationship was optimized to the complete data set. Therefore a modified version of the NRMM relationship was

developed that optimized the empirical constants in the prediction equations for drawbar as a function of RCI_X. The combined linear regression and numerical optimization process was used to determine the empirical constants in the equations (i.e., curve-fits), and the resulting optimized NRMM relationship is shown below.

$$\frac{D^{RCI}}{W_{20}} = f(RCI_X)$$

$$where \begin{cases} CPF \geq 4\,psi & \Rightarrow & \frac{D^{RCI}}{W_{20}} = 0.63 - \frac{5.14}{RCI_X + 8.16} \\ \\ CPF < 4\,psi & \Rightarrow & \frac{D^{RCI}}{W_{20}} = 0.81 - \frac{17.8}{RCI_X + 22.0} \end{cases}$$
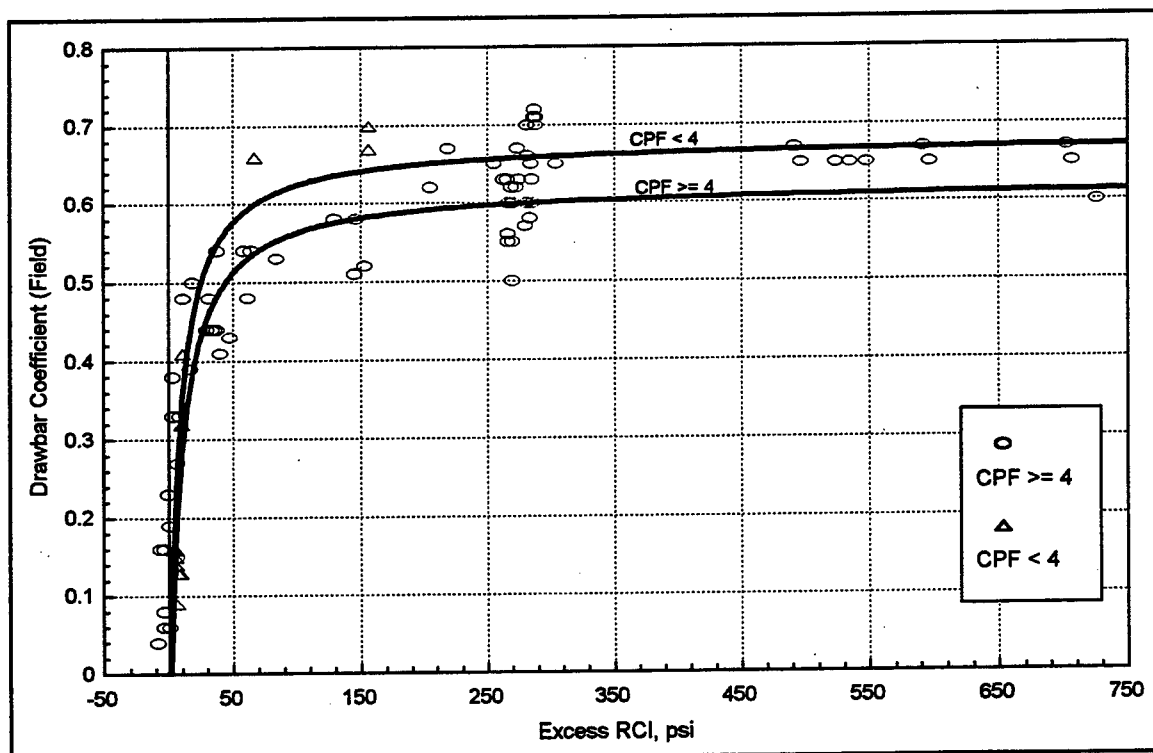
Figure 25. Standard NRMM relationship for drawbar

The field drawbar data were plotted with the optimized NRMM equations on a x-y plot as shown in Figure 26. The figure demonstrates that the new optimized curve-fits describe the field drawbar data better than the standard curve-fits, especially for the data with CPF less than 4 psi. It is emphasized that the optimized curve-fit for CPF less than 4 psi is not recommended for use beyond this study because, as the figure shows, there are only three observations in the high drawbar range and no observations beyond an RCI_x of 160.
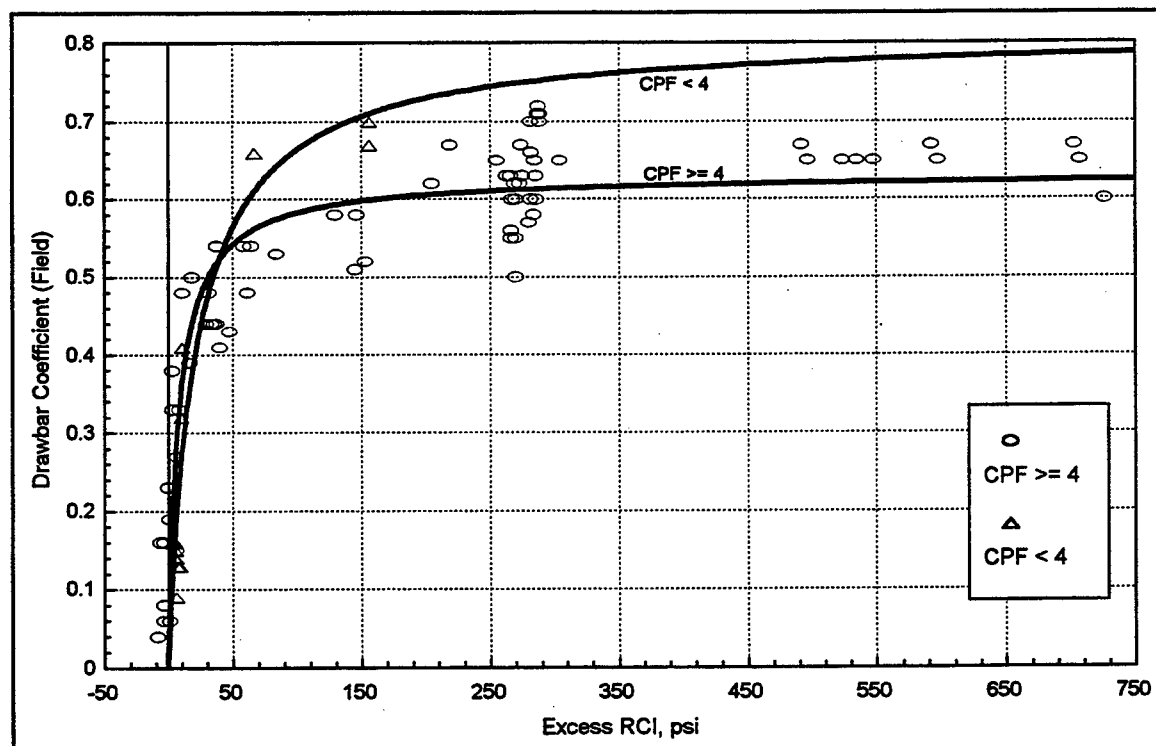
Figure 26. Optimized NRMM relationship for drawbar

The other four existing models for drawbar are all based on existing numerics. The first three numerics, which were developed by WES, were founded on the dimensional analysis research conducted by Freitag [1965] that was described in Chapter I. Freitag used

the laboratory drawbar data described in Chapter II and his associated laboratory sinkage data to develop a numeric that related well to the motion resistance, sinkage, torque output and drawbar performances measured in his laboratory research. Although Freitag's numeric was developed from evaluation of laboratory performance measurements, it is not limited to laboratory use and was evaluated in this research as a parameter for describing field drawbar data. Freitag's numeric is calculated as shown below.

$$N_{c(F)} = \frac{RCI\,n\,b\,d}{w}\left(\frac{\delta}{h}\right)^{1/2}$$

The field drawbar data were plotted versus Freitag's numeric on a x-y plot, and the resulting trend was in a form that could be described well by the rectangular hyperbola equation. Therefore, the combined linear regression and numerical optimization process was used to develop a rectangular hyperbola equation for describing field drawbar performance as a function of $N_{c(F)}$. The resulting equation is shown below and is plotted with the field drawbar data in Figure 27.

$$\frac{D^{RCI}}{W}_{20} = 0.74 - \frac{3.6}{N_{c(F)} + 4.3}$$

The figure demonstrates that the trend is hyperbolic and that Freitag's numeric describes the field drawbar data reasonably well with the exception of the data having CPF less than 4 psi in the low drawbar range. The figure also demonstrates that there is a much better distribution of data throughout the full range for $N_{c(F)}$ than there was for RCI_X.
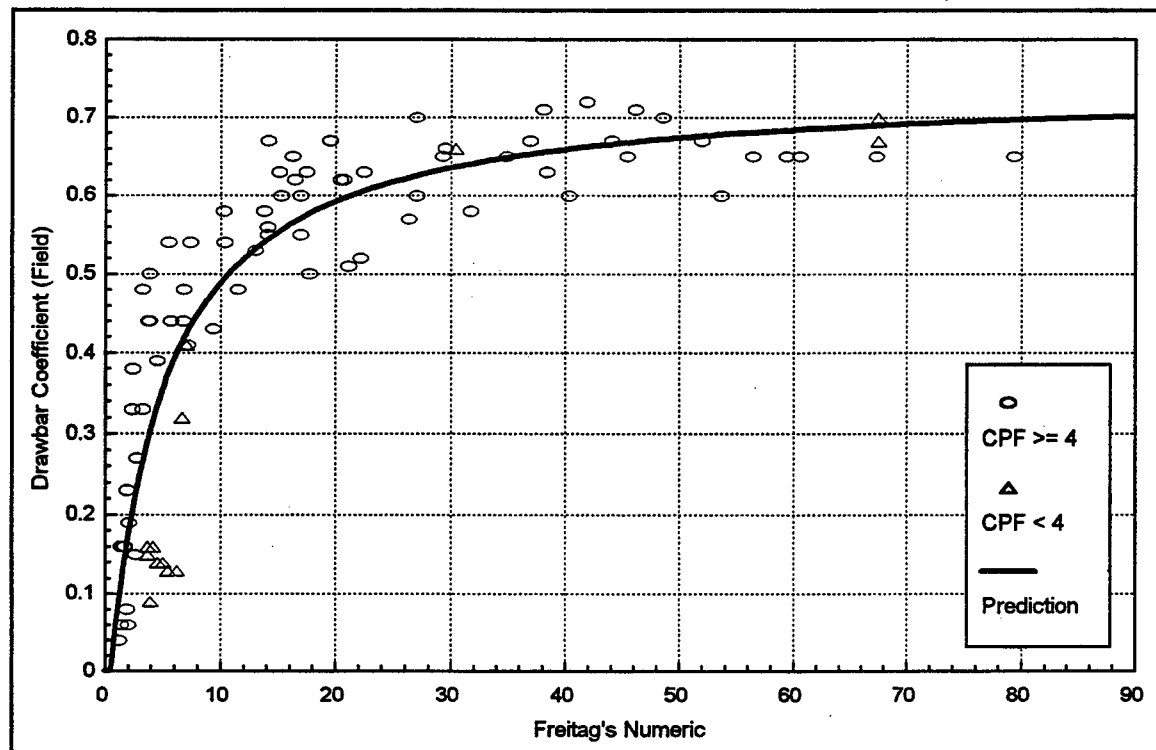
Figure 27. Relationship between Freitag's Numeric and the field drawbar data

The other two WES numerics involved modifications to Freitag's original numeric. Turnage [1972] showed that a modified form of Freitag's numeric described the laboratory performance of several tires with greatly varying shapes better than Freitag's numeric. Turnage's data included the four tires evaluated in Freitag's original research plus a few other tires with different shapes, and this larger mix of tire shapes led him to incorporate an additional consideration for the ratio of tire section width-to-diameter. Turnage's numeric is calculated as shown below.

$$N_{c(T)} = \frac{RCI\,n\,b\,d}{w}\left(\frac{\delta}{h}\right)^{1/2}\left(\frac{2d}{2d+b}\right)$$
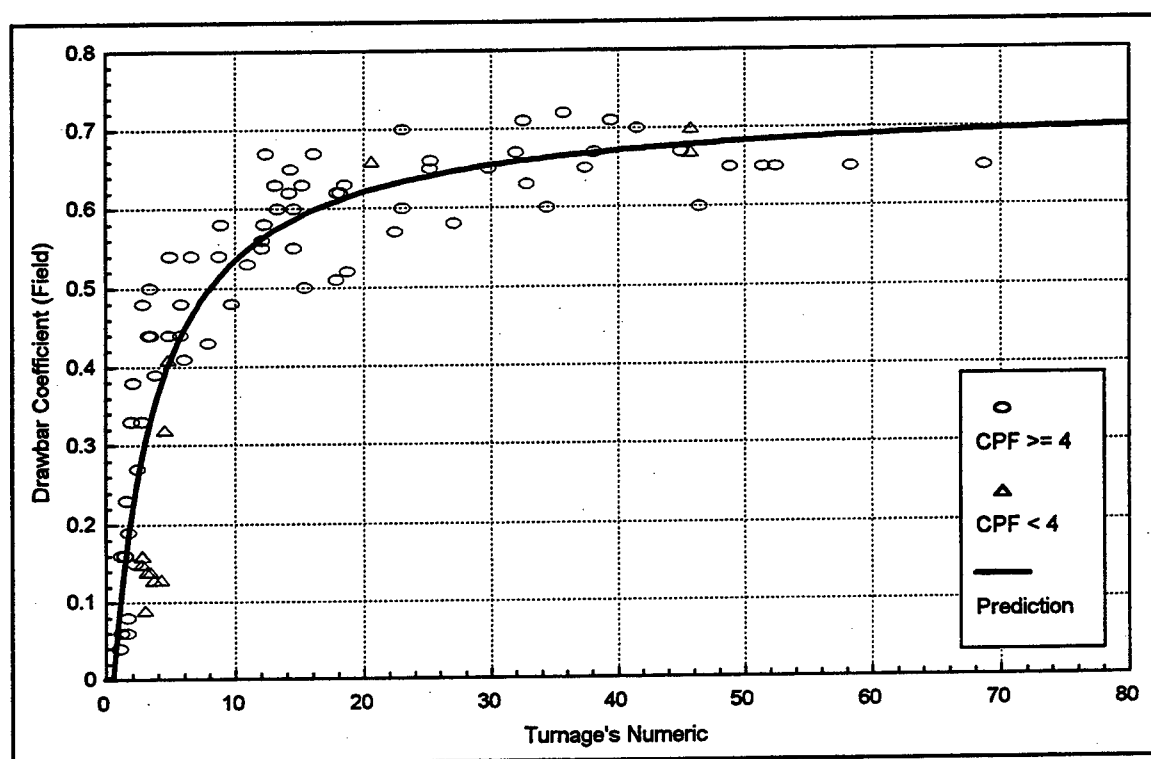
Figure 28. Relationship between Turnage's Numeric and the field drawbar data

The field drawbar data were plotted versus Turnage's numeric on a x-y plot, and the resulting trend was in a form that could be described well by the rectangular hyperbola equation. Therefore, the combined linear regression and numerical optimization process was used to develop a rectangular hyperbola equation for describing field drawbar performance as a function of $N_{c(T)}$. The resulting equation is shown below.

$$\frac{D^{RCI}}{W_{20}} = 0.73 - \frac{2.5}{N_{c(T)} + 2.8}$$

A x-y plot with the field drawbar data and the equation for drawbar versus $N_{c(T)}$ is shown in Figure 28. The figure demonstrates that the trend is hyperbolic and that Turnage's numeric describes the field drawbar data reasonably well. Turnage's numeric is shown to also have

problems describing the data with CPF less than 4 psi in the low drawbar range, but it does appear to be slightly better than Freitag's numeric in this range. The data are shown to be well distributed throughout the full range of $N_{c(T)}$.

The last WES numeric was developed primarily by Smith in collaboration with Turnage [1995]. Smith's numeric was similar to Turnage's numeric in content but much different in form. Smith cast the ratios of tire deflection-to-section height and section width-to-diameter in forms different from both Freitag's and Turnage's numerics. According to Turnage [1995], Smith's numeric should be the best WES numeric for describing field performance. Smith's numeric is calculated as shown below.

$$N_{c(S)} = \frac{RCI\,n\,b\,d}{w}\left(1-\frac{\delta}{h}\right)^{-3/2}\left(1+\frac{b}{d}\right)^{-3/4}$$

The field drawbar data were plotted versus Smith's numeric on a x-y plot, and the resulting trend was in a form that could be described well by the rectangular hyperbola equation. Therefore, the combined linear regression and numerical optimization process was used to develop a rectangular hyperbola equation for describing field drawbar performance as a function of $N_{c(S)}$. The resulting equation is shown below and is plotted with the field drawbar data in Figure 29.

$$\frac{D^{RCI}}{W_{20}} = 0.72 - \frac{7.1}{N_{c(S)} + 7.4}$$

The figure demonstrates that the trend is hyperbolic and that Smith's numeric describes the field drawbar data reasonably well. Smith's numeric is shown to also have slight problems describing the data with CPF less than 4 psi in the low drawbar range, but it appears to be

better than both Freitag's and Turnage's numerics in this range. $N_{c(S)}$ is also shown to produce a good distribution throughout the full range of data.
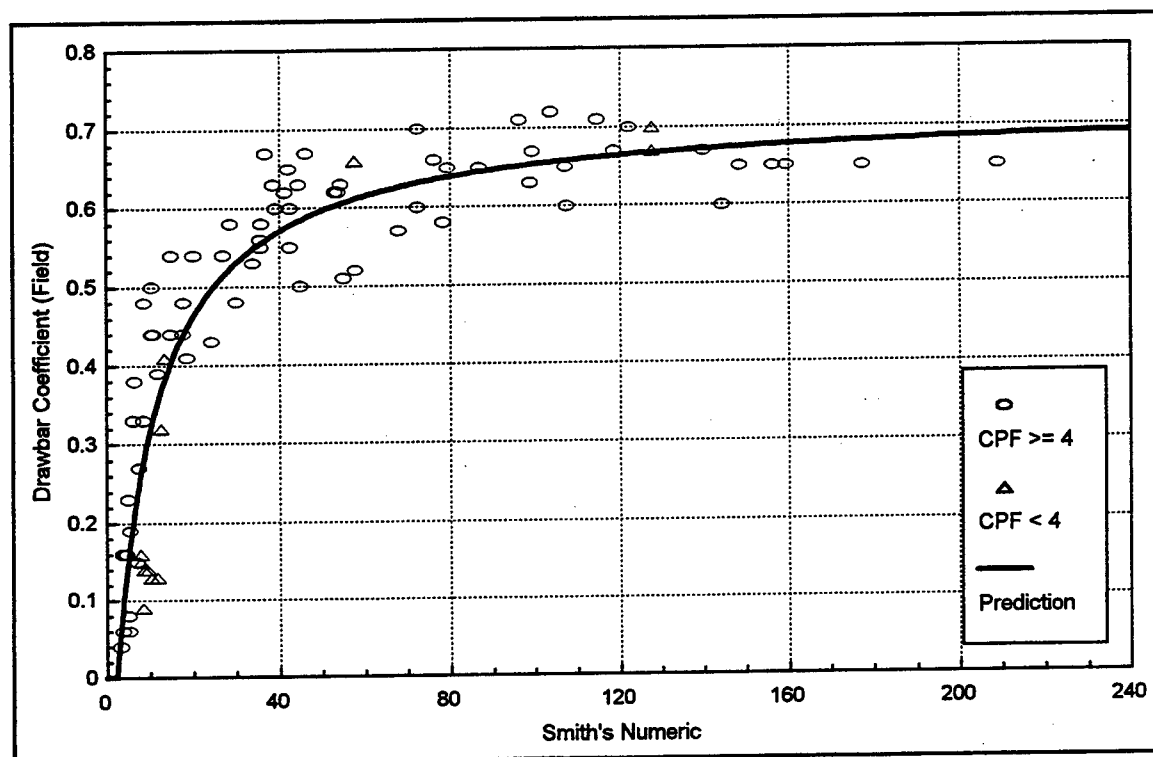
Figure 29. Relationship between Smith's Numeric and the field drawbar data

The last existing model is based on a numeric for drawbar that was recently proposed for use in the United Kingdom by Maclaurin [1997]. Maclaurin's numeric is actually loosely founded on Freitag's original numeric, but its development was accomplished through a significantly different approach. Unlike Turnage's and Smith's numerics which involved modifications to Freitag's numeric, Maclaurin's numeric is completely original. Maclaurin derived his numeric from the results of recent drawbar experiments conducted by DERA with a field deployable, computer controlled, single-wheel tire tester. The formula used for this

drawbar model is actually slightly different from the formula found in the referenced publication. The true formula had the constant 2 for the number of tires per axle, but the variable n was used here for reasons discussed in Chapter IV pertaining to Maclaurin's MMP. Maclaurin's numeric was calculated as shown below.

$$N_M = \frac{RCI\,n\,b^{0.8}\,d^{0.8}\,\delta^{0.4}}{w}$$

The field drawbar data were plotted versus Maclaurin's numeric on a x-y plot, and the resulting trend was in a form that could be described well by the rectangular hyperbola equation. Therefore, the combined linear regression and numerical optimization process was used to develop a rectangular hyperbola equation for describing field drawbar performance as a function of N_M. The resulting equation is shown below and is plotted with the field drawbar data in Figure 30.

$$\frac{D^{RCI}}{W_{20}} = 0.73 - \frac{2.7}{N_M + 3.2}$$

The figure demonstrates that the trend is hyperbolic and that Maclaurin's numeric describes the field drawbar data reasonably well. Just like the three WES numerics, Maclaurin's numeric is shown to have problems describing the data with CPF less than 4 psi in the low drawbar range. N_M, just like the other existing numerics, is shown to produce a good distribution throughout the full range of data.
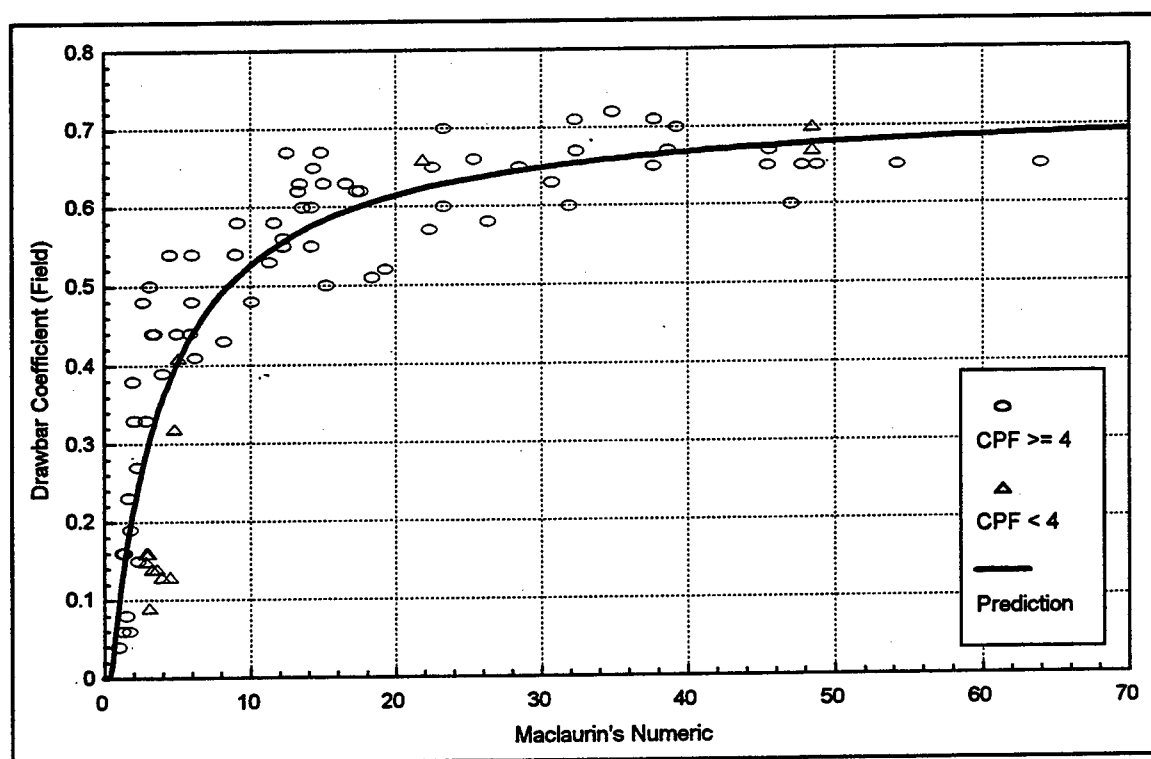
Figure 30. Relationship between Maclaurin's Numeric and the field drawbar data

New Development Models

As stated, four major types of new development models were explored in the drawbar modeling. These included a bearing ratio model, an excess bearing ratio model, an excess RCI ratio model, and a numeric-type model. Only the numeric-type model will be discussed, and only the major variants of the numeric-type model will be presented. Before the individual model variants are addressed, clarification is provided on what is meant by 'bearing ratio model', 'excess bearing ratio model', and 'excess RCI ratio model' (see first few sections on new development models in Chapter IV for clarification on 'numeric-type model'). Explanations are also provided as to why these types of models were explored in the drawbar modeling effort and why the numeric-type model is the only one presented.

The bearing ratio model is based on a dimensionless parameter that is the ratio of soil strength over contact pressure. Therefore, it represents the ratio of resistance over loading for the bearing interaction. The bearing ratio parameter closely resembles the numeric parameter for drawbar, but the bearing ratio parameter uses a logically derived expression for contact pressure similar to the logical derivations of contact pressure used for the VCI_1 modeling in Chapter IV. In fact, the variants explored for the bearing ratio model used the same expressions for contact pressure that resulted from the VCI_1 modeling (i.e., CP2, etc.). The excess bearing ratio model is essentially the same with the exception that it uses excess soil strength (RCI_x) rather than the actual soil strength (RCI). The excess RCI ratio model is somewhat similar, but it uses the ratio of excess soil strength over VCI_1. All three of these types of models are based in part on the ideas utilized in the standard NRMM drawbar relationship and Freitag's original dimensional analysis research.

The bearing ratio model was explored for drawbar because of the decent level of success demonstrated in the existing numerics and the fact that Freitag's numeric worked reasonably well describing VCI_1 which was proven to be almost entirely controlled by contact pressure. However, the bearing ratio model did not work very well (as can be seen in Appendix C), and this led to the idea of trying excess bearing ratio. It was hypothesized that the collapsing effect of RCI_x on drawbar versus RCI might produce a beneficial effect on the bearing ratio model in a similar fashion. The modeling demonstrated that this hypothesis was false, and in fact, the excess bearing ratio model was worse than the bearing ratio model.

The excess RCI ratio model was explored due to the success demonstrated in the RCI_x models (standard and optimized). Dividing RCI_x by VCI_1 has two logical benefits.

First, it makes the modeling parameter dimensionless forcing the units in the relationship to be correct (recall that the drawbar coefficient performance metric is dimensionless). Second, it allows the principal vehicle characteristics to have influence on drawbar performance throughout the full range of soil strengths rather than just at zero drawbar. The excess RCI ratio model demonstrated better potential than the bearing ratio and excess bearing ratio models, but it did not work very well either, falling short of the quality demonstrated in the optimized RCI_x model.

The numeric-type model was explored due to the level of success demonstrated in the existing numerics and due to the success of the numeric-type model in the VCI_1 modeling. As will be shown, the numeric-type model was very successful in the drawbar modeling. The numeric-type model not only worked well describing the field drawbar data, it also provided some potential insight into the controlling mechanism in drawbar performance. Therefore, the major variants of the numeric-type model were the focus of the discussion for the drawbar modeling effort.

As described in Chapter IV, a numeric-type model allows the data to completely define the form of a simple, principal parameter (referred to as a numeric) under the constraint that the parameter's units must be correct. The drawbar coefficient performance metric is dimensionless, and hence the numeric parameter must also be dimensionless. The soil part of the numeric was soil strength measured in RCI which introduces pressure units (i.e., force/length^2). For the vehicle part of the numeric, w/n was used for including force units and the principal tire shape dimensions were used to include the length^2 units. This basic approach was used in all of the individual numeric variants. The only differences in the variants were

the number of principal tire shape dimensions included and the approach used to develop their optimum arrangement.

For each of the numeric-type model variants, the same process was used to develop the relationship between the drawbar performance metric and the numeric. Once the basic mathematical form of the drawbar numeric was decided, a statistical model was used to develop the relationship. The rectangular hyperbola equation was used in the relationships because of its strength in describing the relationship for all of the existing models. Due to the performance differences that were observed between bias ply and radial tire configurations in the VCI_1 modeling, tire construction was considered in the drawbar modeling, but there was no apparent difference in performance between bias ply and radial tire configurations in the field drawbar database.

The first numeric-type model variant used an approach for the vehicle part that was identical to the approach used for the best numeric variant for VCI_1. The approach was to use a product of b, d, and three dimensionless tire ratios where each ratio was raised to a power (p_1, p_2, and p_3). The ratios chosen used d as the characteristic length in dimensionless ratios with each of b, h, and δ so that all four of the principal tire shape dimensions could be included in the final numeric. Three ratios (i.e., powers) were used because there were four length variables less one constraint. This modeling approach allowed inclusion of b, d, h, and δ in the final numeric with each raised to its own numerically optimized power under

the constraint that the summation of the four powers must equal two. The form of the first numeric-type model variant is shown below.

$$\frac{D^{RCI}}{W_{20}} = \beta_0 + \frac{\beta_1}{N_{DI} + \beta_2}$$

$$N_{DI} = \frac{RCI}{w}\left(n \, b \, d \, (b/d)^{P_1} \, (d/h)^{P_2} \, (\delta/d)^{P_3} \right)$$

The combined linear regression and numerical optimization process was used to determine the empirical constants in the relationship. The process resulted in p_1 being -0.90, p_2 being 0.82, and p_3 being 0.45. The resulting final equations are shown below where the numeric has been simplified by collapsing the ratios and collecting like terms.

$$N_{DI} = \frac{RCI}{w}\left(\frac{n \, b^{0.10} \, d^{2.27} \, \delta^{0.45}}{h^{0.82}} \right)$$

$$\frac{D^{RCI}}{W_{20}} = 0.695 - \frac{8.6}{N_{DI} + 7.5}$$

N_{DI} was calculated for each observation in the field drawbar database, and the data were plotted with the equation describing the relationship on a x-y plot as shown in Figure 31. The figure shows that the field drawbar data are described very well by the first numeric-type model variant, and unlike all the existing numerics, N_{DI} had no problem describing the data with CPF < 4 psi in the lower drawbar range.
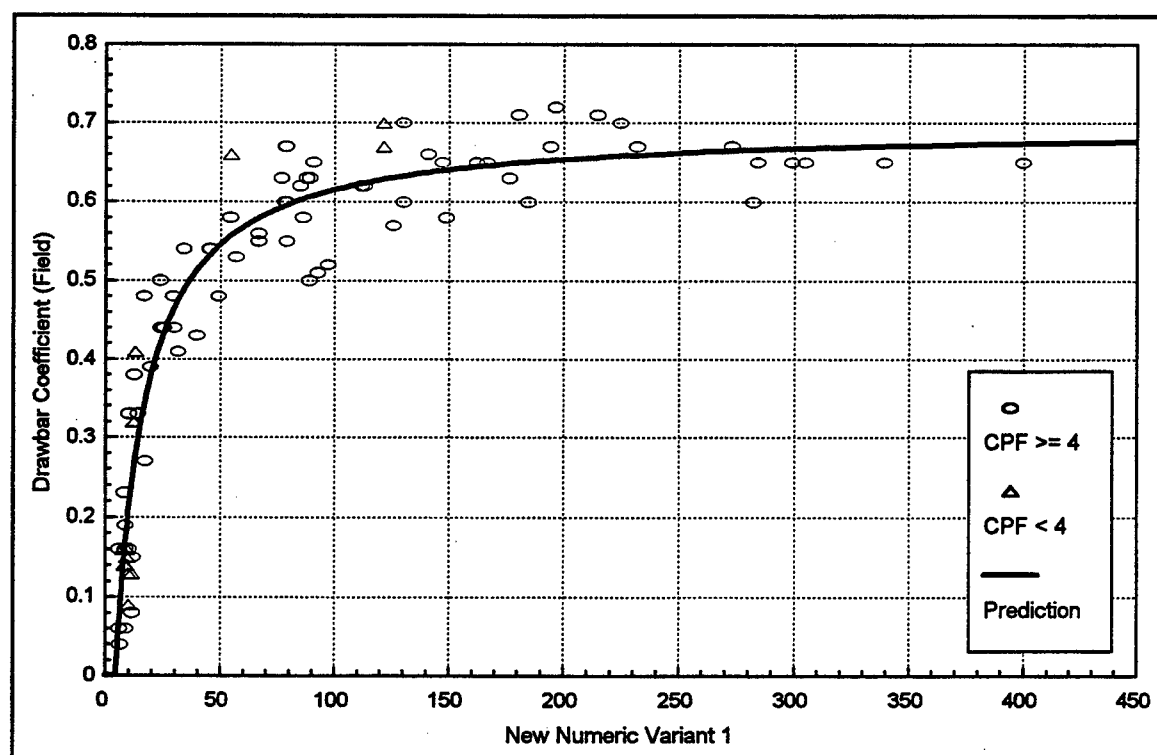
Figure 31. Relationship between new numeric variant 1 and the field drawbar data

Due to the small exponent on section width (i.e., 0.10) in N_{DI}, it was hypothesized

that section height may have caused a reduced influence for section width as a result of the

interrelation between these two variables for the majority of field drawbar observations (see

Chapter II). For this reason, the second numeric-type model variant was developed without

section height included. The fact that Maclaurin's numeric did not consider section height

also supported the removal of this variable. The approach was to use a product of b, d, and

two dimensionless tire ratios where both ratios were raised to a power (p_1 and p_2). The

ratios chosen used d as the characteristic length in dimensionless ratios with both b and δ.

Two ratios (i.e., powers) were used because there were three length variables less one

constraint. This modeling approach allowed inclusion of b, d, and δ in the final numeric with

each raised to its own numerically optimized power under the constraint that the summation of the three powers must equal two. The form of the second numeric-type model variant is shown below.

$$\frac{D^{RCI}}{W_{20}} = \beta_0 + \frac{\beta_1}{N_{D4} + \beta_2}$$

$$N_{D4} = \frac{RCI}{w}\left(n\, b\, d\, (b/d)^{P_1} (\delta/d)^{P_2} \right)$$

The combined linear regression and numerical optimization process was used to determine the empirical constants in the relationship, and the process resulted in p_1 being -1.0 and p_2 being 0.50. The resulting final equations are shown below where the numeric has been simplified by collapsing the ratios and collecting like terms.

$$N_{D4} = \frac{RCI}{w}\left(n\, d^{1.50}\, \delta^{0.50} \right)$$

$$\frac{D^{RCI}}{W_{20}} = 0.69 - \frac{2.55}{N_{D4} + 2.10}$$

N_{D4} was calculated for each observation in the field drawbar database, and the data were plotted with the equation describing the relationship on a x-y plot as shown in Figure 32. The figure shows that the field drawbar data are described very well by this model variant, and N_{D4} is shown to describe the data with a form and quality similar to that of N_{D1}.

The resulting form of N_{D4} was surprising. Section height was removed from consideration in the numeric under the hypothesis that section width would then demonstrate a stronger influence (i.e., a larger exponent), but instead the influence of section width completely disappeared. This result indicates that section width plays a very small role in

drawbar performance, and hence contact pressure is not the controlling factor in drawbar performance. This conclusion is supported by Turnage's [1972] findings that a bearing ratio parameter using actual measured hard-surface contact area did not adequately describe drawbar performance in clay soils, and it is also supported by the poor results obtained in this research for the bearing ratio models. Obviously, this conclusion is not valid at the zero drawbar point (i.e., VCI_1), but these results indicate that a transition in the controlling mechanism occurs very shortly beyond zero drawbar and that something other than contact pressure controls throughout the majority of the drawbar range.
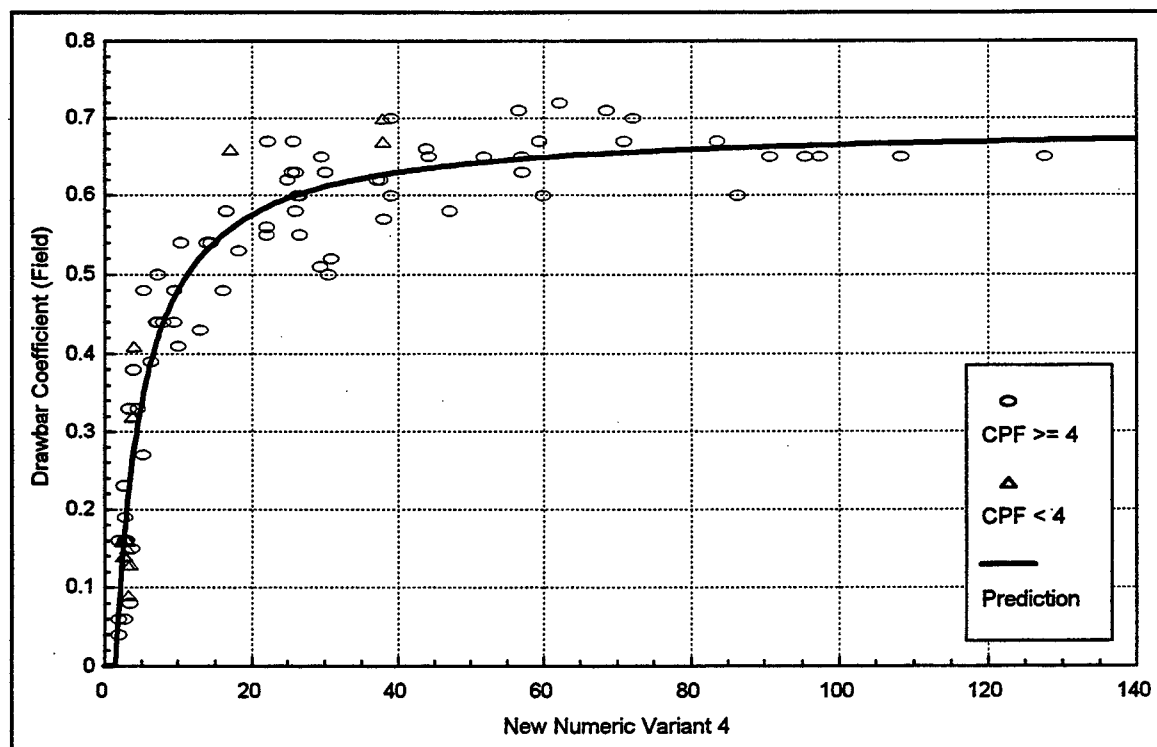
Figure 32. Relationship between new numeric variant 4 and the field drawbar data

The third numeric-type model variant was developed based on a closer look at the form of N_{D4}. It was observed that N_{D4} could be rewritten as shown below.

$$N_{D4} = \frac{RCI}{w}\left(n\,d\sqrt{d\,\delta}\right)$$

It was also recognized that $\sqrt{d\,\delta}$ is very similar to the estimate for hard-surface contact length that results from application of the long chord analogy (i.e., $L_\delta = 2\sqrt{d\,\delta - \delta^2}$). Therefore, it was hypothesized that $\sqrt{d\,\delta}$ could be replaced by the logically derived L_δ in the numeric parameter without affecting the form and quality of the relationship. The form of the third numeric-type model variant is shown below.

$$\frac{D^{RCI}}{W_{20}} = \beta_0 + \frac{\beta_1}{N_{D8} + \beta_2}$$

$$N_{D8} = \frac{RCI}{w}\left(n\,d\,L_\delta\right)$$

The combined linear regression and numerical optimization process was used to determine the empirical constants in the relationship, and the resulting final equations are shown below.

$$N_{D8} = \frac{RCI}{w}\left(n\,d\,L_\delta\right) \qquad where \quad L_\delta = 2\sqrt{d\,\delta - \delta^2}$$

$$\therefore N_{D8} = \frac{RCI}{w}\left(2n\sqrt{d^3\delta - d^2\delta^2}\right)$$

$$\frac{D^{RCI}}{W_{20}} = 0.692 - \frac{5.0}{N_{D8} + 4.1}$$

N_{D8} was calculated for each observation in the field drawbar database, and the data were plotted with the equation describing the relationship on a x-y plot as shown in Figure 33. The

figure verifies that N_{D8} describes the data well and with a form and quality nearly identical to that of N_{D4}.
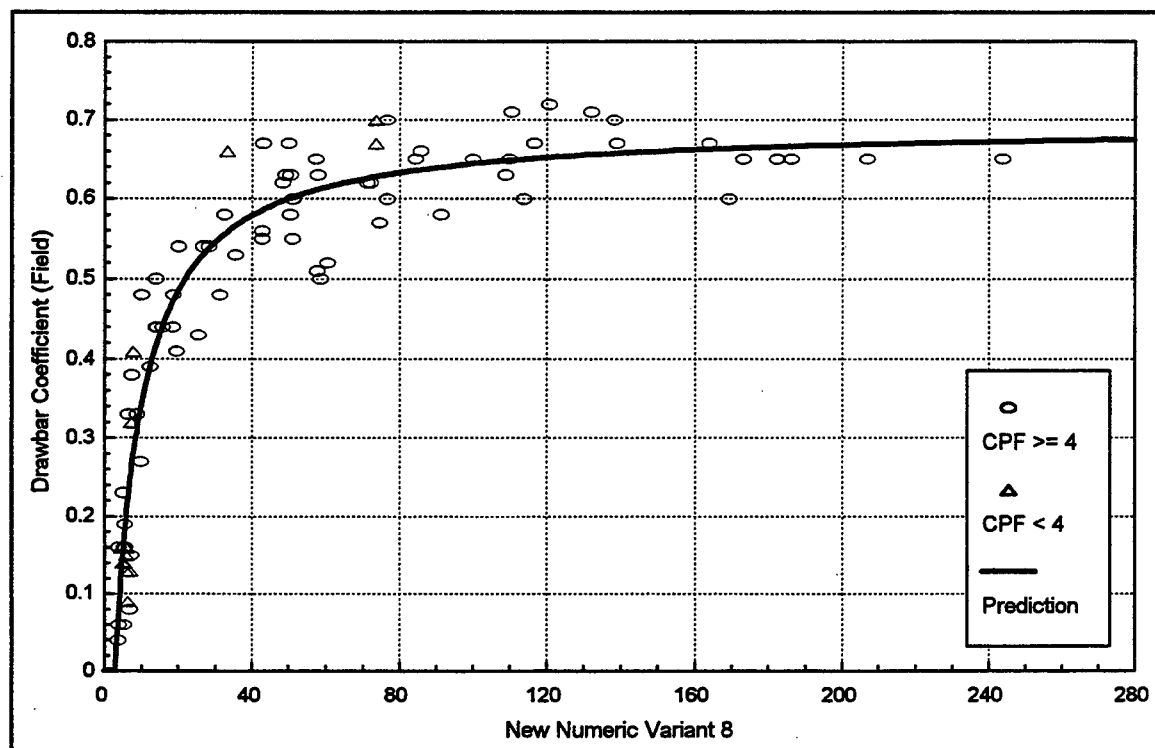
Figure 33. Relationship between new numeric variant 8 and the field drawbar data

An interesting conclusion resulted from the third numeric-type model variant. It appears that the product of tire diameter and hard-surface contact length represents the vehicle side of the controlling mechanism in drawbar performance. This conclusion makes more sense if it is realized that tire diameter could be replaced with tire radius without any effect on the form and quality of the relationship. The product of tire radius and hard-surface contact length indicates that the controlling mechanism in drawbar performance may be the length of the torque moment arm (i.e., active radius) times the length of soil in shear.

In order to gain greater confidence in the validity of N_{D8} as a predictor for drawbar performance, additional drawbar data were explored. Freitag's numeric, which includes a strong influence from section width and was developed entirely from laboratory data, was shown to describe the field drawbar data fairly well. Therefore, N_{D8}, which completely ignores section width and was developed entirely from field data, was evaluated using laboratory drawbar data. The laboratory drawbar data (described in Chapter II) from Freitag's original dimensional analysis research were used for the evaluation.

Before conducting the evaluation of N_{D8} with the laboratory data, the difference between field and laboratory drawbar measurements was observed. Figure 34 shows a x-y plot of drawbar coefficient versus Freitag's numeric. The plot contains the laboratory drawbar measurements and the curve-fit developed earlier for describing the relationship between the field drawbar measurements and Freitag's numeric. The figure shows that the laboratory drawbar measurements follow a trend that is very different from the trend in the field drawbar measurements in terms of form and magnitude. Based on a review of Figure 27, it is probable that the discrepancy below a drawbar coefficient of 0.40 is probably not as large as indicated in Figure 34, but the enormous discrepancy above a drawbar coefficient of 0.40 is undeniable. Despite the difference between drawbar performances observed in the two environments, the quality with which Freitag's numeric described the field data indicates that the same modeling parameter may describe the data well in both environments, although with very different curve-fits.
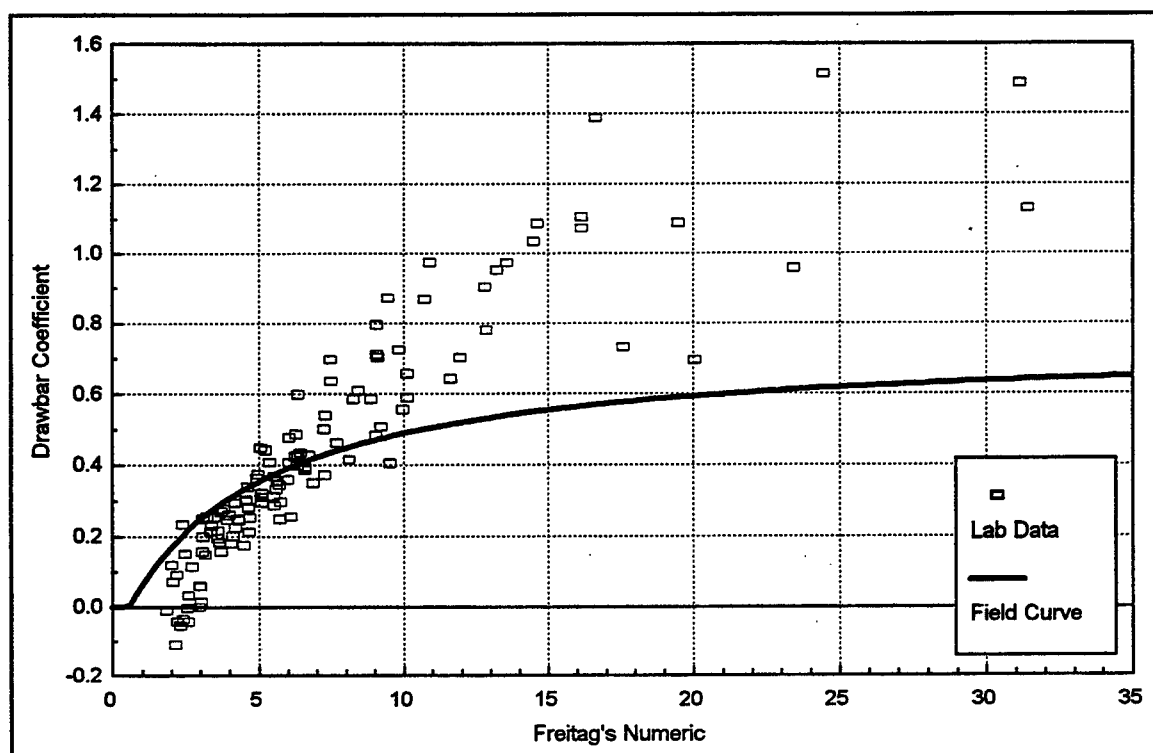
Figure 34. Comparison between laboratory and field drawbar measurements

For evaluating N_{D8} in the laboratory environment, comparison x-y plots were developed as shown in Figure 35. The upper plot (Figure 35a) shows the laboratory drawbar data plotted versus Freitag's numeric, and the lower plot (Figure 35b) shows the same data plotted versus N_{D8}. Although the scales are much different between the upper and lower plots, the absolute horizontal and vertical spread of the data are essentially the same. Therefore, an adequate visual assessment for the difference in quality between the two numerics can be made using the figure.

Figure 35 demonstrates that Freitag's numeric describes the laboratory drawbar data better than N_{D8}. The quality of N_{D8} is not too bad though, and it collapses the data for three of the tires into a central trend very similar in quality and form to that of Freitag's numeric.

a. Performance of Freitag's Numeric

b. Performance of new numeric variant 8
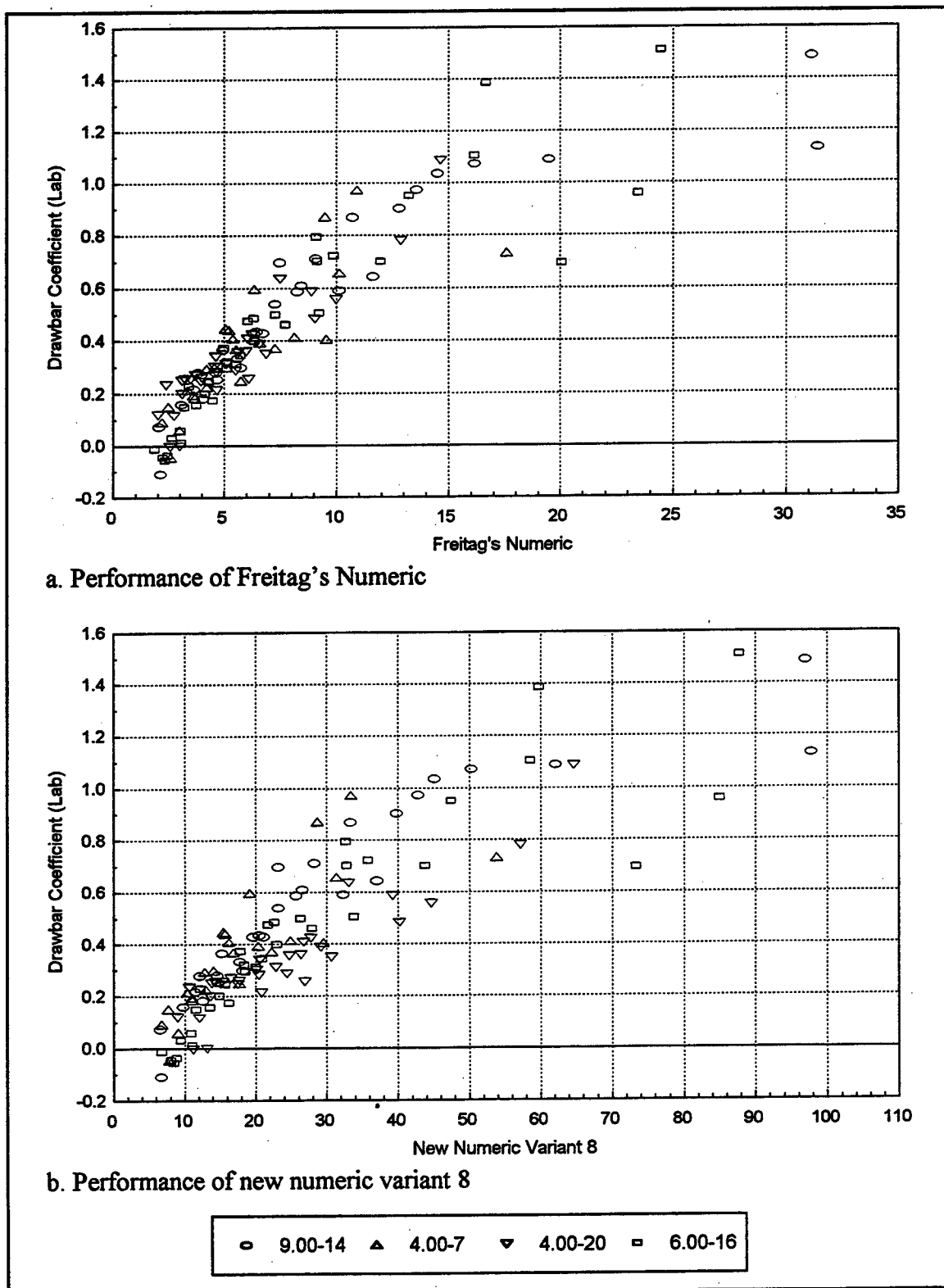
Figure 35. New numeric variant 8 versus Freitag's Numeric in laboratory drawbar data

However, the drawbar performance of the 4.00-20 tire follows a significantly different trend when N_{D8} is used. The 4.00-20 tire had a very small carcass area relative to its diameter, and, as illustrated in Figure 6, it had a very small section height relative to its diameter when compared to the other tires from all three of the databases. This observation led to the hypothesis that the ratio of tire section height to diameter could be used as a potentially improving modification to the numeric parameter. It was noted that this modification should have no detrimental effect on the quality of the numeric in describing the field data since all of the tires from the field drawbar database had h/d ratios that were very similar in magnitude (note that this would not have been the case for b/d).

The last numeric-type model variant was developed for evaluating the potential benefit of the h/d modification. This model variant used a principal parameter that was the product of N_{D8} and h/d raised to a power (p_1). The form of this model variant is shown below.

$$\frac{D^{RCI}}{W}_{20} = \beta_0 + \frac{\beta_1}{N_{D16} + \beta_2}$$

$$N_{D16} = \frac{RCI}{w}\left(2n\sqrt{d^3\delta - d^2\delta^2}\right)\left(\frac{h}{d}\right)^{p_1}$$

A trial and error approach was used to determine the value of p_1 that best collapsed all four of the laboratory tires into a central trend, and a value of 0.6 was visually assessed to work best. Figure 36 shows comparison x-y plots in a layout identical to that of Figure 35. Once again, the absolute horizontal and vertical spread of the data in the upper plot (Figure 36a) and the lower plot (Figure 36b) are essentially the same. Therefore, Figure 36 allows a visual assessment for the difference in quality between Freitag's numeric and N_{D16} to be made. The

a. Performance of Freitag's Numeric

b. Performance of new numeric variant 16
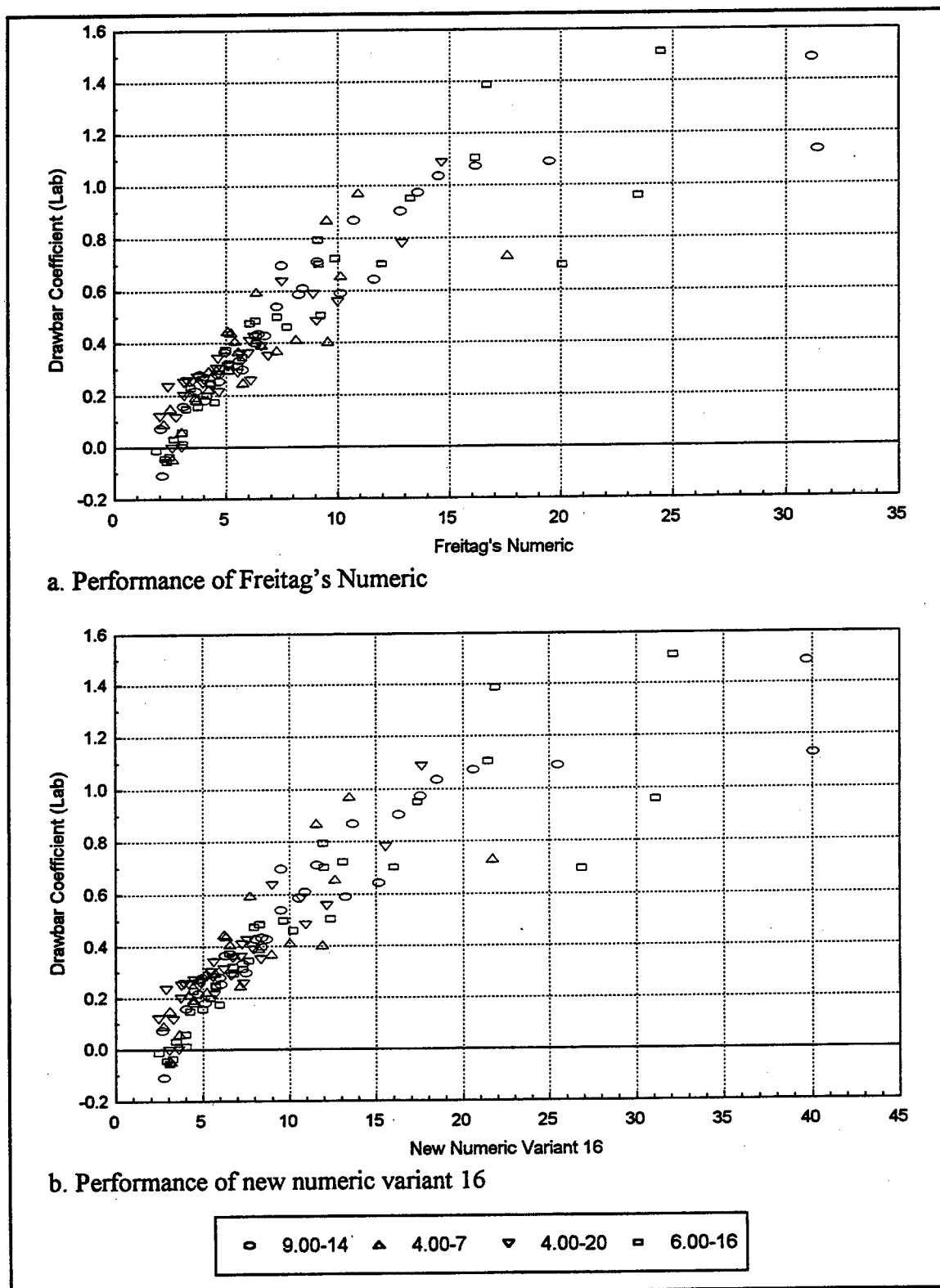
Figure 36. New numeric variant 16 versus Freitag's Numeric in laboratory drawbar data

figure demonstrates that there is no significant difference in quality and form between the two numerics.

Once the appropriate exponent for the h/d modification had been determined using the laboratory data, the combined linear regression and numerical optimization process was used to determine the other empirical constants in the relationship using the field data. The resulting final equations are shown below.

$$N_{D16} = \frac{RCI}{w}\left(2n\sqrt{d^3\delta - d^2\delta^2}\right)\left(\frac{h}{d}\right)^{0.6}$$

$$\frac{D^{RCI}}{W}_{20} = 0.690 - \frac{2.18}{N_{D16} + 1.70}$$

N_{D16} was calculated for each observation in the field drawbar database, and the data were plotted with the equation describing the relationship between drawbar and N_{D16} on a x-y plot as shown in Figure 37. The figure verifies that N_{D16} describes the data well and with a form and quality nearly identical to that of N_{D8}.
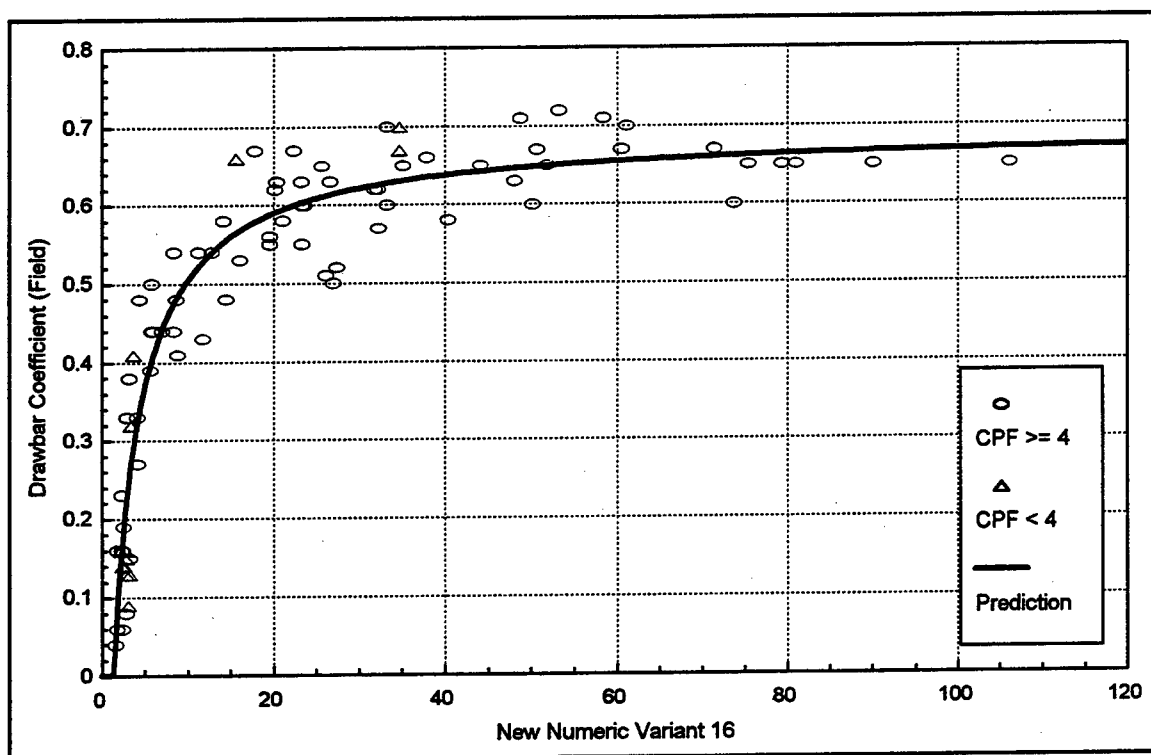
Figure 37. Relationship between new numeric variant 16 and the field drawbar data

Model Comparisons

Several existing and new drawbar relationships were presented in the preceding

sections of this chapter, and a simple x-y plot of each relationship was provided. The x-y

plots allowed a visual interpretation of the quality with which each relationship described the

measured data, but higher accuracy methods of assessing quality were necessary to make

sound comparisons between the various relationships. For this purpose, the standard error

(S_e) and adjusted coefficient of determination (Adj. R^2) measures of quality were used. These

quality measures were determined during the development of each of the many model

variants, and they were used as optimization targets in models that required numerical

optimization as described in Chapter III. Table 6 lists these measures along with their

associated degrees of freedom for each of the relationships. The quality measures shown in the table are based on a consideration of the field drawbar data only (i.e., no laboratory data).

Table 6. Quality comparison for the drawbar modeling results (field data only)

Relationship	Degrees of Freedom	Standard Error	Adjusted R-squared
Standard NRMM (RCI$_x$)	81	0.097	77.8
Optimized NRMM	81	0.079	85.3
Freitag's Numeric	80	0.095	78.7
Turnage's Numeric	80	0.085	82.8
Smith's Numeric	79	0.082	84.1
Maclaurin's Numeric	78	0.090	80.6
New Numeric Variant 1	78	0.063	90.5
New Numeric Variant 4	79	0.063	90.5
New Numeric Variant 8	80	0.063	90.6
New Numeric Variant 16	79	0.064	90.2

Several comparisons can be made using Table 6. First, the table demonstrates that the optimized NRMM relationship described the data significantly better (i.e., lower S_e and higher R^2) than the standard NRMM relationship. For the three existing WES numerics, the table shows that Turnage made significant improvement to Freitag's numeric and that Smith, in collaboration with Turnage, made slightly more improvement. Maclaurin's numeric, which was the existing numeric developed recently by DERA, described the data better than

Freitag's numeric but not as well as Turnage's numeric. In terms of the new relationships, all of the new drawbar numerics essentially described the data with equal quality. Drawbar numeric variant 8, which included the logical L_8, ranked best, and drawbar numeric variant 16, which included consideration of the laboratory drawbar data, ranked a very close last. Most significantly, the table demonstrates that the new drawbar numerics describe the data much better than any of the existing relationships. The optimized NRMM relationship described the data better than any of the existing numerics, but its quality was significantly worse than the new numerics. These results indicate that it is definitely feasible to develop new drawbar relationships that meet the decision criteria stated in the objectives for this research. The results also indicate that the driving factor in drawbar performance may be the product of the torque moment arm at the tires (i.e., active radius) and the length of soil in shear.

CHAPTER VI

SUMMARY AND CONCLUSIONS

Summary

The current traction relationships in NRMM describe the performance of real vehicles in naturally occurring soils reasonably well, but they have some major weaknesses. The weaknesses stem primarily from an inadequate and sometimes illogical consideration of the effects that vehicle characteristics have on traction performance. This research sought to demonstrate the feasibility of developing better traction relationships for NRMM through exploitation of existing performance data. The approach used to demonstrate the feasibility was to conduct a statistical modeling effort for developing some new traction relationships. The applied modeling effort encompassed a systematic and extensive exploration of new and old traction modeling concepts that rely on relatively simple characterizations of the vehicle and the soil. The effort concentrated on VCI_1 and drawbar performance characteristics of pneumatic-tired vehicles interacting with non-slippery, highly plastic clay soils (CH classification by USCS).

Readily accessible sources of VCI_1, field drawbar, and laboratory drawbar performance data were acquired. The range and distribution for each of the critical system variables associated with the performance data were observed, and possible interrelations between the

system variables were explored. The acquired data provided a substantial number of observations from sources that spanned a period of about three decades, and they incorporated a broad range of values with decent distributions for the critical system variables. The data also demonstrated that there are some trends in tire shape that predominate in off-road tire design.

Throughout the modeling effort, some basic concepts were considered. One of these concepts was a simplified force analysis of tire/soil interaction that provides the fundamental logic behind the NRMM traction algorithms. Another concept was a mathematical analogy for the effect of tire deflection on contact area at the tire/soil interface. Some basic analytical tools were used throughout the research as well. These tools were necessary to develop the new relationships, and they included least squares linear regression, iterative numerical optimization routines, and a combined process of both.

In the VCI_1 modeling, several existing and new models were explored. The existing models included the standard NRMM relationship (MI with DCF), three versions of MMP, and Freitag's numeric cast in a VCI form. The new models included various contact pressure models and a numeric-type model. The contact pressure models were based on the theory that tire contact pressure dominates VCI_1 performance. The numeric-type model allowed the data to completely define the form of a simple, single system parameter referred to as a numeric. Several variants were explored for most of the new types of VCI_1 models.

The results of the VCI_1 modeling demonstrated that several new relationships described the data better than any of the existing relationships. The two best variants of the contact pressure models provided the best relationships, and the best numeric variant ranked a close third. The standard NRMM relationship was better than all three versions of MMP

and Freitag's numeric cast in a VCI form, but even a modified version of the NRMM relationship that was fully optimized to the VCI_1 data could not match the quality of the best new relationships.

Several existing and new models were also explored in the drawbar modeling. The existing models included the standard NRMM relationship (RCI_X), three WES numerics (Freitag, Turnage, and Smith), and a recent DERA numeric (Maclaurin). The new models included a bearing ratio model, an excess bearing ratio model, an excess RCI ratio model, and a numeric-type model. The bearing ratio model was based on the ratio of soil strength in RCI over contact pressure, and the excess bearing ratio model used the ratio of RCI_X over contact pressure. The RCI ratio model used the ratio of soil strength in RCI over VCI_1, and the numeric-type model allowed the data to completely define the form of a simple, single system parameter referred to as a numeric. Several variants were explored for all of the new types of drawbar models.

Of the existing models, the standard NRMM relationship described the field drawbar data worst and Smith's numeric did best. However, a modified version of the NRMM relationship that was fully optimized to the field drawbar data demonstrated that RCI_X could describe the data better than any of the four existing numerics. Of the new models, only the numeric-type model proved useful, and nearly all of the new numeric variants described the field drawbar data better than the optimized NRMM relationship and all of the existing numerics. In addition to describing the field drawbar data better than RCI_X and the existing numerics, one of the new numerics even described the laboratory drawbar data with a quality essentially equal to that of Freitag's numeric.

Conclusions

Based on the results obtained from the modeling effort, several significant conclusions were made as follows.

1. The feasibility exists to develop better traction relationships by utilizing existing traction performance data. Moreover, better relationships can be developed that are logical in arrangement, have theoretical foundations, are dimensionally correct, provide a more sound understanding of the role that vehicle characteristics have on traction performance throughout the full range of soil strengths, and describe the existing data better than the current NRMM relationships.

2. VCI_1 performance is completely dominated by soil bearing capacity with tire contact pressure acting as the driving force. Any parameter that is highly correlated with the true average contact pressure under the tires on a wheeled vehicle can be used as a sound predictor of VCI_1 performance.

3. There is a difference in VCI_1 performance resulting strictly from a difference in tire construction such that radial tires outperform bias ply tires by about 2 psi on average.

4. The best CP2 relationship is the best relationship for predicting VCI_1 performance out of all the relationships that were evaluated.

5. There is a change in the controlling mechanism such that drawbar performance beyond a soil strength of VCI_1 is <u>not</u> controlled by tire contact pressure.

6. It appears that the dominant factor in drawbar performance may be the product of the torque moment arm at the tires (i.e., active radius) and the length of soil in shear.

7. Numeric-type models can be extremely useful for developing relationships in areas where little is known about the controlling mechanism.

8. A shortcoming in the Numeric Approach laboratory research resulted from the fact that an attempt was made to develop a single numeric that would represent the controlling vehicle influence for not only drawbar but also for sinkage, motion resistance, and torque output. This research demonstrated that the controlling vehicle influence is not necessarily the same for all four of the performance considerations.

CHAPTER VII

DIRECTIONS FOR FURTHER RESEARCH

The results of this thesis have demonstrated great promise for substantial improvements to the traction prediction capabilities in NRMM. However, much more research is necessary before modifications to NRMM should be considered. Further research should be conducted for VCI_1 performance of wheeled vehicles in non-slippery CH soils. Similar research should also be conducted for VCI_1 performance of wheeled vehicles in the other major USCS soil types and for tracked vehicles in all the major USCS soil types. There are existing data from previous WES studies that could be used for these efforts. Further research should be conducted for traction performance above VCI_1 as well, but the efforts should take a much different direction than the current NRMM implementation.

Further research should be conducted to gain a better understanding of the manner in which the principal tire variables affect hard-surface contact length, loaded section width, and hard-surface contact area. It is apparent that the better a parameter describes hard-surface contact area, the better it will describe VCI_1 performance. Efforts should also be conducted to leverage past research into the nature of stress distributions under tires in soil and into the deflected shape of tires in soil. WES has published research in this area, and information from these and other similar studies could probably provide useful insight.

Potential also exists for improving the soil side of the VCI_1 problem. A review of the root multi-pass data for each of the observations used during this research should be conducted. A digital database that contains the root multi-pass data for most, if not all, of the vehicle configurations is currently available at WES, and this database would greatly simplify the review. Better and simpler critical layer concepts would be the primary goal. A secondary goal would be to verify the VCI_1 measurements for all of the observations prior to establishing new relationships for NRMM (some of the observations appear questionable).

The current NRMM implementation for traction beyond VCI_1 uses drawbar relationships and motion resistance relationships to predict tractive force potential for a particular vehicle/ terrain scenario. This implementation probably originated from the fact that drawbar and motion resistance are measurable quantities that were being researched before a speed-predicting mobility model was ever developed. It probably also had origins from a consideration that motion resistance on powered traction elements could be significantly different from that on non-powered traction elements. A better, more logical implementation for NRMM would be to use tractive force relationships instead of drawbar relationships.

Tractive force is a terrain reaction force that occurs at the vehicle/terrain interface whereas drawbar is a resultant effect on the motion (or towing ability) of the vehicle. The principal vehicle and terrain variables have a direct influence on tractive force and motion resistance and only a secondary influence on drawbar. Tractive force relationships could be developed by adding drawbar and motion resistance data prior to developing relationships rather than adding the two relationships as is done in NRMM now. The error associated with using motion resistance data from non-powered traction elements to estimate motion

resistance for powered traction elements would probably be small relative to the other sources of error (or variability) in traction measurements. This approach would probably produce much more logical relationships and a more sound consideration of the influence that vehicle characteristics have on traction performance.

An example of problems that result from modeling drawbar becomes apparent from a closer look at the data from Figure 33. Figure 38 shows a closeup view of part of the data from Figure 33. The four points delineated in the figure are from a single vehicle configuration with differences in tire deflection only. The figure shows that the best drawbar numeric indicates that drawbar should always increase with increased deflection, but the data indicate what experience has shown [Jones 1992], which is that drawbar on high soil strengths (essentially no sinkage) typically increases when deflection is increased from low magnitudes but then begins to decrease as the deflections get large. This can be attributed to internal motion resistance of the tires increasing at a faster rate than tractive force when tire deflections get too large. This observation is supported by Turnage's [1995] discussion of the importance of considering internal motion resistance when modeling drawbar. It is probable that tractive force does always increase with increased tire deflection.

The last point of discussion for further research is based on the critical layer concept. Critical layer concepts are currently only applied for VCI_1 modeling. Traction beyond VCI_1 is currently modeled based on the 0-6 inch soil layer. This layer is probably appropriate for traction throughout the majority of the soil strength range beyond VCI_1, but in a small zone of strengths just beyond VCI_1, a deeper layer is probably more appropriate. Further research for traction beyond VCI_1 should give consideration to this issue.
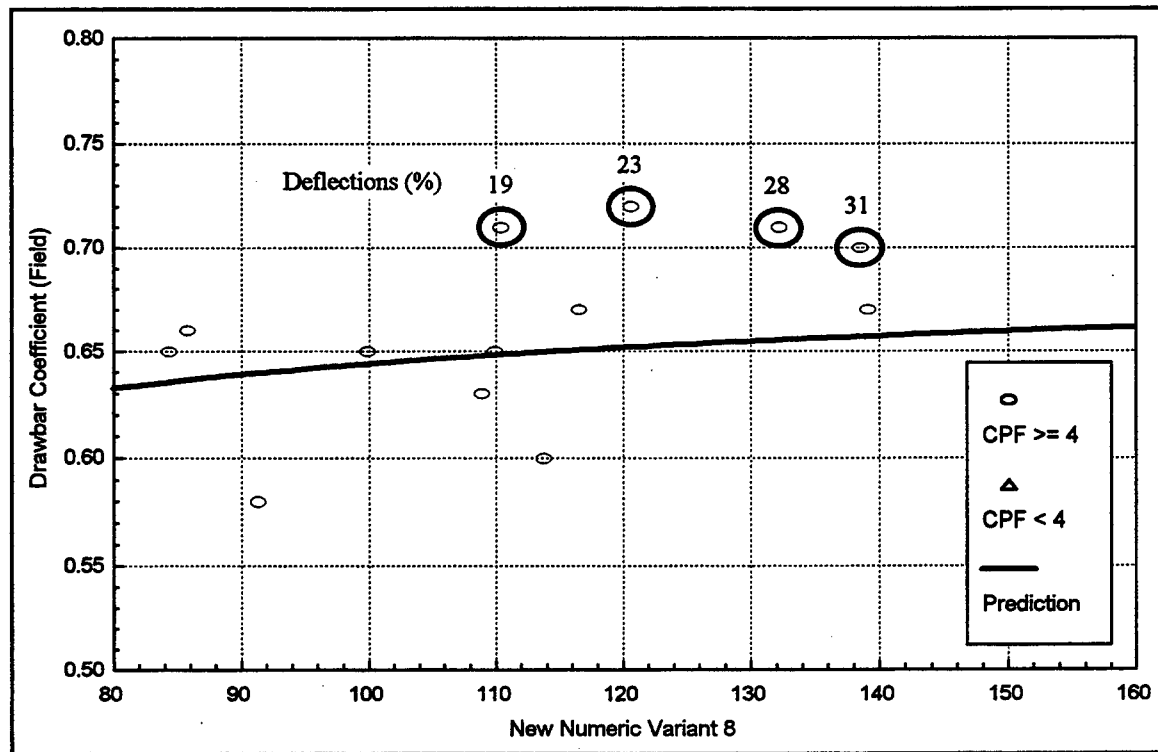
Figure 38. Sample of problems due to modeling drawbar rather than tractive force

BIBLIOGRAPHY

Ahlvin, Richard B. and Haley, Peter W. (December 1992). "NATO Reference Mobility Model Edition II, NRMM II User's Guide," Technical Report GL-92-19, U.S. Army Engineer Waterways Experiment Station, Vicksburg, MS.

Freitag, Dean R. (August 1965). "A Dimensional Analysis of the Performance of Pneumatic Tires on Soft Soils," Technical Report No. 3-688, U.S. Army Engineer Waterways Experiment Station, Vicksburg, MS.

Green, Charles E., and Johnson, Robert H. (April 1991). "Mobility Performance Evaluation of the Palletized Loading System (PLS) Candidate Vehicles," Technical Report GL-91-4, U.S. Army Engineer Waterways Experiment Station, Vicksburg, MS.

Green, Charles E. (July 1986). "Mobility Performance Evaluation of the First Article Preproduction SEE Tractor," Technical Report GL-86-10, U.S. Army Engineer Waterways Experiment Station, Vicksburg, MS.

Johnson, Richard A. (1994). *Miller and Freund's Probability and Statistics for Engineers*. 5th ed., Prentice Hall, Englewood Cliffs, NJ.

Johnson, Robert H., and Green, Charles E. (September 1990). "Mobility Performance Evaluation of the Forward Area Multipurpose Vehicle (FAMV)," Technical Report GL-90-20, U.S. Army Engineer Waterways Experiment Station, Vicksburg, MS.

Johnson, Robert H., and Schreiner, Barton G. (April 1990). "Mobility Test Results of the TATRA 813 8x8 Wheeled Vehicle," Technical Report GL-90-3, U.S. Army Engineer Waterways Experiment Station, Vicksburg, MS.

Jones, Randolph A. (June 1992). "Mobility Performance Tests of the High Mobility Multi-Purpose Wheeled Vehicle With a Central Tire Inflation System and Towed Trailer," Technical Report GL-92-7, U.S. Army Engineer Waterways Experiment Station, Vicksburg, MS.

Kennedy, J. G. and Rush, E. S. (March 1968). "Trafficability of Soils, Eighteenth Supplement, Development of Revised Mobility Index Formula for Self-Propelled Wheeled Vehicles in Fine-Grained Soils," Technical Memorandum No. 3-240, U.S. Army Engineer Waterways Experiment Station, Vicksburg, MS.

Larminie, J. C. (1992). "Modifications to the Mean Maximum Pressure System," *Journal of Terramechanics* 29(2), 239-255.

Maclaurin, B. (August 1997). "Proposed Revisions to MMP Based on the Results of Tractive Performance Trials with Single Pneumatic Tyres and a Modular Track System," DERA/LS4/TR970122/1.0, Defense Evaluation and Research Agency, Farnborough, Hampshire, GU14 0LX.

May, Carl R. and Green, Charles E. (June 1993). "Mobility Assessment of the FSU SA-8 TLAR RSV, 6x6, Amphibious Transporter, Volume 1: Main Text," Technical Report GL-93-8, U.S. Army Engineer Waterways Experiment Station, Vicksburg, MS.

May, Carl R. (March 1991). "Trafficability Tests With the USSR ZIL Model 131, 3-1/2-Ton, 6x6 Truck," Miscellaneous Paper GL-91-8, U.S. Army Engineer Waterways Experiment Station, Vicksburg, MS.

Meyer, Marvin P., Ehrlich, I. Robert, Sloss, David, Murphy, Newell K., Jr., Wismer, Robert D., and Czako, Tibor. (1977). "International Society for Terrain-Vehicle Systems Standards," *Journal of Terramechanics* 14(3), 153-182.

Moore, Dennis W. (August 1989). "Mobility Evaluation of the Technology Demonstrator 5-Ton Truck Testbed," Technical Report GL-89-9, U.S. Army Engineer Waterways Experiment Station, Vicksburg, MS.

Nuttall, C. J., Jr., Wilson, C. W., and Werner, R. A. (July 1966). "One-Pass Performance of Vehicles on Fine-Grained Soils," Contract Report No. 3-152, U.S. Army Engineer Waterways Experiment Station, Vicksburg, MS.

Priddy, Jody D. (June 1995). "Stochastic Vehicle Mobility Forecasts Using the NATO Reference Mobility Model, Report 3, Database Development for Statistical Analysis of the NRMM II Cross-Country Traction Empirical Relationships" Technical Report GL-95-8, U.S. Army Engineer Waterways Experiment Station, Vicksburg, MS.

Rogillio, David M. (March 1990). "Mobility Performance Evaluation of the Renault TRM 2000," Technical Report GL-90-1, U.S. Army Engineer Waterways Experiment Station, Vicksburg, MS.

Rush, E. S. and Robinson, J. H. (April 1971). "Trafficability of Soils, Nineteenth Supplement, Effects of Surface Conditions on Drawbar Pull of a Wheeled Vehicle," Technical Memorandum No. 3-240, U.S. Army Engineer Waterways Experiment Station, Vicksburg, MS.

Schreiner, Barton G. (May 1985). "Field Test Results and Mobility Predictions for the Yugoslav FAP 2026 Cargo Truck," Technical Report GL-85-6, U.S. Army Engineer Waterways Experiment Station, Vicksburg, MS.

Schreiner, Barton G., Moore, Dennis W., and Grimes, Keafur. (April 1985). "Mobility Assessment of the Heavy Expanded Mobility Tactical Truck (HEMTT)–Initial Production Vehicles," Technical Report GL-85-4, U.S. Army Engineer Waterways Experiment Station, Vicksburg, MS.

Schreiner, B. G. (March 1971). "Mobility Exercise A (MEXA) Field Test Program, Report 2, Performance of MEXA and Three Military Vehicles in Soft Soil, Volume 1," Technical Report M-70-11, U.S. Army Engineer Waterways Experiment Station, Vicksburg, MS.

Turnage, Gerald W. (December 1995). "Mobility Numeric System for Predicting In-the-Field Vehicle Performance, Report 1, Historical Review, Planned Development" Miscellaneous Paper GL-95-12, U.S. Army Engineer Waterways Experiment Station, Vicksburg, MS.

Turnage, G. W. (September 1972). "Performance of Soils Under Tire Loads, Report 8, Application of Test Results to Tire Selection for Off-Road Vehicles," Technical Report No. 3-666, U.S. Army Engineer Waterways Experiment Station, Vicksburg, MS.

Willoughby, William E., Jones, Randolph A., Cothren, C. David, Moore, Dennis W., Rogillio, David M., Unger, Robert F., and Prickett, Terri L. (January 1991). "U.S. Army Wheeled Versus Tracked Vehicle Mobility Performance Test Program, Report 1, Mobility in Slippery Soils and Across Gaps, Volume 1: Program Summary," Technical Report GL-91-2, U.S. Army Engineer Waterways Experiment Station, Vicksburg, MS.

Willoughby, William E., Jones, Randolph A., Cothren, C. David, Moore, Dennis W., Rogillio, David M., Unger, Robert F., and Prickett, Terri L. "U.S. Army Wheeled Versus Tracked Vehicle Mobility Performance Test Program, Report 1, Mobility in Slippery Soils and Across Gaps, Volume II: Drawbar Pull, Motion Resistance, and Slope Climbing Tests," (not published), (Copies can be requested from USAEWES, ATTN: CEWES-GM, 3909 Halls Ferry Road, Vicksburg, MS 39180-6199.).

Willoughby, William E. (May 1984). "Trafficability Tests With M923, 5-Ton Truck," Miscellaneous Paper GL-84-6, U.S. Army Engineer Waterways Experiment Station, Vicksburg, MS.

(May 1951). "Trafficability of Soils, Ninth Supplement, Vehicle Classification," Technical Memorandum No. 3-240, U.S. Army Engineer Waterways Experiment Station, Vicksburg, MS.

APPENDIX A

TABLES PRESENTING DETAILED DESCRIPTIONS

OF THE OBSERVATIONS USED DURING

THE TRACTION MODELING

Table A1. General description of the observations used for the VCI$_1$ modeling

| Item No. | Vehicle Identification | Tire Characteristics | | | Chains (Y/N) | GVW lbf | Critical Layer | Measured VCI$_1$ | Data Reference |
		Description	Inflation psi	δ/h percent					
2	TCM MTV	395/80R20 Goodyear MV/T	22	36	No	35070	6-12	25	unpublished
3	TCM LMTV	395/80R20 Goodyear MV/T	24	33	No	22310	6-12	25	unpublished
4	S&S MTV	395/80R20 Michelin Pilot XML	26	35	No	35770	6-12	25	unpublished
5	S&S LMTV	395/80R20 Michelin Pilot XML	24	35	No	23385	6-12	25	unpublished
6	TTC MTV	395/80R20 Goodyear MV/T	32	26	No	35060	6-12	24	unpublished
7	TTC LMTV	395/80R20 Goodyear MV/T	20	35	No	23585	6-12	23	unpublished
8	LAV 84	Michelin11.00R16 XL	52	16	No	27100	6-12	32	unpublished
9	LAV 84	Michelin 11.00R16 XL	29	25	No	27100	6-12	30	unpublished
10	M1008 CUCV	Armstrong 9.50x16.50 Bias	11.3	30	No	6300	3-9	24	unpublished
11	M1008 CUCV	Armstrong 9.50x16.50 Bias	38.3	15	No	6300	3-9	22	unpublished
12	M1008 CUCV	9.50R16.5 Radial	41	15	No	6300	3-9	22	unpublished
13	M1008 CUCV	9.50R16.5 Radial	14.5	30	No	6300	3-9	19	unpublished
14	FSU SA-8	1200x500-508 10PR Bias	14	32	No	35780	6-12	20	TR GL-93-8
15	FSU SA-8	1200x500-508 10PR Bias	28	24	No	35780	6-12	22	TR GL-93-8
16	ZIL-131	12.00-20	7	42	No	21325	6-12	14	MP GL-91-8
17	ZIL-131	12.00-20	22	20	No	21325	6-12	24	MP GL-91-8
18	ZIL-131	12.00-20	10	33	No	21325	6-12	17	MP GL-91-8

Table A1. (continued)

Item No.	Vehicle Identification	Tire Characteristics				GVW lbf	Critical Layer	Measured VCI_1	Data Reference
		Description	Inflation psi	δ/h percent	Chains (Y/N)				
19	M35A2	11.00x20	20	21	No	18225	6-12	26	MP GL-91-8 [a]
20	M35A2	11.00x20	13	29	No	18225	6-12	23	MP GL-91-8 [a]
21	M35A1	11.00x20	35.5	15	No	19410	6-12	29	CR No. 3-152 [a]
22	M35A1	11.00x20	13	35	No	19410	6-12	29	CR No. 3-152 [a]
23	OSHKOSH PLS	425/95R20 XZL	16/22	35	No	86255	6-12	33	TR GL-91-4 [a]
25	PACCAR PLS	17.5R25	42	25	No	80655	6-12	39	TR GL-91-4 [a]
27	GM PLS	425/95R20 XZL	42	25	No	80795	6-12	37	TR GL-91-4 [a]
29	TATRA 813	15.00-21 TO	20/20	35	No	50250	6-12	25	TR GL-90-3
30	TATRA 813	15.00-21 TO	30/30	29	No	50250	6-12	25	TR GL-90-3
31	TATRA 813	15.00-21 TO	20/20	35	No	50250	6-12	29	TR GL-90-3
32	TATRA 813	15.00-21 TO	30/30	29	No	50250	6-12	29	TR GL-90-3
33	FAMV	12.5R16.5 XL	30	22	No	22690	6-12	23	TR GL-90-20
35	TRM 2000	12.5R20 XL	19/23	33	No	13920	6-12	21	TR GL-90-1
36	TECH DEMO	14.00R20 XL	17	35	No	32210	6-12	23	TR GL-89-9
37	M923A1	14.00R20 XL	17	35	No	32190	6-12	23	TR GL-89-9
38	M923	11.00x20 NDCC Goodyear	60/30	17	No	32485	6-12	29	MP GL-84-6
39	M923	11.00x20 NDCC Goodyear	25/25	27	No	32485	6-12	28	MP GL-84-6

Table A1. (continued)

Item No.	Vehicle Identification	Tire Characteristics				GVW lbf	Critical Layer	Measured VCI₁	Data Reference
		Description	Inflation psi	δ/h percent	Chains (Y/N)				
40	M923	14.00R20 Michelin	30	23	No	32260	6-12	29	MP GL-84-6
41	M923	14.00R20 Michelin	10	47	No	32260	6-12	22	MP GL-84-6
42	M923	14.00R20 Goodyear	30	22	No	32105	6-12	28	MP GL-84-6 [a]
43	M923	14.00R20 Goodyear	10	40	No	32105	6-12	23	MP GL-84-6
44	M923	16.00R20 Michelin	25	22	No	33585	6-12	23	MP GL-84-6
45	M923	16.00R20 Michelin	8	37	No	33585	6-12	18	MP GL-84-6
46	M923	16.00R21 Goodyear	25	21	No	33790	6-12	23	MP GL-84-6
47	M923	16.00R21 Goodyear	8	40	No	33790	6-12	18	MP GL-84-6
50	SEE Tractor	12.5R20 XL	unknown	18 [b]	No	16170	6-12	30	TR GL-86-10
51	FAP 2026	15.00-21	44	22	No	38620	6-12	31	TR GL-85-6
52	FAP 2026	15.00-21	13	40	No	38620	6-12	26	TR GL-85-6
57	M985 HEMTT	16.00R20 XL	20/30	29	No	62250	6-12	32	TR GL-85-4
58	M985 HEMTT	16.00R20 XL	20/20	27	No	57770	6-12	27	TR GL-85-4
61	M977 HEMTT	16.00R20 XL	35/40	20	No	60145	6-12	36	TR GL-85-4 [a]
62	M977 HEMTT	16.00R20 XL	20/30	28	No	60145	6-12	29	TR GL-85-4
63	M977 HEMTT	16.00R20 XL	15/19	34	No	60145	6-12	27	TR GL-85-4
64	M977 HEMTT	14.00x20	20/20	34	No	56290	6-12	27	unpublished

Table A1. (continued)

Item No.	Vehicle Identification	Tire Characteristics				GVW lbf	Critical Layer	Measured VCI$_1$	Data Reference
		Description	Inflation psi	δ/h percent	Chains (Y/N)				
65	M977 HEMTT	14.00x20	39/39	20	No	56290	6-12	39	unpublished
66	M977 HEMTT	14.00x20	74/74	14	No	56290	6-12	40	unpublished
72	M151	7.00x16	30	12	No	3560	3-9	22	CR No. 3-152 [a]
73	M151	7.00x16	15	20	No	3560	3-9	20	CR No. 3-152 [a]
74	M151	9.00x14	30	15	No	3560	3-9	14	CR No. 3-152 [a]
75	M151	9.00x14	20	19	No	3560	3-9	17	CR No. 3-152 [a]
76	M151	36x20-14R	15	6	No	3560	3-9	9	CR No. 3-152 [a]
77	M151	36x20-14R	3	15	No	3560	3-9	8	CR No. 3-152 [a]
78	MEXA 8x8	48x31 - 16A	9	20	No	19013	6-12	12	TR M-70-11 [a]
79	MEXA 10x10	42x40 - 16A	7.3	20	No	18030	3-9	9	TR M-70-11 [a]
81	XM410E1	14x18	13	25	No	18504	6-12	18	TR M-70-11 [a]
88	M37	9.00x16	30	13	No	7240	3-9	26	CR No. 3-152 [a]
89	M37	9.00x16	15	20	No	7240	3-9	26	CR No. 3-152 [a]
90	M37	9.00x16	6.5	35	No	7240	3-9	18	CR No. 3-152 [a]
91	M37	46.00 - 18x16 Terra Tires	15	10	No	7240	3-9	10	CR No. 3-152 [a]
92	M37	46.00 - 18x16 Terra Tires	3	25	No	7240	3-9	10	CR No. 3-152 [a]
93	M274 Mule	7.50x10	30	6	No	1190	3-9	8	CR No. 3-152 [a]

Table A1. (continued)

Item No.	Vehicle Identification	Tire Characteristics				GVW lbf	Critical Layer	Measured VCI$_1$	Data Reference
		Description	Inflation psi	δ/h percent	Chains (Y/N)				
94	M274 Mule	7.50x10	10	12	No	1190	3-9	7	CR No. 3-152 [a]
95	M274 Mule	7.50x10	5	15	No	1190	3-9	6	CR No. 3-152 [a]
96	M274 Mule	7.50x10	30	10	No	1940	3-9	12	CR No. 3-152 [a]
97	M274 Mule	7.50x10	10	21	No	1940	3-9	11	CR No. 3-152 [a]
98	M274 Mule	7.50x10	5	35	No	1940	3-9	9	CR No. 3-152 [a]
99	M274 Mule	16.00 - 15x16 Terra Tires	15	10	No	1325	3-9	7	CR No. 3-152 [a]
100	M274 Mule	16.00 - 15x16 Terra Tires	3	22	No	1325	3-9	5	CR No. 3-152 [a]
101	M274 Mule	16.00 - 15x16 Terra Tires	15	15	No	1940	3-9	10	CR No. 3-152 [a]
102	M274 Mule	16.00 - 15x16 Terra Tires	3	39	No	1940	3-9	9	CR No. 3-152 [a]
106	Timberjack 404	23.1x26 10PR Logger Special	16	16	No	16880	6-12	16	unpublished
107	Mudder	46x18-16R	3	20	No	4840	3-9	10	unpublished

[a] - Measured VCI$_1$ values used here are not necessarily those reported in the data reference; a re-evaluation of the basic multi-pass data was performed during the development of these databases as reported by Priddy [1995]

[b] - assumed value

Table A2. Principal vehicle characteristics associated with the VCI$_1$ observations

Item No.	Vehicle Identification	Transmission Type 0=automatic 1=manual	Engine Net Power hp/ton	h_c in.	m	Tire Construction 0=radial 1=bias	Average per-Axle Dimensions					
							w lbf	n	d in.	b in.	h in.	δ in.
2	TCM MTV	0	16.5	15.0	3	0	11690	2	46.4	15.1	11.2	4.00
3	TCM LMTV	0	20.2	15.0	2	0	11155	2	46.4	15.1	11.2	3.70
4	S&S MTV	0	16.2	10.0	3	0	11923	2	46.4	15.0	11.2	3.90
5	S&S LMTV	0	19.2	10.0	2	0	11693	2	46.4	15.0	11.1	3.90
6	TTC MTV	0	17.1	11.0	3	0	11687	2	46.6	15.1	11.3	2.90
7	TTC LMTV	0	19.1	11.0	2	0	11793	2	46.4	15.2	11.2	3.90
8	LAV 84	0	20.3	15.2	4	0	6775	2	38.7	10.9	10.1	1.65
9	LAV 84	0	20.3	15.2	4	0	6775	2	38.7	10.9	10.1	2.48
10	M1008 CUCV	0	42.9	9.8	2	1	3150	2	31.0	9.5	6.9	2.05
11	M1008 CUCV	0	42.9	9.8	2	1	3150	2	31.0	9.5	6.9	1.04
12	M1008 CUCV	0	42.9	9.8	2	0	3150	2	30.9	9.5	6.9	1.04
13	M1008 CUCV	0	42.9	9.8	2	0	3150	2	30.9	9.5	6.9	2.05
14	FSU SA-8	1	16.8	17.0	3	1	11927	2	43.5	18.3	10.0	3.20
15	FSU SA-8	1	16.8	17.0	3	1	11927	2	43.5	18.3	10.0	2.40
16	ZIL-131	1	14.1	13.8	3	1	7108	2	44.9	12.8	10.5	4.40
17	ZIL-131	1	14.1	13.8	3	1	7108	2	44.9	12.8	10.5	2.10
18	ZIL-131	1	14.1	13.8	3	1	7108	2	44.9	12.8	10.5	3.50

Table A2. (continued)

Item No.	Vehicle Identification	Transmission Type 0=automatic 1=manual	Engine Net Power hp/ton	h_c in.	m	Tire Construction 0=radial 1=bias	Average per-Axle Dimensions					
							w lbf	n	d in.	b in.	h in.	δ in.
19	M35A2	1	15.4	12.5	3	1	6075	2	43.6	11.2	10.2	2.19
20	M35A2	1	15.4	12.5	3	1	6075	2	43.6	11.2	10.2	2.91
21	M35A1	1	13.4	12.3	3	1	6470	2	43.6	11.2	10.2	1.53
22	M35A1	1	13.4	12.3	3	1	6470	2	43.6	11.2	10.2	3.57
23	OSHKOSH PLS	0	11.6	14.5	5	0	17251	2	52.4	17.2	14.2	4.99
25	PACCAR PLS	0	11.0	16.9	4	0	20164	2	53.3	17.5	12.8	3.14
27	GM PLS	0	12.4	16.5	4	0	20199	2	52.8	16.8	14.4	3.58
29	TATRA 813	1	10.0	14.0	4	1	12563	2	52.6	16.6	15.0	5.25
30	TATRA 813	1	10.0	14.0	4	1	12563	2	52.6	16.6	15.0	4.35
31	TATRA 813	1	10.0	14.0	4	1	12563	2	52.6	16.6	15.0	5.25
32	TATRA 813	1	10.0	14.0	4	1	12563	2	52.6	16.6	15.0	4.35
33	FAMV	0	18.1	22.0	4	0	5673	2	36.5	11.6	9.4	2.10
35	TRM 2000	1	15.4	16.0	2	0	6960	2	40.5	12.9	9.4	3.12
36	TECH DEMO	0	14.9	13.8	3	0	10737	2	49.5	14.6	12.5	4.38
37	M923A1	0	14.9	13.8	3	0	10730	2	49.5	14.6	12.5	4.38
38	M923	0	15.4	10.5	3	1	10828	3.333	42.8	11.6	9.9	1.66
39	M923	0	15.4	10.5	3	1	10828	3.333	42.8	11.6	9.9	2.64

Table A2. (continued)

Item No.	Vehicle Identification	Transmission Type 0=automatic 1=manual	Engine Net Power hp/ton	h_c in.	m	Tire Construction 0=radial 1=bias	Average per-Axle Dimensions					
							w lbf	n	d in.	b in.	h in.	δ in.
40	M923	0	15.5	13.8	3	0	10753	2	49.3	14.6	12.7	2.87
41	M923	0	15.5	13.8	3	0	10753	2	49.3	14.6	12.7	5.93
42	M923	0	15.6	13.5	3	0	10702	2	48.9	15.0	12.4	2.71
43	M923	0	15.6	13.5	3	0	10702	2	48.9	15.0	12.4	4.96
44	M923	0	14.9	14.3	3	0	11195	2	52.8	16.1	14.5	3.17
45	M923	0	14.9	14.3	3	0	11195	2	52.8	16.1	14.5	5.38
46	M923	0	14.8	14.3	3	0	11263	2	51.4	17.1	13.9	2.89
47	M923	0	14.8	14.3	3	0	11263	2	51.4	17.1	13.9	5.58
50	SEE Tractor	1	13.6	16.9	2	0	8085	2	40.5	12.9	9.4	1.70
51	FAP 2026	1	13.3	15.8	3	1	12873	2	52.5	16.6	13.4	3.00
52	FAP 2026	1	13.3	15.8	3	1	12873	2	52.5	16.6	13.4	5.30
57	M985 HEMTT	0	13.9	13.4	4	0	15563	2	52.8	16.1	14.5	4.16
58	M985 HEMTT	0	15.0	13.4	4	0	14443	2	52.8	16.1	14.5	3.97
61	M977 HEMTT	0	14.4	13.0	4	0	15036	2	52.8	16.1	14.5	2.85
62	M977 HEMTT	0	14.4	13.0	4	0	15036	2	52.8	16.1	14.5	4.03
63	M977 HEMTT	0	14.4	13.0	4	0	15036	2	52.8	16.1	14.5	4.92
64	M977 HEMTT	0	15.3	13.0	4	1	14073	2	49.9	15.1	13.0	4.40

Table A2. (continued)

Item No.	Vehicle Identification	Transmission Type 0=automatic 1=manual	Engine Net Power hp/ton	h_c in.	m	Tire Construction 0=radial 1=bias	Average per-Axle Dimensions					
							w lbf	n	d in.	b in.	h in.	δ in.
65	M977 HEMTT	0	15.3	13.0	4	1	14073	2	49.9	15.1	13.0	2.55
66	M977 HEMTT	0	15.3	13.0	4	1	14073	2	49.9	15.1	13.0	1.80
72	M151	1	34.3	10.3	2	1	1780	2	28.6	7.1	6.7	0.80
73	M151	1	34.3	10.3	2	1	1780	2	28.6	7.1	6.7	1.34
74	M151	1	34.3	9.1	2	1	1780	2	26.2	8.6	6.1	0.92
75	M151	1	34.3	9.1	2	1	1780	2	26.2	8.6	6.1	1.16
76	M151	1	34.3	14.8	2	1	1780	2	37.5	20.2	10.5	0.63
77	M151	1	34.3	14.8	2	1	1780	2	37.5	20.2	10.5	1.58
78	MEXA 8x8	0	22.5	12.0	4	1	4753	2	48.0	31.0	14.0	2.80
79	MEXA 10x10	0	23.7	11.5	5	1	3606	2	42.0	40.0	12.0	2.40
81	XM410E1	0	16.6	15.0	4	1	4626	2	40.0	14.0	9.5	2.38
88	M37	1	21.5	10.8	2	1	3620	2	32.8	10.2	8.2	1.07
89	M37	1	21.5	10.8	2	1	3620	2	32.8	10.2	8.2	1.64
90	M37	1	21.5	10.8	2	1	3620	2	32.8	10.2	8.2	2.87
91	M37	1	21.5	18.4	2	1	3620	2	48.0	20.0	15.2	1.45
92	M37	1	21.5	18.4	2	1	3620	2	48.0	20.0	15.2	3.80
93	M274 Mule	1	25.2	11.5	2	1	595	2	22.5	8.5	6.2	0.37

Table A2. (continued)

Item No.	Vehicle Identification	Transmission Type 0=automatic 1=manual	Engine Net Power hp/ton	h_c in.	m	Tire Construction 0=radial 1=bias	Average per-Axle Dimensions					
							w lbf	n	d in.	b in.	h in.	δ in.
94	M274 Mule	1	25.2	11.5	2	1	595	2	22.5	8.5	6.2	0.74
95	M274 Mule	1	25.2	11.5	2	1	595	2	22.5	8.5	6.2	0.93
96	M274 Mule	1	15.5	11.5	2	1	970	2	22.5	8.5	6.2	0.62
97	M274 Mule	1	15.5	11.5	2	1	970	2	22.5	8.5	6.2	1.30
98	M274 Mule	1	15.5	11.5	2	1	970	2	22.5	8.5	6.2	2.17
99	M274 Mule	1	22.6	9.0	2	1	663	2	17.4	15.1	4.5	0.45
100	M274 Mule	1	22.6	9.0	2	1	663	2	17.4	15.1	4.5	0.99
101	M274 Mule	1	15.5	9.0	2	1	970	2	17.4	15.1	4.5	0.68
102	M274 Mule	1	15.5	9.0	2	1	970	2	17.4	15.1	4.5	1.76
106	Timberjack 404	0	15.4	21.0	2	1	8440	2	62.5	23.2	16.7	2.75
107	Mudder	1	47.5	15.5	2	1	2420	2	48.0	20.0	15.2	3.00

Table A3. General description of the field observations used for the drawbar modeling

Item No.	Vehicle Identification	Tire Characteristics				GVW lbf	Measurements			Data Reference
		Description	Inflation psi	δ/h percent	Chains (Y/N)		Slip %	0-6 RCI	D/W	
1	M977 HEMTT	MI 16.00R20	20/30	27.6	No	60375	20	296	0.63	TR GL-91-2
2	M977 HEMTT	MI 16.00R20	20/30	27.6	No	60375	20	300	0.50	TR GL-91-2
3	M977 HEMTT	MI 16.00R20	35/40	20.6	No	60375	20	300	0.60	TR GL-91-2
4	M977 HEMTT	MI 16.00R20	35/40	20.6	No	60375	20	296	0.63	TR GL-91-2
5	LAV 25	MI 11.00R16	24	30.3	No	26895	20	296	0.62	TR GL-91-2
6	LAV 25	MI 11.00R16	24	30.3	No	26895	20	300	0.62	TR GL-91-2
7	LAV 25	MI 11.00R16	42	20.6	No	26895	20	249	0.67	TR GL-91-2
8	LAV 25	MI 11.00R16	42	20.6	No	26895	20	286	0.65	TR GL-91-2
9	MK48 LVS	GY 16.00R21	22	28.3	No	66000	20	300	0.60	TR GL-91-2
10	MK48 LVS	GY 16.00R21	22	28.3	No	66000	20	300	0.55	TR GL-91-2
11	MK48 LVS	GY 16.00R21	45	19.4	No	66000	20	300	0.56	TR GL-91-2
12	MK48 LVS	GY 16.00R21	45	19.4	No	66000	20	300	0.55	TR GL-91-2
14	M37	9.00x16	6.5	35	No	7240	20	30	0.48	CR No. 3-152
15	M37	9.00x16	6.5	35	No	7240	20	16	0.16	CR No. 3-152
16	M37	9.00x16	6.5	35	No	7240	20	11	0.04	CR No. 3-152
17	M37	9.00x16	6.5	35	No	7240	20	22	0.38	CR No. 3-152
18	M37	9.00x16	13.4	35	No	7240	20	516	0.65	TM No. 3-240 19th Sup.

Table A3. (continued)

Item No.	Vehicle Identification	Tire Characteristics				GVW lbf	Measurements			Data Reference
		Description	Inflation psi	δ/h percent	Chains (Y/N)		Slip %	0-6 RCI	D/W	
19	M37	9.00x16	13.4	35	No	7240	20	726	0.65	TM No. 3-240 19th Sup.
20	M37	9.00x16	13.4	35	No	7240	20	616	0.65	TM No. 3-240 19th Sup.
21	M37	9.00x16	13.4	35	No	7240	20	543	0.65	TM No. 3-240 19th Sup.
22	M37	9.00x16	13.4	35	No	7240	20	554	0.65	TM No. 3-240 19th Sup.
23	M37	9.00x16	30	13	No	7240	20	154	0.58	unpublished
24	M37	9.00x16	39.1	15	No	7240	20	516	0.67	TM No. 3-240 19th Sup.
25	M37	9.00x16	39.1	15	No	7240	20	726	0.67	TM No. 3-240 19th Sup.
26	M37	9.00x16	39.1	15	No	7240	20	616	0.67	TM No. 3-240 19th Sup.
28	M37	9.00x16	39.1	15	No	7240	20	750	0.60	TM No. 3-240 19th Sup.
29	M274 Mule	7.50-10	unknown	15 [a]	No	1900	20	9	0.06	unpublished
30	M274 Mule	7.50-10	unknown	15 [a]	No	1900	20	9	0.16	unpublished
31	M274 Mule	7.50-10	unknown	15 [a]	No	1900	20	12	0.23	unpublished
32	M274 Mule	7.50-10	unknown	15 [a]	No	1900	20	13	0.19	unpublished
33	M274 Mule	7.50-10	unknown	15 [a]	No	1900	20	15	0.33	unpublished
34	M274 Mule	7.50-10	unknown	15 [a]	No	1900	20	21	0.33	unpublished
35	M274 Mule	7.50-10	unknown	15 [a]	No	1900	20	29	0.39	unpublished
36	M274 Mule	7.50-10	unknown	15 [a]	No	1900	20	44	0.48	unpublished

Table A3. (continued)

<div style="text-align:right">-128-</div>

Item No.	Vehicle Identification	Tire Characteristics				GVVW lbf	Measurements			Data Reference
		Description	Inflation psi	δ/h percent	Chains (Y/N)		Slip %	0-6 RCI	D/W	
37	M274 Mule	7.50-10	unknown	15 [a]	No	1900	20	60	0.43	unpublished
38	M274 Mule	7.50-10	unknown	15 [a]	No	1900	20	74	0.48	unpublished
39	M998 HMMWV	Bias	20/22	14.1	No	7570	20	300	0.60	TR GL-91-2
40	M998 HMMWV	Bias	20/22	14.1	No	7570	20	300	0.70	TR GL-91-2
41	M998 HMMWV	36x12.50-16.5	20/30	15/18	No	8420	20	300	0.57	TR GL-92-7
42	M998 HMMWV	Radial	20/22	16.7	No	7570	20	298	0.66	TR GL-91-2
43	M998 HMMWV	37x12.50R16.5	14/22	22/25	No	8420	20	300	0.58	TR GL-92-7
44	M998 HMMWV	37x12.50R16.5	10/15	26/31	No	8420	20	300	0.65	TR GL-92-7
45	M998 HMMWV	37x12.50R16.5	7/10	31/38	No	8420	20	300	0.63	TR GL-92-7
46	M998 HMMWV	37x12.50R16.5	6/8	33/43	No	8420	20	300	0.60	TR GL-92-7
47	M1025 HMMWV	37x12.50R16.5	14/22	22/16	No	6305	20	300	0.71	TR GL-92-7
48	M1025 HMMWV	37x12.50R16.5	10/15	26/20	No	6305	20	300	0.72	TR GL-92-7
49	M1025 HMMWV	37x12.50R16.5	7/10	32/24	No	6305	20	300	0.71	TR GL-92-7
50	M1025 HMMWV	37x12.50R16.5	6/8	34/28	No	6305	20	300	0.70	TR GL-92-7
51	LAV 25	12.50R20 XL	15	38.5	No	28840	20	325	0.65	TR GL-91-2
52	LAV 25	12.50R20 XL	30	24.9	No	28840	20	228	0.62	TR GL-91-2
53	M35A1	11.00x20	13	35	No	19410	20	21	0.08	CR No. 3-152

Table A3. (continued)

| Item No. | Vehicle Identification | Tire Characteristics | | | | GVW lbf | Measurements | | | Data Reference |
		Description	Inflation psi	δ/h percent	Chains (Y/N)		Slip %	0-6 RCI	D/W	
54	M35A1	11.00x20	13	35	No	19410	20	62	0.54	CR No. 3-152
55	M35A1	11.00x20	13	35	No	19410	20	83	0.54	CR No. 3-152
56	M35A1	11.00x20	13	35	No	19410	20	43	0.50	CR No. 3-152
57	M35A1	11.00x20	13	35	No	19410	20	18	0.16	CR No. 3-152
58	M35A1	11.00x20	13	35	No	19410	20	31	0.27	CR No. 3-152
59	M35A1	11.00x20	35.5	15	No	19410	20	66	0.44	CR No. 3-152
60	M35A1	11.00x20	35.5	15	No	19410	20	64	0.44	CR No. 3-152
61	M35A2	11.00x20	20.1	25	No	18225	22	172	0.58	TR M-70-11
62	DA-1500	MI 24R21 XL	25	23.8	No	62470	20	567	0.65	TR GL-91-2
63	Timberjack 404	23.1x26	16	18.4/11.0	No	16880	20	15	0.06	unpublished
64	Timberjack 404	23.1x26	16	18.4/11.0	No	16880	20	20	0.15	unpublished
65	Timberjack 404	23.1x26	16	18.4/11.0	No	16880	20	43	0.44	unpublished
66	Timberjack 404	23.1x26	16	18.4/11.0	No	16880	20	51	0.44	unpublished
67	Timberjack 404	23.1x26	16	18.4/11.0	No	16880	20	54	0.41	unpublished
68	Timberjack 404	23.1x26	16	18.4/11.0	No	16880	20	78	0.54	unpublished
69	Timberjack 404	23.1x26	16	18.4/11.0	No	16880	20	98	0.53	unpublished
70	Timberjack 404	23.1x26	16	18.4/11.0	No	16880	20	159	0.51	unpublished

Table A3. (continued)

| Item No. | Vehicle Identification | Tire Characteristics | | | | | | Measurements | | | Data Reference |
		Description	Inflation psi	δ/h percent	Chains (Y/N)	GVW lbf	Slip %	0-6 RCI	D/W	
71	Timberjack 404	23.1x26	16	18.4/11.0	No	16880	20	167	0.52	unpublished
72	FSU SA-8	1200x500-508	28	24	No	35780	20	298	0.67	TR GL-93-8
73	FSU SA-8	1200x500-508	14	31.6	No	35780	20	297	0.63	TR GL-93-8
74	MEXA 10x10	42x40 -16A	7.3	20	No	18030	19	162	0.67	TR M-70-11
75	MEXA 10x10	42x40 -16A	7.3	20	No	18030	18	162	0.70	TR M-70-11
76	MEXA 10x10	42x40 -16A	7.3	20	No	18030	27	13	0.13	TR M-70-11
77	MEXA 10x10	42x40 -16A	7.3	20	No	18030	23	15	0.13	TR M-70-11
78	MEXA 10x10	42x40 -16A	7.3	20	No	18030	18	73	0.66	TR M-70-11
79	MEXA 10x10	42x40 -16A	7.3	20	No	18030	21	17	0.41	TR M-70-11
80	MEXA 10x10	42x40 -16A	7.3	20	No	18030	18	16	0.32	TR M-70-11
81	MEXA 10x10	42x40 -16A	7.3	20	No	18030	20	10	0.16	TR M-70-11
82	MEXA 10x10	42x40 -16A	7.3	20	No	18030	16	11	0.14	TR M-70-11
83	MEXA 10x10	42x40 -16A	7.3	20	No	18030	24	12	0.14	TR M-70-11
84	MEXA 8x8	48x31 -16A	9	20	No	19013	30	13	0.16	TR M-70-11
85	MEXA 8x8	48x31 -16A	9	20	No	19013	20	13	0.15	TR M-70-11
86	MEXA 8x8	48x31 -16A	9	20	No	19013	23	14	0.09	TR M-70-11

a - assumed value

Table A4. Principal vehicle characteristics associated with the field drawbar observations

Item No.	Vehicle Identification	m	Tire Construction 0=radial 1=bias	w lbf	n	Average per-Axle Dimensions d in.	b in.	h in.	δ in.	Calculated CPF psi
1	M977 HEMTT	4	0	15094	2	52.8	16.1	14.5	4.00	17.8
2	M977 HEMTT	4	0	15094	2	52.8	16.1	14.5	4.00	17.8
3	M977 HEMTT	4	0	15094	2	52.8	16.1	14.5	2.99	17.8
4	M977 HEMTT	4	0	15094	2	52.8	16.1	14.5	2.99	17.8
5	LAV 25	4	0	6724	2	38.7	10.9	10.1	3.06	15.9
6	LAV 25	4	0	6724	2	38.7	10.9	10.1	3.06	15.9
7	LAV 25	4	0	6724	2	38.7	10.9	10.1	2.08	15.9
8	LAV 25	4	0	6724	2	38.7	10.9	10.1	2.08	15.9
9	MK48 LVS	4	0	16500	2	51.4	17.1	13.9	3.93	18.8
10	MK48 LVS	4	0	16500	2	51.4	17.1	13.9	3.93	18.8
11	MK48 LVS	4	0	16500	2	51.4	17.1	13.9	2.70	18.8
12	MK48 LVS	4	0	16500	2	51.4	17.1	13.9	2.70	18.8
14	M37	2	1	3620	2	32.8	10.2	8.2	2.87	10.8
15	M37	2	1	3620	2	32.8	10.2	8.2	2.87	10.8
16	M37	2	1	3620	2	32.8	10.2	8.2	2.87	10.8
17	M37	2	1	3620	2	32.8	10.2	8.2	2.87	10.8
18	M37	2	1	3620	2	32.8	10.2	8.2	2.87	10.8

Table A4. (continued)

Item No.	Vehicle Identification	m	Tire Construction 0=radial 1=bias	Average per-Axle Dimensions						Calculated CPF psi
				w lbf	n	d in.	b in.	h in.	δ in.	
19	M37	2	1	3620	2	32.8	10.2	8.2	2.87	10.8
20	M37	2	1	3620	2	32.8	10.2	8.2	2.87	10.8
21	M37	2	1	3620	2	32.8	10.2	8.2	2.87	10.8
22	M37	2	1	3620	2	32.8	10.2	8.2	2.87	10.8
23	M37	2	1	3620	2	32.8	10.2	8.2	1.07	10.8
24	M37	2	1	3620	2	32.8	10.2	8.2	1.23	10.8
25	M37	2	1	3620	2	32.8	10.2	8.2	1.23	10.8
26	M37	2	1	3620	2	32.8	10.2	8.2	1.23	10.8
28	M37	2	1	3620	2	32.8	10.2	8.2	1.23	10.8
29	M274 Mule	2	1	950	2	22.5	8.5	6.2	0.93	5.0
30	M274 Mule	2	1	950	2	22.5	8.5	6.2	0.93	5.0
31	M274 Mule	2	1	950	2	22.5	8.5	6.2	0.93	5.0
32	M274 Mule	2	1	950	2	22.5	8.5	6.2	0.93	5.0
33	M274 Mule	2	1	950	2	22.5	8.5	6.2	0.93	5.0
34	M274 Mule	2	1	950	2	22.5	8.5	6.2	0.93	5.0
35	M274 Mule	2	1	950	2	22.5	8.5	6.2	0.93	5.0
36	M274 Mule	2	1	950	2	22.5	8.5	6.2	0.93	5.0

Table A4. (continued)

Item No.	Vehicle Identification	m	Tire Construction 0=radial 1=bias	Average per-Axle Dimensions							Calculated CPF psi
				w lbf	n	d in.	b in.	h in.	δ in.		
37	M274 Mule	2	1	950	2	22.5	8.5	6.2	0.93		5.0
38	M274 Mule	2	1	950	2	22.5	8.5	6.2	0.93		5.0
39	M998 HMMWV	2	1	3785	2	36.3	12.5	9.0	1.27		8.3
40	M998 HMMWV	2	1	3785	2	36.3	12.5	9.0	1.27		8.3
41	M998 HMMWV	2	1	4210	2	36.3	12.5	9.0	1.49		9.3
42	M998 HMMWV	2	0	3785	2	36.7	12.5	9.4	1.57		8.3
43	M998 HMMWV	2	0	4210	2	36.7	12.5	9.4	2.21		9.2
44	M998 HMMWV	2	0	4210	2	36.7	12.5	9.4	2.68		9.2
45	M998 HMMWV	2	0	4210	2	36.7	12.5	9.4	3.24		9.2
46	M998 HMMWV	2	0	4210	2	36.7	12.5	9.4	3.57		9.2
47	M1025 HMMWV	2	0	3153	2	36.7	12.5	9.4	1.79		6.9
48	M1025 HMMWV	2	0	3153	2	36.7	12.5	9.4	2.16		6.9
49	M1025 HMMWV	2	0	3153	2	36.7	12.5	9.4	2.63		6.9
50	M1025 HMMWV	2	0	3153	2	36.7	12.5	9.4	2.91		6.9
51	LAV 25	4	0	7210	2	40.5	12.9	9.4	3.62		13.8
52	LAV 25	4	0	7210	2	40.5	12.9	9.4	2.34		13.8
53	M35A1	3	1	6470	2	43.6	11.2	10.2	3.57		13.3

Table A4. (continued)

Item No.	Vehicle Identification	m	Tire Construction 0=radial 1=bias	Average per-Axle Dimensions						Calculated CPF psi
				w lbf	n	d in.	b in.	h in.	δ in.	
54	M35A1	3	1	6470	2	43.6	11.2	10.2	3.57	13.3
55	M35A1	3	1	6470	2	43.6	11.2	10.2	3.57	13.3
56	M35A1	3	1	6470	2	43.6	11.2	10.2	3.57	13.3
57	M35A1	3	1	6470	2	43.6	11.2	10.2	3.57	13.3
58	M35A1	3	1	6470	2	43.6	11.2	10.2	3.57	13.3
59	M35A1	3	1	6470	2	43.6	11.2	10.2	1.53	13.3
60	M35A1	3	1	6470	2	43.6	11.2	10.2	1.53	13.3
61	M35A2	3	1	6075	2	43.6	11.2	10.2	2.55	12.4
62	DA-1500	4	0	15618	2	54.8	23.4	15.7	3.74	12.2
63	Timberjack 404	2	1	8440	2	62.5	23.2	16.7	2.50	5.8
64	Timberjack 404	2	1	8440	2	62.5	23.2	16.7	2.50	5.8
65	Timberjack 404	2	1	8440	2	62.5	23.2	16.7	2.50	5.8
66	Timberjack 404	2	1	8440	2	62.5	23.2	16.7	2.50	5.8
67	Timberjack 404	2	1	8440	2	62.5	23.2	16.7	2.50	5.8
68	Timberjack 404	2	1	8440	2	62.5	23.2	16.7	2.50	5.8
69	Timberjack 404	2	1	8440	2	62.5	23.2	16.7	2.50	5.8
70	Timberjack 404	2	1	8440	2	62.5	23.2	16.7	2.50	5.8

Table A4. (continued)

Item No.	Vehicle Identification	m	Tire Construction 0=radial 1=bias	Average per-Axle Dimensions						Calculated CPF psi
				w lbf	n	d in.	b in.	h in.	δ in.	
71	Timberjack 404	2	1	8440	2	62.5	23.2	16.7	2.50	5.8
72	FSU SA-8	3	1	11927	2	43.5	18.3	10.0	2.40	15.0
73	FSU SA-8	3	1	11927	2	43.5	18.3	10.0	3.20	15.0
74	MEXA 10x10	5	1	3606	2	42.0	40.0	12.0	2.40	2.1
75	MEXA 10x10	5	1	3606	2	42.0	40.0	12.0	2.40	2.1
76	MEXA 10x10	5	1	3606	2	42.0	40.0	12.0	2.40	2.1
77	MEXA 10x10	5	1	3606	2	42.0	40.0	12.0	2.40	2.1
78	MEXA 10x10	5	1	3606	2	42.0	40.0	12.0	2.40	2.1
79	MEXA 10x10	5	1	3606	2	42.0	40.0	12.0	2.40	2.1
80	MEXA 10x10	5	1	3606	2	42.0	40.0	12.0	2.40	2.1
81	MEXA 10x10	5	1	3606	2	42.0	40.0	12.0	2.40	2.1
82	MEXA 10x10	5	1	3606	2	42.0	40.0	12.0	2.40	2.1
83	MEXA 10x10	5	1	3606	2	42.0	40.0	12.0	2.40	2.1
84	MEXA 8x8	4	1	4753	2	48.0	31.0	14.0	2.80	3.2
85	MEXA 8x8	4	1	4753	2	48.0	31.0	14.0	2.80	3.2
86	MEXA 8x8	4	1	4753	2	48.0	31.0	14.0	2.80	3.2

Table A5. General description of the laboratory observations used for the drawbar modeling and the associated principal tire characteristics

Test No.	Tire Characteristics		Tire Dimensions					Measurements		
	Description	δ/h percent	w lbf	d in.	b in.	h in.	delta in.	Slip %	CI psi	D/W
297	9.00-14 treadless bias ply	0.150	226	28.3	8.3	6.4	0.96	20	16	0.434
298	9.00-14 treadless bias ply	0.150	428	28.3	8.3	6.4	0.96	20	17	0.217
299	9.00-14 treadless bias ply	0.250	427	28.3	8.3	6.4	1.60	20	17	0.253
300	9.00-14 treadless bias ply	0.250	824	28.3	8.3	6.4	1.60	20	15	-0.108
301	9.00-14 treadless bias ply	0.150	617	28.3	8.3	6.4	0.96	20	14	0.073
303	9.00-14 treadless bias ply	0.150	440	28.3	8.3	6.4	0.96	20	49	0.590
304	9.00-14 treadless bias ply	0.150	227	28.3	8.3	6.4	0.96	20	29	0.643
305	9.00-14 treadless bias ply	0.150	456	28.3	8.3	6.4	0.96	20	28	0.333
306	9.00-14 treadless bias ply	0.150	645	28.3	8.3	6.4	0.96	20	27	0.278
307	9.00-14 treadless bias ply	0.150	857	28.3	8.3	6.4	0.96	20	29	0.158
308	9.00-14 treadless bias ply	0.150	238	28.3	8.3	6.4	0.96	20	51	1.088
310	9.00-14 treadless bias ply	0.250	446	28.3	8.3	6.4	1.60	20	32	0.610
311	9.00-14 treadless bias ply	0.250	860	28.3	8.3	6.4	1.60	20	34	0.280
312	9.00-14 treadless bias ply	0.250	441	28.3	8.3	6.4	1.60	20	51	0.973
313	9.00-14 treadless bias ply	0.150	650	28.3	8.3	6.4	0.96	20	52	0.540
314	9.00-14 treadless bias ply	0.350	230	28.3	8.3	6.4	2.24	20	52	1.130
390	9.00-14 treadless bias ply	0.350	445	28.3	8.3	6.4	2.24	20	41	0.903

Table A5. (continued)

Test No.	Tire Characteristics			Tire Dimensions					Measurements		
	Description	δ/h percent	w lbf	d in.	b in.	h in.	delta in.	Slip %	CI psi	D/W
408	9.00-14 treadless bias ply	0.350	447	28.3	8.3	6.4	2.24	20	24	0.698
409	9.00-14 treadless bias ply	0.350	649	28.3	8.3	6.4	2.24	20	23	0.365
410	9.00-14 treadless bias ply	0.350	447	28.3	8.3	6.4	2.24	20	52	1.072
411	9.00-14 treadless bias ply	0.350	674	28.3	8.3	6.4	2.24	20	52	0.868
412	9.00-14 treadless bias ply	0.350	656	28.3	8.3	6.4	2.24	20	39	0.587
413	9.00-14 treadless bias ply	0.350	878	28.3	8.3	6.4	2.24	20	40	0.429
414	9.00-14 treadless bias ply	0.350	232	28.3	8.3	6.4	2.24	20	52	1.487
415	9.00-14 treadless bias ply	0.350	872	28.3	8.3	6.4	2.24	20	57	0.712
416	9.00-14 treadless bias ply	0.350	860	28.3	8.3	6.4	2.24	20	25	0.181
417	9.00-14 treadless bias ply	0.350	230	28.3	8.3	6.4	2.24	20	24	1.035
418	9.00-14 treadless bias ply	0.150	872	28.3	8.3	6.4	0.96	20	55	0.298
419	9.00-14 treadless bias ply	0.250	892	28.3	8.3	6.4	1.60	20	51	0.429
363	4.00-7 treadless bias ply	0.150	111	14.1	4.2	3.1	0.47	20	49	0.658
364	4.00-7 treadless bias ply	0.250	114	14.1	4.2	3.1	0.78	20	42	0.974
365	4.00-7 treadless bias ply	0.150	235	14.1	4.2	3.1	0.47	20	43	0.226
366	4.00-7 treadless bias ply	0.250	101	14.1	4.2	3.1	0.78	20	60	0.733
367	4.00-7 treadless bias ply	0.250	219	14.1	4.2	3.1	0.78	20	60	0.416

Table A5. (continued)

Test No.	Tire Characteristics		Tire Dimensions					Measurements		
	Description	δ/h percent	w lbf	d in.	b in.	h in.	delta in.	Slip %	CI psi	D/W
368	4.00-7 treadless bias ply	0.150	101	14.1	4.2	3.1	0.47	20	42	0.406
370	4.00-7 treadless bias ply	0.250	234	14.1	4.2	3.1	0.78	20	40	0.449
371	4.00-7 treadless bias ply	0.150	100	14.1	4.2	3.1	0.47	20	25	0.250
372	4.00-7 treadless bias ply	0.250	102	14.1	4.2	3.1	0.78	20	25	0.373
373	4.00-7 treadless bias ply	0.150	343	14.1	4.2	3.1	0.47	20	37	0.152
374	4.00-7 treadless bias ply	0.250	336	14.1	4.2	3.1	0.78	20	41	0.196
375	4.00-7 treadless bias ply	0.150	440	14.1	4.2	3.1	0.47	20	42	0.093
376	4.00-7 treadless bias ply	0.250	437	14.1	4.2	3.1	0.78	20	38	-0.043
377	4.00-7 treadless bias ply	0.350	445	14.1	4.2	3.1	1.09	20	38	0.061
378	4.00-7 treadless bias ply	0.350	215	14.1	4.2	3.1	1.09	20	33	0.409
379	4.00-7 treadless bias ply	0.350	325	14.1	4.2	3.1	1.09	20	34	0.185
380	4.00-7 treadless bias ply	0.150	337	14.1	4.2	3.1	0.47	20	67	0.300
383	4.00-7 treadless bias ply	0.150	223	14.1	4.2	3.1	0.47	20	64	0.395
384	4.00-7 treadless bias ply	0.250	343	14.1	4.2	3.1	0.78	20	64	0.370
385	4.00-7 treadless bias ply	0.150	451	14.1	4.2	3.1	0.47	20	66	0.215
386	4.00-7 treadless bias ply	0.250	451	14.1	4.2	3.1	0.78	20	64	0.295
387	4.00-7 treadless bias ply	0.350	229	14.1	4.2	3.1	1.09	20	62	0.873

Table A5. (continued)

Tire Characteristics			Tire Dimensions					Measurements		
Test No.	Description	δ/h percent	w lbf	d in.	b in.	h in.	delta in.	Slip %	CI psi	D/W
388	4.00-7 treadless bias ply	0.350	337	14.1	4.2	3.1	1.09	20	61	0.599
389	4.00-7 treadless bias ply	0.350	451	14.1	4.2	3.1	1.09	20	67	0.443
269	4.00-20 treadless bias ply	0.150	205	28	4.2	3.2	0.48	20	21	0.214
270	4.00-20 treadless bias ply	0.250	206	28	4.2	3.2	0.80	20	23	0.388
271	4.00-20 treadless bias ply	0.150	407	28	4.2	3.2	0.48	20	18	0.120
272	4.00-20 treadless bias ply	0.250	388	28	4.2	3.2	0.80	20	18	0.116
273	4.00-20 treadless bias ply	0.150	444	28	4.2	3.2	0.48	20	45	0.340
274	4.00-20 treadless bias ply	0.250	442	28	4.2	3.2	0.80	20	47	0.425
275	4.00-20 treadless bias ply	0.150	219	28	4.2	3.2	0.48	20	48	0.557
276	4.00-20 treadless bias ply	0.250	233	28	4.2	3.2	0.80	20	51	0.781
277	4.00-20 treadless bias ply	0.350	209	28	4.2	3.2	1.12	20	44	1.086
278	4.00-20 treadless bias ply	0.350	428	28	4.2	3.2	1.12	20	46	0.636
279	4.00-20 treadless bias ply	0.150	219	28	4.2	3.2	0.48	20	33	0.351
280	4.00-20 treadless bias ply	0.250	221	28	4.2	3.2	0.80	20	34	0.484
281	4.00-20 treadless bias ply	0.250	648	28	4.2	3.2	0.80	20	44	0.261
282	4.00-20 treadless bias ply	0.350	645	28	4.2	3.2	1.12	20	43	0.283
283	4.00-20 treadless bias ply	0.350	235	28	4.2	3.2	1.12	20	30	0.587

Table A5. (continued)

Test No.	Tire Characteristics		Tire Dimensions					Measurements		
	Description	δ/h percent	w lbf	d in.	b in.	h in.	delta in.	Slip %	CI psi*	D/W
284	4.00-20 treadless bias ply	0.350	457	28	4.2	3.2	1.12	20	30	0.304
285	4.00-20 treadless bias ply	0.350	706	28	4.2	3.2	1.12	20	56	0.287
286	4.00-20 treadless bias ply	0.150	628	28	4.2	3.2	0.48	20	51	0.270
287	4.00-20 treadless bias ply	0.150	456	28	4.2	3.2	0.48	20	31	0.250
288	4.00-20 treadless bias ply	0.250	461	28	4.2	3.2	0.80	20	31	0.247
289	4.00-20 treadless bias ply	0.350	230	28	4.2	3.2	1.12	20	20	0.408
290	4.00-20 treadless bias ply	0.350	420	28	4.2	3.2	1.12	20	18	0.000
291	4.00-20 treadless bias ply	0.250	655	28	4.2	3.2	0.80	20	36	0.256
292	4.00-20 treadless bias ply	0.350	659	28	4.2	3.2	1.12	20	33	0.256
293	4.00-20 treadless bias ply	0.350	639	28	4.2	3.2	1.12	20	56	0.257
294	4.00-20 treadless bias ply	0.350	629	28	4.2	3.2	1.12	20	54	0.360
295	4.00-20 treadless bias ply	0.350	426	28	4.2	3.2	1.12	20	19	0.200
400	4.00-20 treadless bias ply	0.450	658	28	4.2	3.2	1.44	20	47	0.357
401	4.00-20 treadless bias ply	0.080	314	28	4.2	3.2	0.26	20	48	0.312
402	4.00-20 treadless bias ply	0.080	308	28	4.2	3.2	0.26	20	22	0.234
403	4.00-20 treadless bias ply	0.450	648	28	4.2	3.2	1.44	20	21	-0.003
321	6.00-16 treadless bias ply	0.150	241	28.3	6.6	5.3	0.80	20	19	0.346

Table A5. (continued)

Test No.	Tire Characteristics		Tire Dimensions					Measurements		
	Description	δ/h percent	w lbf	d in.	b in.	h in.	delta in.	Slip %	CI psi	D/W
322	6.00-16 treadless bias ply	0.250	243	28.3	6.6	5.3	1.33	20	20	0.463
323	6.00-16 treadless bias ply	0.150	231	28.3	6.6	5.3	0.80	20	64	0.696
324	6.00-16 treadless bias ply	0.250	239	28.3	6.6	5.3	1.33	20	60	0.958
325	6.00-16 treadless bias ply	0.150	429	28.3	6.6	5.3	0.80	20	22	0.158
326	6.00-16 treadless bias ply	0.250	438	28.3	6.6	5.3	1.33	20	21	0.176
327	6.00-16 treadless bias ply	0.150	629	28.3	6.6	5.3	0.80	20	21	-0.035
328	6.00-16 treadless bias ply	0.250	645	28.3	6.6	5.3	1.33	20	21	0.014
329	6.00-16 treadless bias ply	0.150	236	28.3	6.6	5.3	0.80	20	39	0.703
330	6.00-16 treadless bias ply	0.250	237	28.3	6.6	5.3	1.33	20	41	1.105
331	6.00-16 treadless bias ply	0.350	231	28.3	6.6	5.3	1.86	20	19	0.796
332	6.00-16 treadless bias ply	0.350	445	28.3	6.6	5.3	1.86	20	20	0.375
333	6.00-16 treadless bias ply	0.350	653	28.3	6.6	5.3	1.86	20	20	0.230
334	6.00-16 treadless bias ply	0.150	828	28.3	6.6	5.3	0.80	20	21	-0.010
335	6.00-16 treadless bias ply	0.250	848	28.3	6.6	5.3	1.33	20	20	-0.042
336	6.00-16 treadless bias ply	0.350	847	28.3	6.6	5.3	1.86	20	20	0.033
337	6.00-16 treadless bias ply	0.250	847	28.3	6.6	5.3	1.33	20	21	-0.053
338	6.00-16 treadless bias ply	0.250	683	28.3	6.6	5.3	1.33	20	22	0.060

Table A5. (continued)

Test No.	Tire Characteristics		Tire Dimensions					Measurements		
	Description	δ/h percent	w lbf	d in.	b in.	h in.	delta in.	Slip %	CI psi	D/W
339	6.00-16 treadless bias ply	0.150	676	28.3	6.6	5.3	0.80	20	40	0.250
340	6.00-16 treadless bias ply	0.250	658	28.3	6.6	5.3	1.33	20	36	0.296
341	6.00-16 treadless bias ply	0.350	677	28.3	6.6	5.3	1.86	20	37	0.478
342	6.00-16 treadless bias ply	0.350	239	28.3	6.6	5.3	1.86	20	36	1.389
343	6.00-16 treadless bias ply	0.350	460	28.3	6.6	5.3	1.86	20	38	0.704
344	6.00-16 treadless bias ply	0.150	891	28.3	6.6	5.3	0.80	20	39	0.150
345	6.00-16 treadless bias ply	0.250	887	28.3	6.6	5.3	1.33	20	39	0.202
346	6.00-16 treadless bias ply	0.350	886	28.3	6.6	5.3	1.86	20	41	0.322
351	6.00-16 treadless bias ply	0.150	455	28.3	6.6	5.3	0.80	20	58	0.508
354	6.00-16 treadless bias ply	0.250	657	28.3	6.6	5.3	1.33	20	51	0.502
355	6.00-16 treadless bias ply	0.350	235	28.3	6.6	5.3	1.86	20	52	1.514
356	6.00-16 treadless bias ply	0.350	443	28.3	6.6	5.3	1.86	20	53	0.952
357	6.00-16 treadless bias ply	0.250	455	28.3	6.6	5.3	1.33	20	48	0.725
359	6.00-16 treadless bias ply	0.150	876	28.3	6.6	5.3	0.80	20	52	0.246
360	6.00-16 treadless bias ply	0.250	864	28.3	6.6	5.3	1.33	20	51	0.314
361	6.00-16 treadless bias ply	0.350	844	28.3	6.6	5.3	1.86	20	48	0.487
362	6.00-16 treadless bias ply	0.250	710	28.3	6.6	5.3	1.33	20	48	0.401

APPENDIX B

SUMMARY OF ALL MODEL VARIANTS EXPLORED

DURING THE VCI_1 MODELING

Table B1. Quality comparison for all VCI_1 model variants

Model No.	Model Description	Degrees of Freedom	Standard Error (psi)	Adjusted R-squared
EXISTING COMPARISON MODELS				
C1 [a]	Standard NRMM Model: Mobility Index with Deflection Correction Factor (MI&DCF)	70, 69, 68, or 67	2.68	90.3
C2 [a]	Rowland's Mean Maximum Pressure (MMP_R)	73	2.91	88.5
C3 [a]	Larminie's Mean Maximum Pressure (MMP_L)	73	2.96	88.1
C4 [a]	Maclaurin's Mean Maximum Pressure (MMP_M)	74	3.01	87.7
PRELIMINARY NEW DEVELOPMENT MODELS				
P1	CPF	77	3.60	82.4
P2	CPF*DCF	76	2.79	89.4
P3	Hard Surface Contact Pressure Parameter (CPH)	77	2.91	88.5
P4	Soft Soil Contact Pressure Parameter (CPS)	77	3.50	83.3
P5	Modified CPH version 1: Replaced d with 3.876*h which originates from the correlation between d and h	76	3.29	85.3
P6	Modified CPH version 2: Assumed δ^2 is negligible in the contact length estimator	77	2.99	87.8
P7 [a]	Freitag's Clay Numeric cast in a VCI form ($N_{c(F)}^{VCI}$)	76	2.82	89.2
P8	Turnage's Clay Numeric cast in a VCI form ($N_{c(T)}^{VCI}$)	76	2.94	88.2
P9	Smith's Clay Numeric cast in a VCI form ($N_{c(S)}^{VCI}$)	75	2.93	88.4
P10	Maclaurin's Motion Resistance Numeric cast in a VCI form (N_{MR}^{VCI})	74	3.77	80.7
P11	Average Contact Pressure Parameter No. 1 (CP1)	77	2.66	90.4
P12	Modified CP1 version 0a: Used d/2 instead of $\frac{1}{2} LC_{zl}$	77	2.68	90.3
P13	Modified CP1 version 0b: Used $\sqrt{d(\delta + h_c) - (\delta + h_c)^2}$ instead of $\frac{1}{2} LC_{zl}$	77	2.66	90.4
PRINCIPAL NEW DEVELOPMENT MODELS				
1a	Modified MI&DCF Model: Optimized Curve Fit to Database	70, 69, 68, or 67	2.52	91.4
1b	Modified MI&DCF Model: Used CPF/10 instead of WF	69	2.80	89.4

Table B1. (continued)

Model No.	Model Description	Degrees of Freedom	Standard Error (psi)	Adjusted R-squared
1c	Modified MI&DCF Model: Used CPF/10 instead of WF and left out WLF	70	2.90	88.6
1d	Modified MI&DCF Model: Partially Optimized to Database (Curve Fits and WF only)	70, 69, 68, or 67	2.48	91.7
1e [a]	Modified MI&DCF Model: Fully Optimized to Database (GF and EF have no effect)	70, 69, 68, or 67	2.44	91.9
2	CP1 and m	75	2.65	90.4
3	Modified CP1 version 1: Empirical adjustments to the 3 parts of the contact length using 3 constants	74	2.69	90.2
4	Modified CP1 version 2: Empirical adjustment to the hard-surface deflection using a constant	76	2.67	90.3
5	CP1 with modified TF (product)	76	2.64	90.5
6	CP1 and w	75	2.69	90.2
7	CP1 and Aspect Ratio (h/b)	75	2.54	91.2
8	Modified CP1 version 3: Empirical adjustment to the contact area using aspect ratio	76	2.50	91.5
9	$CP1\frac{1}{3}$ with modified TF (product)	75	2.46	91.8
10	Modified CP1 version 4: Empirical adjustment to the contact area using d/b	76	2.52	91.3
11	Modified CP1 version 5: Empirical adjustment to the contact area using h/d	76	2.66	90.4
12a	Modified CP1 version 6a: Empirical adjustment to the contact area using h/b, d/b, and h/d	74	2.52	91.4
12b	Modified CP1 version 6b: Empirical adjustment to the contact area using h/b and d/b	75	2.50	91.5
13	Modified CP1 version 7: Empirical adjustment to the contact area using a constant and h/b	76	2.50	91.5
14	Modified CP1 version 8: Empirical adjustments to (1) the additional contact length due to sinkage using a constant and (2) the contact area using aspect ratio	75	2.47	91.7
15	Modified CP1 version 9: Empirical adjustments to (1) $\frac{1}{2} LC_{z1}$ using a constant and (2) $\sqrt{d\delta - \delta^2}$ using aspect ratio	75	2.48	91.7

Table B1. (continued)

Model No.	Model Description	Degrees of Freedom	Standard Error (psi)	Adjusted R-squared
16	Modified CP1 version 10: Empirical adjustments to (1) the additional contact length due to sinkage using a constant and (2) $\sqrt{d\delta - \delta^2}$ using aspect ratio	75	2.47	91.7
17	Modified CP1 version 11: Empirical adjustments to (1) $2\sqrt{d\delta - \delta^2}$ using a constant, (2) the additional contact length due to sinkage using a constant, and (3) the contact area using aspect ratio	74	2.49	91.6
18	Modified CP1 version 12: Removed 1/m and made empirical adjustments to (1) $2\sqrt{d\delta - \delta^2}$ using a constant, (2) the additional contact length due to sinkage using a constant, and (3) the contact area using aspect ratio	74	2.50	91.5
19	Modified CP1 version 13: Empirical adjustments to (1) the two parts of the additional contact length due to sinkage using constants and (2) the contact area using aspect ratio	74	2.48	91.6
20	$CP1_8'$ and Tire Construction Factor (TCF)	74	2.40	92.1
21	Modified CP1 version 14: Empirical adjustments to (1) the additional contact length due to sinkage using a constant and (2) the contact area using aspect ratio and TCF	74	2.42	92.1
22	$CP1_8'$ with modified TF (product) and TCF	73	2.42	92.1
23	$CP1_8'$ and modified TCF [Form 1]	73	2.41	92.1
24	CPI_8' and modified TCF [Form 2]	73	2.39	92.3
25	CPI_8' and h/b	73	2.50	91.5
26	CPH and modified CPS version 1: Included 1/m in CPS	76	2.62	90.7
27	Modified CPH version 3 and modified CPS version 2: Included 1/m in CPS and made empirical adjustment to both hard surface and soft soil parameter contact areas using aspect ratio	74	2.47	91.7
28	Modified CPH version 3 and modified CPS version 3: Empirical adjustment to both hard surface and soft soil parameter contact areas using aspect ratio	74	2.51	91.4
29	Numeric version 1: MMP style numeric with constraint for pressure units	75	2.65	90.5
30	Numeric version 2: MMP style numeric without the constraint for pressure units	74	2.53	91.3

Table B1. (continued)

Model No.	Model Description	Degrees of Freedom	Standard Error (psi)	Adjusted R-squared
31a	Numeric version 3a: Numeric using bd and 4 dimensionless ratios of tire variables [b/d, d/h, δ/d, and h/b] which allows inclusion of b, d, h, and δ with optimal exponents under the constraint of pressure units	73	2.53	91.3
31b	Numeric version 3b: Numeric using bd and 3 dimensionless ratios of tire variables [b/d, d/h, and δ/d] which allows inclusion of b, d, h, and δ with optimal exponents under the constraint of pressure units	74	2.51	91.4
32	Modified CP1 version 15 and TCF: Empirical adjustments to (1) $\sqrt{d\delta - \delta^2}$ using a constant and (2) the contact area using aspect ratio	74	2.39	92.2
33	Modified CP1 version 16 and TCF: Empirical adjustments to (1) $2\sqrt{d\delta - \delta^2}$ using a constant, (2) the $\sqrt{d\delta - \delta^2}$ part of the additional contact length due to sinkage using a constant, and (3) the contact area using aspect ratio	73	2.41	92.1
34	Modified CP1 version 17 and TCF: Empirical adjustments to (1) $\sqrt{d\delta - \delta^2}$ using a constant, (2) the additional contact length due to sinkage using a constant, and (3) the contact area using aspect ratio	73	2.41	92.1
35	Modified CP1 version 18 and TCF: Empirical adjustments to (1) $\sqrt{d\delta - \delta^2}$ using a constant, (2) $\frac{1}{2}LC_{z1}$ using a constant, and (3) the contact area using aspect ratio	73	2.41	92.1
36 [a]	Modified CP1 version 19 and TCF: Empirical adjustments to (1) $\frac{1}{2}LC_{z1}$ using a constant and (2) the contact area using aspect ratio	74	2.39	92.2
37	Modified CP1 version 20 and TCF: Empirical adjustments to (1) the additional contact length due to sinkage using a constant, (2) $\frac{1}{2}LC_{z1}$ using a constant, and (3) the contact area using aspect ratio	73	2.40	92.2
38	Modified CP1 version 21 and TCF: Replaced $\frac{1}{2}LC_{z1}$ with $c_1 d/2$ and made an empirical adjustment to the contact area using aspect ratio	74	2.39	92.2
39	Modified CP1 version 22 and TCF: Replaced $\frac{1}{2}LC_{z1}$ with $\frac{1}{2}LC_{z3}$ (i.e., changed z from h_c to $c_1 d$) and made an empirical adjustment to the contact area using aspect ratio	74	2.40	92.2
40	Modified CP1 version 23 and TCF: Replaced $\frac{1}{2}LC_{z1}$ with $\frac{1}{2}LC_{z4}$ (i.e., changed z from h_c to $c_1 h$) and made an empirical adjustment to the contact area using aspect ratio	74	2.40	92.2

Table B1. (continued)

Model No.	Model Description	Degrees of Freedom	Standard Error (psi)	Adjusted R-squared
41	Modified CP1 version 24 and TCF: Replaced $\frac{1}{2} LC_{z1}$ with $\frac{1}{2} LC_{z5}$ (i.e., changed z from h_c to $\frac{1}{4} d$) and made empirical adjustments to (1) the additional contact length due to sinkage using a constant and (2) the contact area using aspect ratio	73	2.42	92.0
42	Modified CP1 version 25 and TCF: Replaced $\frac{1}{2} LC_{z1}$ with $\frac{1}{2} LC_{z3}$ (i.e., changed z from h_c to $c_1 d$) and made empirical adjustments to (1) $\sqrt{d\delta - \delta^2}$ using a constant and (2) the contact area using aspect ratio	73	2.41	92.1
43	Modified CP1 version 26 and TCF: Replaced $\frac{1}{2} LC_{z1}$ with $\frac{1}{2} LC_{z3}$ (i.e., changed z from h_c to $c_1 d$) and made an empirical adjustment to $\sqrt{d\delta - \delta^2}$ using aspect ratio	74	2.40	92.2
44	Modified CP1 version 27 and TCF: Replaced $\frac{1}{2} LC_{z1}$ with $\frac{1}{2} LC_{z3}$ (i.e., changed z from h_c to $c_1 d$) and made empirical adjustments to (1) the additional contact length due to sinkage using a constant and (2) $\sqrt{d\delta - \delta^2}$ using aspect ratio	73	2.40	92.1
45	Modified CP1 version 28 and TCF: Removed 1/m, replaced $\frac{1}{2} LC_{z1}$ with $\frac{1}{2} LC_{z3}$ (i.e., changed z from h_c to $c_1 d$), and made empirical adjustments to (1) the additional contact length due to sinkage using a constant and (2) $\sqrt{d\delta - \delta^2}$ using aspect ratio	73	2.40	92.2
46	CPH_3' and TCF	75	2.62	90.7
47	CPS_3' and TCF	75	3.15	86.5
48 [a]	Modified Average Contact Pressure Parameter No. 2 (CP2) version 1 and TCF: Used $c_1 d$ for internal length adjustment and made empirical adjustment to the contact area using aspect ratio	74	2.37	92.4
49	Modified CP2 version 2 and TCF: Split the contact length into 2 parts and simplified the adjustment/correction part to $c_1 d$	74	2.39	92.3
50	Recast $CP2_1'$ and TCF: Split the contact length into 2 parts	74	2.37	92.4
51 [a]	N_{3b} and TCF	73	2.40	92.2

[a] - These models were discussed in the main text

VCI$_1$ Model C1
Standard NRMM Model: Mobility Index with Deflection Correction Factor (MI&DCF)

$$MI = \left(\frac{CPF\ WF}{TEF\ GF} + WLF - CF \right)(EF)(TF)$$

where $CPF = \dfrac{w}{0.5\,n\,d\,b}$

$WF = c_{WF1}\,(w/1000) + c_{WF2}$

where

$w < 2{,}000\ lbf$	$\Rightarrow$	$c_{WF1} = 0.553$	and	$c_{WF2} = 0$
$2{,}000 \le w < 13{,}500\ lbf$	$\Rightarrow$	$c_{WF1} = 0.033$	and	$c_{WF2} = 1.050$
$13{,}500 \le w < 20{,}000\ lbf$	$\Rightarrow$	$c_{WF1} = 0.142$	and	$c_{WF2} = -0.420$
$20{,}000 \le w$	$\Rightarrow$	$c_{WF1} = 0.278$	and	$c_{WF2} = -3.115$

$TEF = \dfrac{10 + b}{100}$

$GF = 1 + 0.05\,c_{GF}$ where $c_{GF} = 1$ if tire chains are used or 0 if not

$WLF = \dfrac{w}{2000}$

$CF = \dfrac{h_c}{10}$

$EF = 1 + 0.05\,c_{EF}$ where $c_{EF} = 1$ if $PWR < 10$ hp/ton or 0 if not

$TF = 1 + 0.05\,c_{TF}$ where $c_{TF} = 1$ if manual transmission or 0 if automatic

$$\therefore MI = \left(\frac{w}{0.5\,n\,d\,b(0.10 + 0.01b)}\ \frac{c_{WF1}\,(w/1000) + c_{WF2}}{1 + 0.05\,c_{GF}} + \frac{w}{2000} - \frac{h_c}{10} \right)\left(1 + 0.05\,c_{EF}\right)\left(1 + 0.05\,c_{TF}\right)$$

$$DCF = \left(\frac{0.15}{\delta/h} \right)^{0.25}$$

$VCI_1 = f(MI, DCF)$

where $MI \le 115$ $\Rightarrow$ $f(MI, DCF) = \left(11.48 + 0.2\,MI - \dfrac{39.2}{MI + 3.74} \right) DCF$

$MI > 115$ $\Rightarrow$ $f(MI, DCF) = \left(4.1\,MI^{0.446} \right) DCF$

VCI$_1$ Model C2
Rowland's Mean Maximum Pressure (MMP$_R$)

$$MMP_R = \frac{0.97\,K\,GVW}{n\,m\,b^{0.85}\,d^{1.15}\,\sqrt{\delta/h}}$$

where for all-drive vehicles $m = 2 \Rightarrow K = 3.66$ $m = 3 \Rightarrow K = 3.90$

$m = 4 \Rightarrow K = 4.10$ $m = 5 \Rightarrow K = 4.32$

$$VCI_1 = 3.65 + 0.477\,MMP_R$$

VCI$_1$ Model C3
Larminie's Mean Maximum Pressure (MMP$_L$)

$$MMP_L = \frac{0.97\,K'\,GVW}{n\,m\,b^{0.85}\,d^{1.15}\,\sqrt{\delta/d}}$$

where for all-drive vehicles $m = 2 \Rightarrow K' = 1.83$ $m = 3 \Rightarrow K' = 1.95$

$m = 4 \Rightarrow K' = 2.05$ $m = 5 \Rightarrow K' = 2.16$

$$VCI_1 = 3.68 + 0.480\,MMP_L$$

VCI$_1$ Model C4
Maclaurin's Mean Maximum Pressure (MMP$_M$)

$$MMP_M = \frac{GVW}{n\,m\,b^{0.8}\,d^{0.8}\,\delta^{0.4}}$$

$$VCI_1 = 2.53 + 1.35\,MMP_M$$

VCI$_1$ Model P1
CPF

$$CPF = \frac{w}{\frac{1}{2}\,n\,d\,b}$$

$$VCI_1 = 4.61 + 1.45\,CPF$$

VCI$_1$ Model P2
CPF*DCF

$$CPF*DCF = \frac{w}{\frac{1}{2}\,n\,d\,b}\left(\frac{0.15}{\delta/h}\right)^{0.25}$$

$$\therefore CPF*DCF = \frac{1.245\,w}{n\,d\,b\,(\delta/h)^{0.25}}$$

$$VCI_1 = 3.14 + 1.79\,(CPF*DCF)$$

VCI$_1$ Model P3
Hard Surface Contact Pressure Parameter (CPH)

$$CPH = \frac{w}{2\,n\,b\,\sqrt{d\,\delta - \delta^2}}$$

$$VCI_1 = 3.12 + 1.53\,CPH$$

VCI$_1$ Model P4
Soft Soil Contact Pressure Parameter (CPS)

$$CPS = \frac{w}{n\,b\,LC_{z1}}$$

$$\text{where}\quad h_c < \frac{d}{2} - \delta \quad\Rightarrow\quad LC_{z1} = 2\sqrt{d(\delta + h_c) - (\delta + h_c)^2}$$

$$h_c \geq \frac{d}{2} - \delta \quad\Rightarrow\quad LC_{z1} = d$$

$$VCI_1 = 4.83 + 2.75\,CPS$$

VCI$_1$ Model P5
Modified CPH version 1: Replaced d with 3.876*h which originates from the correlation between d and h

$$CPH_1' = \frac{w}{2\,n\,b\,\sqrt{3.876\,h\,\delta - \delta^2}}$$

$$VCI_1 = 3.67 + 1.46\,CPH_1'$$

VCI$_1$ Model P6
Modified CPH version 2: Assumed δ^2 is negligible in the contact length estimator

$$CPH_2' = \frac{w}{2\,n\,b\,\sqrt{d\,\delta}}$$

$$VCI_1 = 3.26 + 1.57\,CPH_2'$$

VCI$_1$ Model P7
Freitag's Clay Numeric cast in a VCI form ($N_{c(F)}^{VCI}$)

$$N_{c(F)}^{VCI} = \frac{w}{n\,b\,d}\left(\frac{\delta}{h}\right)^{-1/2}$$

$$\therefore N_{c(F)}^{VCI} = \frac{w}{n\,b\,d\,\sqrt{\delta/h}}$$

$$VCI_1 = 2.99 + 1.58\,N_{c(F)}^{VCI}$$

VCI₁ Model P8
Turnage's Clay Numeric cast in a VCI form $(N_{c(T)}^{VCI})$

$$N_{c(T)}^{VCI} = \frac{w}{n\,b\,d}\left(\frac{\delta}{h}\right)^{-1/2}\left(1 + \frac{b}{2\,d}\right)$$

$$\therefore\ N_{c(T)}^{VCI} = \frac{w}{n\,b\,d\,\sqrt{\delta/h}}\left(1 + \frac{b}{2\,d}\right)$$

$$VCI_1 = 2.44 + 1.40\,N_{c(T)}^{VCI}$$

VCI₁ Model P9
Smith's Clay Numeric cast in a VCI form $(N_{c(S)}^{VCI})$

$$N_{c(S)}^{VCI} = \frac{w}{n\,b\,d}\left(1 - \frac{\delta}{h}\right)^{3/2}\left(1 + \frac{b}{d}\right)^{3/4}$$

$$VCI_1 = 3.09 + 4.09\,N_{c(S)}^{VCI}$$

VCI₁ Model P10
Maclaurin's Motion Resistance Numeric cast in a VCI form (N_{MR}^{VCI})

$$N_{MR}^{VCI} = \frac{W}{n\,m\,b^{0.5}\,d^{0.95}\,\delta^{0.55}}$$

$$VCI_1 = 2.30 + 1.26\,N_{MR}^{VCI}$$

VCI₁ Model P11
Average Contact Pressure Parameter No. 1 (CP1)

$$CP1 = \frac{w}{n\,b\left[2\sqrt{d\,\delta - \delta^2} + 1/m\left(\tfrac{1}{2}LC_{z1} - \sqrt{d\,\delta - \delta^2}\right)\right]}$$

$$VCI_1 = 4.19 + 1.70\,CP1$$

VCI$_1$ Model P12

Modified CP1 version 0a: Used d/2 instead of ½ LC_{zI}

$$CP1'_{0a} = \frac{w}{n\,b\left[2\sqrt{d\,\delta - \delta^2} + 1/m\left(d/2 - \sqrt{d\,\delta - \delta^2}\right)\right]}$$

$$VCI_1 = 4.13 + 1.73\,CP1'_{0a}$$

VCI$_1$ Model P13

Modified CP1 version 0b: Used $\sqrt{d(\delta + h_c) - (\delta + h_c)^2}$ instead of ½ LC_{zI}

$$CP1'_{0b} = \frac{w}{n\,b\left[2\sqrt{d\,\delta - \delta^2} + 1/m\left(\sqrt{d(\delta + h_c) - (\delta + h_c)^2} - \sqrt{d\,\delta - \delta^2}\right)\right]}$$

$$VCI_1 = 4.18 + 1.70\,CP1'_{0b}$$

VCI$_1$ Model 1a

Modified MI&DCF Model: Optimized Curve Fit to Database

$$MI = \left(\frac{w}{0.5\,n\,d\,b\,(0.10 + 0.01b)}\,\frac{c_{WF1}\,(w/1000) + c_{WF2}}{1 + 0.05\,c_{GF}} + \frac{w}{2000} - \frac{h_c}{10}\right)\left(1 + 0.05\,c_{EF}\right)\left(1 + 0.05\,c_{TF}\right)$$

$$DCF'_a = \left(\frac{0.15}{\delta/h}\right)^{0.29}$$

$$VCI_1 = f(MI, DCF'_a)$$

$$where \quad MI \leq 115 \quad \rightarrow \quad f(MI, DCF'_a) = \left(9.95 + 0.232\,MI - \frac{39.1}{MI + 4.49}\right)DCF'_a$$

$$MI > 115 \quad \rightarrow \quad f(MI, DCF'_a) = \left(7.80\,MI^{0.324}\right)DCF'_a$$

VCI$_1$ Model 1b
Modified MI&DCF Model: Used CPF/10 instead of WF

$$MI_b' = \left(\frac{CPF^2}{10 \, TEF \, GF} + WLF - CF \right)(EF)(TF)$$

$$\therefore MI_b' = \left(\frac{w^2}{2.5 \, n^2 \, d^2 \, b^2 \, (0.10 + 0.01b)} \, \frac{1}{1 + 0.05 \, c_{GF}} + \frac{w}{2000} - \frac{h_c}{10} \right) \left(1 + 0.05 \, c_{EF} \right) \left(1 + 0.05 \, c_{TF} \right)$$

$$DCF_b' = \left(\frac{0.15}{\delta/h} \right)^{0.28}$$

$$VCI_1 = \left(42.4 + 0.074 \, MI_b' - \frac{3890}{MI_b' + 110} \right) DCF_b'$$

VCI$_1$ Model 1c
Modified MI&DCF Model: Used CPF/10 instead of WF and left out WLF

$$MI_c' = \left(\frac{CPF^2}{10 \, TEF \, GF} - CF \right)(EF)(TF)$$

$$\therefore MI_c' = \left(\frac{w^2}{2.5 \, n^2 \, d^2 \, b^2 \, (0.10 + 0.01b)} \, \frac{1}{1 + 0.05 \, c_{GF}} - \frac{h_c}{10} \right) \left(1 + 0.05 \, c_{EF} \right) \left(1 + 0.05 \, c_{TF} \right)$$

$$DCF_c' = \left(\frac{0.15}{\delta/h} \right)^{0.26}$$

$$VCI_1 = \left(26.5 + 0.122 \, MI_c' - \frac{1120}{MI_c' + 58.8} \right) DCF_c'$$

VCI$_1$ Model 1d
Modified MI&DCF Model: Partially Optimized to Database (WF only)

$$MI'_d = \left(\frac{CPF\ WF'_d}{TEF\ GF} + WLF - CF \right) (EF)\,(TF)$$

$$WF'_d = c_{WF1}\,(w/1000) + c_{WF2}$$

where
$$w < 2{,}338\ lbf \quad \rightarrow \quad c_{WF1} = 0.467 \quad and \quad c_{WF2} = \quad 0$$

$$2{,}338 \le w < 12{,}564\ lbf \quad \rightarrow \quad c_{WF1} = 0.044 \quad and \quad c_{WF2} = \quad 0.988$$

$$12{,}564 \le w \quad \rightarrow \quad c_{WF1} = 0.093 \quad and \quad c_{WF2} = \quad 0.372$$

$$\therefore MI'_d = \left(\frac{w}{0.5\,n\,d\,b\,(0.10 + 0.01b)}\ \frac{c_{WF1}\,(w/1000) + c_{WF2}}{1 + 0.05\,c_{GF}} + \frac{w}{2000} - \frac{h_c}{10} \right)\left(1 + 0.05\,c_{EF}\right)\left(1 + 0.05\,c_{TF}\right)$$

$$DCF'_d = \left(\frac{0.15}{\delta/h} \right)^{0.31}$$

$$VCI_1 = f(MI'_d, DCF'_d)$$

where $MI'_d \le 115 \quad \rightarrow \quad f(MI'_d, DCF'_d) = \left(10.2 + 0.223\,MI'_d - \dfrac{28.1}{MI'_d + 2.62} \right) DCF'_d$

$$MI'_d > 115 \quad \rightarrow \quad f(MI'_d, DCF'_d) = \left(3.21\,MI'^{\,0.507}_d \right) DCF'_d$$

VCI₁ Model 1e
Modified MI&DCF Model: Fully Optimized to Database (GF and EF have no effect)

$$MI'_e = \left(\frac{CPF \; WF'_e}{TEF'_e \; GF} + WLF'_e - CF'_e \right)(EF)\,(TF'_e)$$

$$WF'_e = c_{WF1}\,(w/1000) + c_{WF2}$$

where $\quad w < 2{,}338 \; lbf \quad \rightarrow \quad c_{WF1} = 0.467 \quad and \quad c_{WF2} = \quad 0$

$\qquad\qquad 2{,}338 \leq w < 12{,}564 \; lbf \quad \rightarrow \quad c_{WF1} = 0.044 \quad and \quad c_{WF2} = \quad 0.988$

$\qquad\qquad 12{,}564 \leq w \qquad\qquad \rightarrow \quad c_{WF1} = 0.093 \quad and \quad c_{WF2} = \quad 0.372$

$$TEF'_e = \frac{8.3 + 1.13\,b}{100}$$

$$WLF'_e = \frac{w}{2000}$$

$$CF'_e = \frac{h_c}{6.9}$$

$$TF'_e = 1 + 0.10\,c_{TF} \qquad where \quad c_{TF} = 1 \; if \; manual \; transmission \; or \; 0 \; if \; automatic$$

$$\therefore MI'_e = \left(\frac{w}{0.5\,n\,d\,b\,(0.083 + 0.0113\,b)} \; \frac{c_{WF1}\,(w/1000) + c_{WF2}}{1 + 0.05\,c_{GF}} + \frac{w}{2000} - \frac{h_c}{6.9} \right)\left(1 + 0.05\,c_{EF}\right)\left(1 + 0.10\,c_{TF}\right)$$

$$DCF'_e = \left(\frac{0.15}{\delta/h} \right)^{0.30}$$

$$VCI_1 = f(MI'_e, DCF'_e)$$

$$where \quad MI'_e \leq 115 \quad \rightarrow \quad f(MI'_e, DCF'_e) = \left(10.2 + 0.222\,MI'_e - \frac{28.1}{MI'_e + 2.62} \right)DCF'_e$$

$$MI'_e > 115 \quad \rightarrow \quad f(MI'_e, DCF'_e) = \left(3.216\,MI'^{\,0.506}_e \right)DCF'_e$$

VCI₁ Model 2
CP1 and m

$$VCI_1 = 4.19 + 1.68\,CP1 + 0.000166\,m^6$$

VCI$_1$ Model 3
Modified CP1 version 1: Empirical adjustments to the 3 parts of the contact length using 3 constants

$$CPI_1' = \frac{w}{nb\left[c_1 2\sqrt{d\delta - \delta^2} + 1/m\left(c_2 \frac{1}{2}LC_{z1} - c_3\sqrt{d\delta - \delta^2}\right)\right]}$$

Numerical Optimization yields $c_1 = 1.6$, $c_2 = 1.1$, $c_3 = 0.26$

$$\therefore CPI_1' = \frac{w}{nb\left[3.2\sqrt{d\delta - \delta^2} + 1/m\left(0.55LC_{z1} - 0.26\sqrt{d\delta - \delta^2}\right)\right]}$$

$$VCI_1 = 4.19 + 2.80\, CPI_1'$$

VCI$_1$ Model 4
Modified CP1 version 2: Empirical adjustment to the hard-surface deflection using a constant

$$CPI_2' = \frac{w}{nb\left[2\sqrt{dc_1\delta - (c_1\delta)^2} + 1/m\left(\frac{1}{2}LC_{z2} - \sqrt{dc_1\delta - (c_1\delta)^2}\right)\right]}$$

$$\text{where } h_c < \frac{d}{2} - c_1\delta \quad \rightarrow \quad LC_{z2} = 2\sqrt{d(c_1\delta + h_c) - (c_1\delta + h_c)^2}$$

$$h_c \geq \frac{d}{2} - c_1\delta \quad \rightarrow \quad LC_{z2} = d$$

Numerical Optimization yields $c_1 = 1.1$

$$\therefore CPI_2' = \frac{w}{nb\left[2\sqrt{1.1d\delta - 1.2\delta^2} + 1/m\left(\frac{1}{2}LC_{z2} - \sqrt{1.1d\delta - 1.2\delta^2}\right)\right]}$$

$$\text{where } h_c < \frac{d}{2} - 1.1\delta \quad \rightarrow \quad LC_{z2} = 2\sqrt{d(1.1\delta + h_c) - (1.1\delta + h_c)^2}$$

$$h_c \geq \frac{d}{2} - 1.1\delta \quad \rightarrow \quad LC_{z2} = d$$

$$VCI_1 = 4.11 + 1.77\, CPI_2'$$

VCI$_1$ Model 5
CP1 with modified TF (product)

$$TF'_{MS} = 1 + c_1 c_{TF} \qquad \text{where} \quad c_{TF} = 1 \text{ if manual transmission or } 0 \text{ if automatic}$$

Numerical Optimization yields $c_1 = 0.05$

$$\therefore TF'_{MS} = 1 + 0.05\, c_{TF}$$

$$VCI_1 = 3.81 + 1.71\left(CP1\, TF'_{MS}\right)$$

VCI$_1$ Model 6
CP1 and w

$$VCI_1 = 4.05 + 1.74\, CP1 - 0.0081\left(\frac{w}{1000}\right)^{1.6}$$

VCI$_1$ Model 7
CP1 and Aspect Ratio (h/b)

$$VCI_1 = 3.78 + 1.58\, CP1 + 5.24\left(\frac{h}{b}\right)^{5.6}$$

VCI$_1$ Model 8
Modified CP1 version 3: Empirical adjustment to the contact area using aspect ratio

$$CP1'_3 = \frac{w}{n\, b\left[2\sqrt{d\delta - \delta^2} + 1/m\left(\tfrac{1}{2}LC_{z1} - \sqrt{d\delta - \delta^2}\right)\right](h/b)^{p_1}}$$

Numerical Optimization yields $p_1 = -0.46$

$$\therefore CP1'_3 = \frac{w}{n\, b\left[2\sqrt{d\delta - \delta^2} + 1/m\left(\tfrac{1}{2}LC_{z1} - \sqrt{d\delta - \delta^2}\right)\right](b/h)^{0.46}}$$

$$VCI_1 = 5.10 + 1.79\, CP1'_3$$

VCI₁ Model 9

CP1′₃ with modified TF (product)

$$CP1_3' = \frac{w}{n\,b\left[2\sqrt{d\delta - \delta^2} + 1/m\left(\frac{1}{2}LC_{z1} - \sqrt{d\delta - \delta^2}\right)\right](h/b)^{p_1}}$$

$$TF_{M9}' = 1 + c_1 c_{TF} \qquad \text{where} \quad c_{TF} = 1 \; \textit{if manual transmission or } 0 \textit{ if automatic}$$

Numerical Optimization yields $p_1 = -0.47$ and $c_1 = 0.06$

$$\therefore CP1_3' = \frac{w}{n\,b\left[2\sqrt{d\delta - \delta^2} + 1/m\left(\frac{1}{2}LC_{z1} - \sqrt{d\delta - \delta^2}\right)\right](b/h)^{0.47}}$$

$$TF_{M9}' = 1 + 0.06\,c_{TF}$$

$$VCI_1 = 4.72 + 1.79\left(CP1_3'\,TF_{M9}'\right)$$

VCI₁ Model 10

Modified CP1 version 4: Empirical adjustment to the contact area using d/b

$$CP1_4' = \frac{w}{n\,b\left[2\sqrt{d\delta - \delta^2} + 1/m\left(\frac{1}{2}LC_{z1} - \sqrt{d\delta - \delta^2}\right)\right](d/b)^{p_1}}$$

Numerical Optimization yields $p_1 = -0.49$

$$\therefore CP1_4' = \frac{w}{n\,b\left[2\sqrt{d\delta - \delta^2} + 1/m\left(\frac{1}{2}LC_{z1} - \sqrt{d\delta - \delta^2}\right)\right](b/d)^{0.49}}$$

$$VCI_1 = 5.09 + 0.917\,CP1_4'$$

VCI$_1$ Model 11
Modified CP1 version 5: Empirical adjustment to the contact area using h/d

$$CP1_5' = \frac{w}{n b \left[2\sqrt{d\delta - \delta^2} + 1/m\left(\frac{1}{2}LC_{z1} - \sqrt{d\delta - \delta^2}\right)\right](h/d)^{P_1}}$$

Numerical Optimization yields $p_1 = -0.24$

$$\therefore CP1_5' = \frac{w}{n b \left[2\sqrt{d\delta - \delta^2} + 1/m\left(\frac{1}{2}LC_{z1} - \sqrt{d\delta - \delta^2}\right)\right](d/h)^{0.24}}$$

$VCI_1 = 4.20 + 2.37\, CP1_5'$

VCI$_1$ Model 12a
Modified CP1 version 6a: Empirical adjustment to the contact area using h/b, d/b, and h/d

$$CP1_{6a}' = \frac{w}{n b \left[2\sqrt{d\delta - \delta^2} + 1/m\left(\frac{1}{2}LC_{z1} - \sqrt{d\delta - \delta^2}\right)\right](h/b)^{P_1}(d/b)^{P_2}(h/d)^{P_3}}$$

Numerical Optimization yields $p_1 = -0.29$, $p_2 = -0.24$, *and* $p_3 = -0.05$

$$\therefore CP1_{6a}' = \frac{w}{n b \left[2\sqrt{d\delta - \delta^2} + 1/m\left(\frac{1}{2}LC_{z1} - \sqrt{d\delta - \delta^2}\right)\right]\left(\frac{b^{0.53}}{h^{0.34}d^{0.19}}\right)}$$

$VCI_1 = 5.20 + 1.39\, CP1_{6a}'$

VCI$_1$ Model 12b
Modified CP1 version 6b: Empirical adjustment to the contact area using h/b and d/b

$$CP1_{6b}' = \frac{w}{n b \left[2\sqrt{d\delta - \delta^2} + 1/m\left(\frac{1}{2}LC_{z1} - \sqrt{d\delta - \delta^2}\right)\right](h/b)^{P_1}(d/b)^{P_2}}$$

Numerical Optimization yields $p_1 = -0.34$, *and* $p_2 = -0.20$

$$\therefore CP1_{6b}' = \frac{w}{n b \left[2\sqrt{d\delta - \delta^2} + 1/m\left(\frac{1}{2}LC_{z1} - \sqrt{d\delta - \delta^2}\right)\right]\left(\frac{b^{0.54}}{h^{0.34}d^{0.20}}\right)}$$

$VCI_1 = 5.20 + 1.37\, CP1_{6b}'$

VCI$_1$ Model 13

Modified CP1 version 7: Empirical adjustment to the contact area using a constant and h/b

$$CPI_7' = \frac{w}{n\,c_1 b\left[2\sqrt{d\delta - \delta^2} + 1/m\left(\frac{1}{2}LC_{z1} - \sqrt{d\delta - \delta^2}\right)\right](h/b)^{P_1}}$$

Numerical Optimization yields $c_1 = 1$ *and* $p_1 = -0.46$

$$\therefore CPI_7' = \frac{w}{n\,b\left[2\sqrt{d\delta - \delta^2} + 1/m\left(\frac{1}{2}LC_{z1} - \sqrt{d\delta - \delta^2}\right)\right](b/h)^{0.46}}$$

$$VCI_1 = 5.10 + 1.79\,CPI_7'$$

VCI$_1$ Model 14

Modified CP1 version 8: Empirical adjustments to (1) the additional contact length due to sinkage using a constant and (2) the contact area using aspect ratio

$$CPI_8' = \frac{w}{n\,b\left[2\sqrt{d\delta - \delta^2} + c_1(1/m)\left(\frac{1}{2}LC_{z1} - \sqrt{d\delta - \delta^2}\right)\right](h/b)^{P_1}}$$

Numerical Optimization yields $c_1 = 0.59$ *and* $p_1 = -0.50$

$$\therefore CPI_8' = \frac{w}{n\,b\left[2\sqrt{d\delta - \delta^2} + 0.59/m\left(\frac{1}{2}LC_{z1} - \sqrt{d\delta - \delta^2}\right)\right](b/h)^{0.50}}$$

$$VCI_1 = 4.76 + 1.73\,CPI_8'$$

VCI$_1$ Model 15

Modified CP1 version 9: Empirical adjustments to (1) $\frac{1}{2} LC_{zi}$ using a constant and (2) $\sqrt{d\delta - \delta^2}$ using aspect ratio

$$CP1_9' = \frac{w}{n\, b \left[2\sqrt{d\delta - \delta^2}\, (h/b)^{p_1} + 1/m \left(c_1 \frac{1}{2} LC_{zi} - \sqrt{d\delta - \delta^2}\, (h/b)^{p_1} \right) \right]}$$

Numerical Optimization yields $c_1 = 0.79$ *and* $p_1 = -0.66$

$$\therefore CP1_9' = \frac{w}{n\, b \left[2\sqrt{d\delta - \delta^2}\, (b/h)^{0.66} + 1/m \left(0.395\, LC_{zi} - \sqrt{d\delta - \delta^2}\, (b/h)^{0.66} \right) \right]}$$

$$VCI_1 = 4.63 + 1.74\, CP1_9'$$

VCI$_1$ Model 16

Modified CP1 version 10: Empirical adjustments to (1) the additional contact length due to sinkage using a constant and (2) $\sqrt{d\delta - \delta^2}$ using aspect ratio

$$CP1_{10}' = \frac{w}{n\, b \left[2\sqrt{d\delta - \delta^2}\, (h/b)^{p_1} + c_1(1/m) \left(\frac{1}{2} LC_{zi} - \sqrt{d\delta - \delta^2}\, (h/b)^{p_1} \right) \right]}$$

Numerical Optimization yields $c_1 = 0.69$ *and* $p_1 = -0.62$

$$\therefore CP1_{10}' = \frac{w}{n\, b \left[2\sqrt{d\delta - \delta^2}\, (b/h)^{0.62} + 0.69/m \left(\frac{1}{2} LC_{zi} - \sqrt{d\delta - \delta^2}\, (b/h)^{0.62} \right) \right]}$$

$$VCI_1 = 4.68 + 1.76\, CP1_{10}'$$

VCI$_1$ Model 17

Modified CP1 version 11: Empirical adjustments to (1) $2\sqrt{d\delta - \delta^2}$ using a constant, (2) the additional contact length due to sinkage using a constant, and (3) the contact area using aspect ratio

$$CPI'_{11} = \frac{w}{n\,b\left[2c_1\sqrt{d\delta - \delta^2} + c_2(1/m)\left(\frac{1}{2}LC_{zl} - \sqrt{d\delta - \delta^2}\right)\right](h/b)^{p_1}}$$

Numerical Optimization yields $c_1 = 1.2$, $c_2 = 0.74$, *and* $p_1 = -0.50$

$$\therefore CPI'_{11} = \frac{w}{n\,b\left[2.4\sqrt{d\delta - \delta^2} + 0.74/m\left(\frac{1}{2}LC_{zl} - \sqrt{d\delta - \delta^2}\right)\right](b/h)^{0.50}}$$

$$VCI_1 = 4.79 + 2.08\,CPI'_{11}$$

VCI$_1$ Model 18

Modified CP1 version 12: Removed 1/m and made empirical adjustments to (1) $2\sqrt{d\delta - \delta^2}$ using a constant, (2) the additional contact length due to sinkage using a constant, and (3) the contact area using aspect ratio

$$CPI'_{12} = \frac{w}{n\,b\left[2c_1\sqrt{d\delta - \delta^2} + c_2\left(\frac{1}{2}LC_{zl} - \sqrt{d\delta - \delta^2}\right)\right](h/b)^{p_1}}$$

Numerical Optimization yields $c_1 = 1.5$, $c_2 = 0.44$, *and* $p_1 = -0.56$

$$\therefore CPI'_{12} = \frac{w}{n\,b\left[3.0\sqrt{d\delta - \delta^2} + 0.44\left(\frac{1}{2}LC_{zl} - \sqrt{d\delta - \delta^2}\right)\right](b/h)^{0.56}}$$

$$VCI_1 = 4.33 + 2.79\,CPI'_{12}$$

VCI$_1$ Model 19
Modified CP1 version 13: Empirical adjustments to (1) the two parts of the additional contact length due to sinkage using constants and (2) the contact area using aspect ratio

$$CPI'_{13} = \frac{w}{n b \left[2\sqrt{d\delta - \delta^2} + 1/m \left(c_1 \tfrac{1}{2} LC_{zl} - c_2 \sqrt{d\delta - \delta^2} \right) \right] (h/b)^{P_1}}$$

Numerical Optimization yields $c_1 = 0.62$, $c_2 = 0.72$, *and* $p_1 = -0.51$

$$\therefore CPI'_{13} = \frac{w}{n b \left[2\sqrt{d\delta - \delta^2} + 1/m \left(0.31 LC_{zl} - 0.72\sqrt{d\delta - \delta^2} \right) \right] (b/h)^{0.51}}$$

$$VCI_1 = 4.74 + 1.71 \, CPI'_{13}$$

VCI$_1$ Model 20
CPI'_8 and Tire Construction Factor (TCF)

$$CPI'_8 = \frac{w}{n b \left[2\sqrt{d\delta - \delta^2} + c_1(1/m) \left(\tfrac{1}{2} LC_{zl} - \sqrt{d\delta - \delta^2} \right) \right] (h/b)^{P_1}}$$

$TCF = c_{TCF}$ *where* $c_{TCF} = 0$ *if radial construction or* 1 *if bias ply construction*

Numerical Optimization yields $c_1 = 0.71$ *and* $p_1 = -0.45$

$$\therefore CPI'_8 = \frac{w}{n b \left[2\sqrt{d\delta - \delta^2} + 0.71/m \left(\tfrac{1}{2} LC_{zl} - \sqrt{d\delta - \delta^2} \right) \right] (b/h)^{0.45}}$$

$$VCI_1 = 3.09 + 1.82 \, CPI'_8 + 1.50 \, TCF$$

VCI$_1$ Model 21

Modified CP1 version 14: Empirical adjustments to (1) the additional contact length due to sinkage using a constant and (2) the contact area using aspect ratio and TCF

$$CPI'_{14} = \frac{w}{n\,b\left[2\sqrt{d\delta - \delta^2} + c_1(1/m)\left(\tfrac{1}{2}LC_{zl} - \sqrt{d\delta - \delta^2}\right)\right](h/b)^{p_1}(1 + c_2 TCF)}$$

Numerical Optimization yields $c_1 = 0.72$, $p_1 = -0.47$, *and* $c_2 = -0.06$

$$\therefore CPI'_{14} = \frac{w}{n\,b\left[2\sqrt{d\delta - \delta^2} + 0.72/m\left(\tfrac{1}{2}LC_{zl} - \sqrt{d\delta - \delta^2}\right)\right](b/h)^{0.47}(1 - 0.06\,TCF)}$$

$$VCI_1 = 4.52 + 1.72\,CPI'_{14}$$

VCI$_1$ Model 22

CPI'_8 with modified TF (product) and TCF

$$CPI'_8 = \frac{w}{n\,b\left[2\sqrt{d\delta - \delta^2} + c_1(1/m)\left(\tfrac{1}{2}LC_{zl} - \sqrt{d\delta - \delta^2}\right)\right](h/b)^{p_1}}$$

$$TF'_{M22} = 1 + c_2\,c_{TF} \qquad \text{where} \quad c_{TF} = 1 \text{ if manual transmission or } 0 \text{ if automatic}$$

Numerical Optimization yields $c_1 = 0.72$, $p_1 = -0.46$, *and* $c_2 = 0.01$

$$\therefore CPI'_8 = \frac{w}{n\,b\left[2\sqrt{d\delta - \delta^2} + 0.72/m\left(\tfrac{1}{2}LC_{zl} - \sqrt{d\delta - \delta^2}\right)\right](b/h)^{0.46}}$$

$$TF'_{M22} = 1 + 0.01\,c_{TF}$$

$$VCI_1 = 3.18 + 1.81\left(CPI'_8\,TF'_{M22}\right) + 1.39\,TCF$$

VCI$_1$ Model 23
$CP1_8'$ and modified TCF [Form 1]

$$CP1_8' = \frac{w}{n\,b\left[2\sqrt{d\delta - \delta^2} + c_1(1/m)\left(\frac{1}{2}LC_{z1} - \sqrt{d\delta - \delta^2}\right)\right](h/b)^{P_1}}$$

$$TCF_{M23}' = \left(c_{TCF} + 1\right)\left(\frac{h}{b}\right)^{P_2} \quad \text{where } c_{TCF} = 0 \text{ if radial construction or 1 if bias ply}$$

Numerical Optimization yields $c_1 = 0.68$, $p_1 = -0.50$, *and* $p_2 = -0.27$

$$\therefore CP1_8' = \frac{w}{n\,b\left[2\sqrt{d\delta - \delta^2} + 0.68/m\left(\frac{1}{2}LC_{z1} - \sqrt{d\delta - \delta^2}\right)\right](b/h)^{0.50}}$$

$$TCF_{M23}' = \left(c_{TCF} + 1\right)\left(\frac{b}{h}\right)^{0.27}$$

$$VCI_1 = 1.33 + 1.85\,CP1_8' + 1.39\,TCF_{M23}'$$

VCI$_1$ Model 24
$CP1_8'$ and modified TCF [Form 2]

$$CP1_8' = \frac{w}{n\,b\left[2\sqrt{d\delta - \delta^2} + c_1(1/m)\left(\frac{1}{2}LC_{z1} - \sqrt{d\delta - \delta^2}\right)\right](h/b)^{P_1}}$$

$$TCF_{M24}' = \left[\left(c_{TCF} + 1\right)\left(\frac{b}{h}\right)\right]^{P_2} \quad \text{where } c_{TCF} = 0 \text{ if radial construction or 1 if bias ply}$$

Numerical Optimization yields $c_1 = 0.78$, $p_1 = -0.60$, *and* $p_2 = -6$

$$\therefore CP1_8' = \frac{w}{n\,b\left[2\sqrt{d\delta - \delta^2} + 0.78/m\left(\frac{1}{2}LC_{z1} - \sqrt{d\delta - \delta^2}\right)\right](b/h)^{0.60}}$$

$$TCF_{M24}' = \left[\left(c_{TCF} + 1\right)\left(\frac{b}{h}\right)\right]^{-6}$$

$$VCI_1 = 4.85 + 1.88\,CP1_8' - 4.73\,TCF_{M24}'$$

VCI$_1$ Model 25
CPI'_8 and h/b

$$CPI'_8 = \frac{w}{n\,b\left[2\sqrt{d\delta - \delta^2} + c_1(1/m)\left(\frac{1}{2}LC_{z1} - \sqrt{d\delta - \delta^2}\right)\right](h/b)^{p_1}}$$

Numerical Optimization yields $c_1 = 0.60$ *and* $p_1 = -0.45$

$$\therefore CPI'_8 = \frac{w}{n\,b\left[2\sqrt{d\delta - \delta^2} + 0.60/m\left(\frac{1}{2}LC_{z1} - \sqrt{d\delta - \delta^2}\right)\right](b/h)^{0.45}}$$

$$VCI_1 = 4.64 + 1.70\,CPI'_8 + 0.712\left(\frac{h}{b}\right)^{6.4}$$

VCI$_1$ Model 26
CPH and modified CPS version 1: Included 1/m in CPS

$$CPH = \frac{w}{2\,n\,b\,\sqrt{d\delta - \delta^2}}$$

$$CPS'_1 = \frac{w}{n\,b\,(1/m)\,LC_{z1}}$$

$$VCI_1 = 3.97 + 1.16\,CPH + 0.190\,CPS'_1$$

VCI₁ Model 27

Modified CPH version 3 and modified CPS version 2: Included 1/m in CPS and made empirical adjustment to both hard surface and soft soil parameter contact areas using aspect ratio

$$CPH_3' = \frac{w}{2\,n\,b\,\sqrt{d\delta - \delta^2}\,(h/b)^{p_1}}$$

$$CPS_2' = \frac{w}{n\,b\,(1/m)\,LC_{zl}\,(h/b)^{p_2}}$$

Numerical Optimization yields $p_1 = -0.80$ and $p_2 = 1.2$

$$\therefore CPH_3' = \frac{w}{2\,n\,b\,\sqrt{d\delta - \delta^2}\,(b/h)^{0.80}}$$

$$CPS_2' = \frac{w}{n\,b\,(1/m)\,LC_{zl}\,(h/b)^{1.2}}$$

$$VCI_1 = 4.55 + 1.41\,CPH_3' + 0.107\,CPS_2'$$

VCI₁ Model 28

Modified CPH version 3 and modified CPS version 3: Empirical adjustment to both hard surface and soft soil parameter contact areas using aspect ratio

$$CPH_3' = \frac{w}{2\,n\,b\,\sqrt{d\delta - \delta^2}\,(h/b)^{p_1}}$$

$$CPS_3' = \frac{w}{n\,b\,LC_{zl}\,(h/b)^{p_2}}$$

Numerical Optimization yields $p_1 = -1.1$ and $p_2 = 0.92$

$$\therefore CPH_3' = \frac{w}{2\,n\,b\,\sqrt{d\delta - \delta^2}\,(b/h)^{1.1}}$$

$$CPS_3' = \frac{w}{n\,b\,LC_{zl}\,(h/b)^{0.92}}$$

$$VCI_1 = 3.93 + 1.38\,CPH_3' + 0.593\,CPS_3'$$

VCI₁ Model 29
Numeric version 1: MMP style numeric with constraint for pressure units

$$N_1 = \frac{w}{n\, b^{P_1}\, d^{P_2}\, \delta^{(2-P_1-P_2)}}$$

Numerical Optimization yields $p_1 = 1.45$ and $p_2 = 0.22$

$$\therefore N_1 = \frac{w}{n\, b^{1.45}\, d^{0.22}\, \delta^{0.33}}$$

$$VCI_1 = 4.06 + 0.717\, N_1$$

VCI₁ Model 30
Numeric version 2: MMP style numeric without the constraint for pressure units

$$N_2 = \frac{w}{n\, b^{P_1}\, d^{P_2}\, \delta^{P_3}}$$

Numerical Optimization yields $p_1 = 1.57$, $p_2 = -0.32$, and $p_3 = 0.41$

Note: $p_1 + p_2 + p_3 = 1.66$

$$\therefore N_2 = \frac{w\, d^{0.32}}{n\, b^{1.57}\, \delta^{0.41}}$$

$$VCI_1 = 5.40 + 0.128\, N_2$$

VCI₁ Model 31a
Numeric version 3a: Numeric using bd and 4 dimensionless ratios of tire variables [b/d, d/h, δ/d, and h/b] which allows inclusion of b, d, h, and δ with optimal exponents under the constraint of pressure units

$$N_{3a} = \frac{w}{n\, b\, d\, (b/d)^{P_1}\, (d/h)^{P_2}\, (\delta/d)^{P_3}\, (h/b)^{P_4}}$$

Numerical Optimization yields $p_1 = 0.11$, $p_2 = 0.28$, $p_3 = 0.36$ and $p_4 = -0.39$

$$\therefore N_{3a} = \frac{w\, h^{0.67}}{n\, b^{1.50}\, d^{0.81}\, \delta^{0.36}}$$

$$VCI_1 = 4.08 + 1.56\, N_{3a}$$

VCI$_1$ Model 31b

Numeric version 3b: Numeric using bd and 3 dimensionless ratios of tire variables [b/d, d/h, and δ/d] which allows inclusion of b, d, h, and δ with optimal exponents under the constraint of pressure units

$$N_{3b} = \frac{w}{n\,b\,d\,(b/d)^{p_1}\,(d/h)^{p_2}\,(\delta/d)^{p_3}}$$

Numerical Optimization yields $p_1 = 0.50$, $p_2 = 0.67$ and $p_3 = 0.36$

$$\therefore N_{3b} = \frac{w\,h^{0.67}}{n\,b^{1.50}\,d^{0.81}\,\delta^{0.36}}$$

$$VCI_1 = 4.08 + 1.56\,N_{3b}$$

VCI$_1$ Model 32

Modified CP1 version 15 and TCF: Empirical adjustments to (1) $\sqrt{d\delta - \delta^2}$ using a constant and (2) the contact area using aspect ratio

$$CP1'_{15} = \frac{w}{n\,b\left[2\,c_1\sqrt{d\delta - \delta^2} + (1/m)\left(\tfrac{1}{2}LC_{zl} - c_1\sqrt{d\delta - \delta^2}\right)\right](h/b)^{p_1}}$$

Numerical Optimization yields $c_1 = 1.4$ and $p_1 = -0.47$

$$\therefore CP1'_{15} = \frac{w}{n\,b\left[2.8\sqrt{d\delta - \delta^2} + (1/m)\left(\tfrac{1}{2}LC_{zl} - 1.4\sqrt{d\delta - \delta^2}\right)\right](b/h)^{0.47}}$$

$$VCI_1 = 2.84 + 2.47\,CP1'_{15} + 1.58\,TCF$$

VCI$_1$ Model 33

Modified CP1 version 16 and TCF: Empirical adjustments to (1) $2\sqrt{d\delta - \delta^2}$ using a constant, (2) the $\sqrt{d\delta - \delta^2}$ part of the additional contact length due to sinkage using a constant, and (3) the contact area using aspect ratio

$$CP1'_{16} = \frac{w}{nb\left[2c_1\sqrt{d\delta - \delta^2} + (1/m)\left(\frac{1}{2}LC_{zI} - c_2\sqrt{d\delta - \delta^2}\right)\right](h/b)^{p_1}}$$

Numerical Optimization yields $c_1 = 1.2$, $c_2 = 1.6$ *and* $p_1 = -0.49$

$$\therefore CP1'_{16} = \frac{w}{nb\left[2.4\sqrt{d\delta - \delta^2} + (1/m)\left(\frac{1}{2}LC_{zI} - 1.6\sqrt{d\delta - \delta^2}\right)\right](b/h)^{0.49}}$$

$$VCI_1 = 2.71 + 2.10\,CP1'_{16} + 1.71\,TCF$$

VCI$_1$ Model 34

Modified CP1 version 17 and TCF: Empirical adjustments to (1) $\sqrt{d\delta - \delta^2}$ using a constant, (2) the additional contact length due to sinkage using a constant, and (3) the contact area using aspect ratio

$$CP1'_{17} = \frac{w}{nb\left[2c_1\sqrt{d\delta - \delta^2} + c_2(1/m)\left(\frac{1}{2}LC_{zI} - c_1\sqrt{d\delta - \delta^2}\right)\right](h/b)^{p_1}}$$

Numerical Optimization yields $c_1 = 1.6$, $c_2 = 1.4$ *and* $p_1 = -0.49$

$$\therefore CP1'_{17} = \frac{w}{nb\left[3.2\sqrt{d\delta - \delta^2} + 1.4/m\left(\frac{1}{2}LC_{zI} - 1.6\sqrt{d\delta - \delta^2}\right)\right](b/h)^{0.49}}$$

$$VCI_1 = 2.71 + 2.81\,CP1'_{17} + 1.74\,TCF$$

VCI_1 Model 35

Modified CP1 version 18 and TCF: Empirical adjustments to (1) $\sqrt{d\delta - \delta^2}$ using a constant, (2) $\frac{1}{2}LC_{zi}$ using a constant, and (3) the contact area using aspect ratio

$$CP1'_{18} = \frac{w}{nb\left[2c_1\sqrt{d\delta - \delta^2} + 1/m\left(c_2\frac{1}{2}LC_{zi} - c_1\sqrt{d\delta - \delta^2}\right)\right](h/b)^{P_1}}$$

Numerical Optimization yields $c_1 = 1.1$, $c_2 = 0.83$ *and* $p_1 = -0.47$

$$\therefore CP1'_{18} = \frac{w}{nb\left[2.2\sqrt{d\delta - \delta^2} + 1/m\left(0.415\,LC_{zi} - 1.1\sqrt{d\delta - \delta^2}\right)\right](b/h)^{0.47}}$$

$VCI_1 = 2.90 + 1.96\,CP1'_{18} + 1.59\,TCF$

VCI_1 Model 36

Modified CP1 version 19 and TCF: Empirical adjustments to (1) $\frac{1}{2}LC_{zi}$ using a constant and (2) the contact area using aspect ratio

$$CP1'_{19} = \frac{w}{nb\left[2\sqrt{d\delta - \delta^2} + 1/m\left(c_1\frac{1}{2}LC_{zi} - \sqrt{d\delta - \delta^2}\right)\right](h/b)^{P_1}}$$

Numerical Optimization yields $c_1 = 0.74$ *and* $p_1 = -0.47$

$$\therefore CP1'_{19} = \frac{w}{nb\left[2\sqrt{d\delta - \delta^2} + 1/m\left(0.37\,LC_{zi} - \sqrt{d\delta - \delta^2}\right)\right](b/h)^{0.47}}$$

$VCI_1 = 2.88 + 1.78\,CP1'_{19} + 1.58\,TCF$

VCI₁ Model 37

Modified CP1 version 20 and TCF: Empirical adjustments to (1) the additional contact length due to sinkage using a constant, (2) $\frac{1}{2}LC_{zi}$ using a constant, and (3) the contact area using aspect ratio

$$CPI'_{20} = \frac{w}{nb\left[2\sqrt{d\delta - \delta^2} + c_1\left(c_2 \frac{1}{2}LC_{zi} - \sqrt{d\delta - \delta^2}\right)\right](h/b)^{p_1}}$$

Numerical Optimization yields $c_1 = 0.51$, $c_2 = 0.75$ *and* $p_1 = -0.50$

$$\therefore CPI'_{20} = \frac{w}{nb\left[2\sqrt{d\delta - \delta^2} + 0.51\left(0.375\,LC_{zi} - \sqrt{d\delta - \delta^2}\right)\right](b/h)^{0.50}}$$

$$VCI_1 = 2.08 + 1.92\,CPI'_{20} + 1.89\,TCF$$

VCI₁ Model 38

Modified CP1 version 21 and TCF: Replaced $\frac{1}{2}LC_{zi}$ with $c_1 d/2$ and made an empirical adjustment to the contact area using aspect ratio

$$CPI'_{21} = \frac{w}{nb\left[2\sqrt{d\delta - \delta^2} + 1/m\left(c_1 d/2 - \sqrt{d\delta - \delta^2}\right)\right](h/b)^{p_1}}$$

Numerical Optimization yields $c_1 = 0.711$ *and* $p_1 = -0.48$

$$\therefore CPI'_{21} = \frac{w}{nb\left[2\sqrt{d\delta - \delta^2} + 1/m\left(0.356\,d - \sqrt{d\delta - \delta^2}\right)\right](b/h)^{0.48}}$$

$$VCI_1 = 2.75 + 1.79\,CPI'_{21} + 1.63\,TCF$$

VCI$_1$ Model 39

Modified CP1 version 22 and TCF: Replaced $\frac{1}{2}LC_{z1}$ with $\frac{1}{2}LC_{z3}$ (i.e., changed z from h_c to $c_1 d$) and made an empirical adjustment to the contact area using aspect ratio

$$CP1'_{22} = \frac{w}{n\,b\left[2\sqrt{d\delta - \delta^2} + 1/m\left(\frac{1}{2}LC_{z3} - \sqrt{d\delta - \delta^2}\right)\right](h/b)^{p_1}}$$

$$\text{where} \quad c_1 d < \frac{d}{2} - \delta \quad \rightarrow \quad LC_{z3} = 2\sqrt{d(\delta + c_1 d) - (\delta + c_1 d)^2}$$

$$c_1 d \geq \frac{d}{2} - \delta \quad \rightarrow \quad LC_{z3} = d$$

Numerical Optimization yields $c_1 = 0.16$ *and* $p_1 = -0.46$

$$\therefore CP1'_{22} = \frac{w}{n\,b\left[2\sqrt{d\delta - \delta^2} + 1/m\left(\sqrt{d(\delta + 0.16d) - (\delta + 0.16d)^2} - \sqrt{d\delta - \delta^2}\right)\right](b/h)^{0.46}}$$

$$VCI_1 = 3.02 + 1.83\,CP1'_{22} + 1.51\,TCF$$

VCI$_1$ Model 40

Modified CP1 version 23 and TCF: Replaced $\frac{1}{2}LC_{z1}$ with $\frac{1}{2}LC_{z4}$ (i.e., changed z from h_c to $c_1 h$) and made an empirical adjustment to the contact area using aspect ratio

$$CP1'_{23} = \frac{w}{n\,b\left[2\sqrt{d\delta - \delta^2} + 1/m\left(\frac{1}{2}LC_{z4} - \sqrt{d\delta - \delta^2}\right)\right](h/b)^{p_1}}$$

$$\text{where} \quad c_1 h < \frac{d}{2} - \delta \quad \Rightarrow \quad LC_{z4} = 2\sqrt{d(\delta + c_1 h) - (\delta + c_1 h)^2}$$

$$c_1 h \geq \frac{d}{2} - \delta \quad \rightarrow \quad LC_{z4} = d$$

Numerical Optimization yields $c_1 = 0.69$ *and* $p_1 = -0.48$

$$\therefore CP1'_{23} = \frac{w}{n\,b\left[2\sqrt{d\delta - \delta^2} + 1/m\left(\frac{1}{2}LC_{z4} - \sqrt{d\delta - \delta^2}\right)\right](b/h)^{0.48}}$$

$$\text{where} \quad 0.69h < \frac{d}{2} - \delta \quad \rightarrow \quad LC_{z4} = 2\sqrt{d(\delta + 0.69h) - (\delta + 0.69h)^2}$$

$$0.69h \geq \frac{d}{2} - \delta \quad \Rightarrow \quad LC_{z4} = d$$

$$VCI_1 = 3.12 + 1.84\,CP1'_{23} + 1.49\,TCF$$

VCI$_1$ Model 41

Modified CP1 version 24 and TCF: Replaced $\frac{1}{2} LC_{z1}$ with $\frac{1}{2} LC_{z5}$ (i.e., changed z from h_c to $\frac{1}{4} d$) and made empirical adjustments to (1) the additional contact length due to sinkage using a constant and (2) the contact area using aspect ratio

$$CP1'_{24} = \frac{w}{nb\left[2\sqrt{d\delta - \delta^2} + c_1(1/m)\left(\frac{1}{2}LC_{z5} - \sqrt{d\delta - \delta^2}\right)\right](h/b)^{p_1}}$$

where $\frac{1}{4}d < \frac{d}{2} - \delta \quad \rightarrow \quad LC_{z5} = 2\sqrt{d(\delta + \frac{1}{4}d) - (\delta + \frac{1}{4}d)^2}$

$\frac{1}{4}d \geq \frac{d}{2} - \delta \quad \rightarrow \quad LC_{z5} = d$

Numerical Optimization yields $c_1 = 0.81$ *and* $p_1 = -0.46$

$$\therefore CP1'_{24} = \frac{w}{nb\left[2\sqrt{d\delta - \delta^2} + 0.81/m\left(\frac{1}{2}LC_{z5} - \sqrt{d\delta - \delta^2}\right)\right](b/h)^{0.46}}$$

$VCI_1 = 3.03 + 1.84\,CP1'_{24} + 1.51\,TCF$

VCI$_1$ Model 42

Modified CP1 version 25 and TCF: Replaced $\frac{1}{2} LC_{z1}$ with $\frac{1}{2} LC_{z3}$ (i.e., changed z from h_c to $c_1 d$) and made empirical adjustments to (1) $\sqrt{d\delta - \delta^2}$ using a constant and (2) the contact area using aspect ratio

$$CP1'_{25} = \frac{w}{nb\left[2c_2\sqrt{d\delta - \delta^2} + 1/m\left(\frac{1}{2}LC_{z3} - c_2\sqrt{d\delta - \delta^2}\right)\right](h/b)^{p_1}}$$

Numerical Optimization yields $c_1 = 0.49$, $c_2 = 1.4$ *and* $p_1 = -0.48$

$$\therefore CP1'_{25} = \frac{w}{nb\left[2.8\sqrt{d\delta - \delta^2} + 1/m\left(\frac{1}{2}LC_{z3} - 1.4\sqrt{d\delta - \delta^2}\right)\right](b/h)^{0.48}}$$

where $0.49d < \frac{d}{2} - \delta \quad \rightarrow \quad LC_{z3} = 2\sqrt{d(\delta + 0.49d) - (\delta + 0.49d)^2}$

$0.49d \geq \frac{d}{2} - \delta \quad \rightarrow \quad LC_{z3} = d$

$VCI_1 = 2.75 + 2.51\,CP1'_{25} + 1.63\,TCF$

VCI$_1$ Model 43

Modified CP1 version 26 and TCF: Replaced $\frac{1}{2}LC_{z1}$ with $\frac{1}{2}LC_{z3}$ (i.e., changed z from h_c to $c_1 d$) and made an empirical adjustment to $\sqrt{d\delta - \delta^2}$ using aspect ratio

$$CP1'_{26} = \frac{w}{nb\left[2\sqrt{d\delta - \delta^2}\,(h/b)^{P_1} + 1/m\left(\frac{1}{2}LC_{z3} - \sqrt{d\delta - \delta^2}\,(h/b)^{P_1}\right)\right]}$$

Numerical Optimization yields $c_1 = 0.25$ *and* $p_1 = -0.625$

$$\therefore CP1'_{26} = \frac{w}{nb\left[2\sqrt{d\delta - \delta^2}\,(b/h)^{0.625} + 1/m\left(\frac{1}{2}LC_{z3} - \sqrt{d\delta - \delta^2}\,(b/h)^{0.625}\right)\right]}$$

$$where\quad 0.25d < \frac{d}{2} - \delta \quad\Rightarrow\quad LC_{z3} = 2\sqrt{d(\delta + 0.25d) - (\delta + 0.25d)^2}$$

$$0.25d \geq \frac{d}{2} - \delta \quad\Rightarrow\quad LC_{z3} = d$$

$$VCI_1 = 2.84 + 1.89\,CP1'_{26} + 1.62\,TCF$$

VCI$_1$ Model 44

Modified CP1 version 27 and TCF: Replaced $\frac{1}{2}LC_{z1}$ with $\frac{1}{2}LC_{z3}$ (i.e., changed z from h_c to $c_1 d$) and made empirical adjustments to (1) the additional contact length due to sinkage using a constant and (2) $\sqrt{d\delta - \delta^2}$ using aspect ratio

$$CP1'_{27} = \frac{w}{nb\left[2\sqrt{d\delta - \delta^2}\,(h/b)^{P_1} + c_2(1/m)\left(\frac{1}{2}LC_{z3} - \sqrt{d\delta - \delta^2}\,(h/b)^{P_1}\right)\right]}$$

Numerical Optimization yields $c_1 = 0.070$, $c_2 = 2.3$ *and* $p_1 = -0.84$

$$\therefore CP1'_{27} = \frac{w}{nb\left[2\sqrt{d\delta - \delta^2}\,(b/h)^{0.84} + 2.3/m\left(\frac{1}{2}LC_{z3} - \sqrt{d\delta - \delta^2}\,(b/h)^{0.84}\right)\right]}$$

$$where\quad 0.070d < \frac{d}{2} - \delta \quad\Rightarrow\quad LC_{z3} = 2\sqrt{d(\delta + 0.070d) - (\delta + 0.070d)^2}$$

$$0.070d \geq \frac{d}{2} - \delta \quad\Rightarrow\quad LC_{z3} = d$$

$$VCI_1 = 2.44 + 1.93\,CP1'_{27} + 1.81\,TCF$$

VCI$_1$ Model 45
Modified CP1 version 28 and TCF: Removed 1/m, replaced $\frac{1}{2} LC_{zl}$ with $\frac{1}{2} LC_{z3}$ (i.e., changed z from h_c to $c_1 d$), and made empirical adjustments to (1) the additional contact length due to sinkage using a constant and (2) $\sqrt{d\delta - \delta^2}$ using aspect ratio

$$CP1'_{28} = \frac{w}{n b \left[2\sqrt{d\delta - \delta^2} \, (h/b)^{P_1} + c_2 \left(\frac{1}{2} LC_{z3} - \sqrt{d\delta - \delta^2} \, (h/b)^{P_1} \right) \right]}$$

Numerical Optimization yields $c_1 = 0.11$, $c_2 = 0.80$ *and* $p_1 = -0.92$

$$\therefore CP1'_{28} = \frac{w}{n b \left[2\sqrt{d\delta - \delta^2} \, (b/h)^{0.92} + 0.80 \left(\frac{1}{2} LC_{z3} - \sqrt{d\delta - \delta^2} \, (b/h)^{0.92} \right) \right]}$$

where $0.11d < \dfrac{d}{2} - \delta \quad \Rightarrow \quad LC_{z3} = 2\sqrt{d(\delta + 0.11d) - (\delta + 0.11d)^2}$

$\qquad 0.11d \geq \dfrac{d}{2} - \delta \quad \Rightarrow \quad LC_{z3} = d$

$VCI_1 = 1.91 + 2.09 \, CP1'_{28} + 1.96 \, TCF$

VCI$_1$ Model 46
CPH'_3 and TCF

$$CPH'_3 = \frac{w}{2 n b \sqrt{d\delta - \delta^2} \, (h/b)^{P_1}}$$

Numerical Optimization yields $p_1 = -0.60$

$$\therefore CPH'_3 = \frac{w}{2 n b \sqrt{d\delta - \delta^2} \, (b/h)^{0.60}}$$

$VCI_1 = 3.58 + 1.66 \, CPH'_3 + 0.75 \, TCF$

VCI$_1$ Model 47
CPS_3' **and TCF**

$$CPS_3' = \frac{w}{n \, b \, LC_{zl} \, (h/b)^{p_1}}$$

Numerical Optimization yields $p_1 = -0.50$

$$\therefore CPS_3' = \frac{w}{n \, b \, LC_{zl} \, (b/h)^{0.50}}$$

$$VCI_1 = 2.30 + 3.21 \, CPS_3' + 2.84 \, TCF$$

VCI$_1$ Model 48
Modified Average Contact Pressure Parameter No. 2 (CP2) version 1 and TCF: Used $c_1 d$
for internal length adjustment and made empirical adjustment to the contact area using
aspect ratio

$$CP2_1' = \frac{w}{2 \, n \, b \, \sqrt{d(\delta + c_1 d) - (\delta + c_1 d)^2} \, (h/b)^{p_1}}$$

Numerical Optimization yields $c_1 = 0.026$ *and* $p_1 = -0.52$

$$\therefore CP2_1' = \frac{w}{2 \, n \, b \, \sqrt{d(\delta + 0.026 \, d) - (\delta + 0.026 \, d)^2} \, (b/h)^{0.52}}$$

$$VCI_1 = 1.95 + 2.03 \, CP2_1' + 1.95 \, TCF$$

VCI$_1$ Model 49
Modified CP2 version 2 and TCF: Split the contact length into 2 parts and simplified the
adjustment/correction part to $c_1 d$

$$CP2_2' = \frac{w}{2 \, n \, b \left(\sqrt{d\delta - \delta^2} + c_1 d \right) (h/b)^{p_1}}$$

Numerical Optimization yields $c_1 = 0.12$ *and* $p_1 = -0.50$

$$\therefore CP2_2' = \frac{w}{2 \, n \, b \left(\sqrt{d\delta - \delta^2} + 0.12 \, d \right) (b/h)^{0.50}}$$

$$VCI_1 = 1.86 + 2.58 \, CP2_2' + 1.96 \, TCF$$

VCI$_1$ Model 50
Recast $CP2'_1$ and TCF: Split the contact length into 2 parts

$$CP2'_1 = \frac{w}{2\,n\,b\left[\sqrt{d\,\delta - \delta^2} + \left(\sqrt{d(\delta + c_1 d) - (\delta + c_1 d)^2} - \sqrt{d\,\delta - \delta^2}\right)\right](h/b)^{p_1}}$$

Numerical Optimization yields $c_1 = 0.026$ and $p_1 = -0.52$

$$\therefore CP2'_1 = \frac{w}{2\,n\,b\left[\sqrt{d\,\delta - \delta^2} + \left(\sqrt{d(\delta + 0.026\,d) - (\delta + 0.026\,d)^2} - \sqrt{d\,\delta - \delta^2}\right)\right](b/h)^{0.52}}$$

$$VCI_1 = 1.95 + 2.03\,CP2'_1 + 1.95\,TCF$$

VCI$_1$ Model 51
N_{3b} and TCF

$$N_{3b} = \frac{w}{n\,b\,d\,(b/d)^{p_1}\,(d/h)^{p_2}\,(\delta/d)^{p_3}}$$

Numerical Optimization yields $p_1 = 0.42$, $p_2 = 0.66$ and $p_3 = 0.32$

$$\therefore N_{3b} = \frac{w\,h^{0.66}}{n\,b^{1.42}\,d^{0.92}\,\delta^{0.32}}$$

$$VCI_1 = 1.56 + 2.03\,N_{3b} + 2.03\,TCF$$

APPENDIX C

SUMMARY OF ALL MODEL VARIANTS EXPLORED

DURING THE DRAWBAR MODELING

Table C1. Quality comparison for all drawbar model variants (field data only)

Model No.	Model Description	Degrees of Freedom	Standard Error (D/W)	Adjusted R-squared
EXISTING COMPARISON MODELS				
C1 [a]	Standard NRMM Model: Excess Rating Cone Index (RCI_x)	81	0.097	77.8
C2 [a]	Freitag's Clay Numeric ($N_{c(F)}$)	80	0.095	78.7
C3 [a]	Turnage's Clay Numeric ($N_{c(T)}$)	80	0.085	82.8
C4 [a]	Smith's Clay Numeric ($N_{c(S)}$)	79	0.082	84.1
C5 [a]	Maclaurin's Drawbar Numeric (N_M)	78	0.090	80.6
PRELIMINARY NEW DEVELOPMENT MODELS				
P1	Bearing Ratio No. 1: Ratio of Soil Strength over Contact Pressure using RCI and $CP2_1'$	79	0.120	65.6
P2	Bearing Ratio No. 2: Ratio of Soil Strength over Contact Pressure using RCI and CPH	81	0.098	77.3
P3	Bearing Ratio No. 3: Ratio of Soil Strength over Contact Pressure using RCI and CPH_3'	80	0.123	64.3
P4	Excess Bearing Ratio No. 1: Ratio of Soil Strength over Contact Pressure using RCI_x and $CP2_1'$	79	0.127	61.7
P5	Excess Bearing Ratio No. 2: Ratio of Soil Strength over Contact Pressure using RCI_x and CPH	81	0.110	71.3
P6	Excess Bearing Ratio No. 3: Ratio of Soil Strength over Contact Pressure using RCI_x and CPH_3'	80	0.129	60.7
P7	Excess RCI Ratio No. 1: Ratio of RCI_x over VCI_1	81	0.103	74.7
P8	Excess RCI Ratio No. 2: Ratio of RCI_x over VCI_1 with aspect ratio (product)	81	0.087	82.1
PRINCIPAL NEW DEVELOPMENT MODELS				
1a [a]	Modified NRMM Model: Optimized Curve Fits to Database	81	0.079	85.3
1b	Modified NRMM Model: Removed CPF Separation Criteria and Optimized Single Curve Fit to Database	81	0.084	83.4
2	Excess Bearing Ratio No. 4: Ratio of Soil Strength over Contact Pressure using RCI_x and $CP2_3'$	79	0.084	83.2

Table C1. (continued)

Model No.	Model Description	Degrees of Freedom	Standard Error (D/W)	Adjusted R-squared
3 [a]	Drawbar Numeric No. 1 (N_{D1}): Numeric using bd and 3 dimensionless ratios of tire variables [b/d, d/h, and δ/d] which allows inclusion of b, d, h, and δ with optimal exponents under the constraint of pressure units	78	0.063	90.5
4	Drawbar Numeric No. 2 (N_{D2}): Numeric using bd and 3 dimensionless ratios of tire variables [b/h, d/b, and δ/d] which allows inclusion of b, d, h, and δ with optimal exponents under the constraint of pressure units (check model)	78	0.063	90.5
5	Drawbar Numeric No. 3 (N_{D3}): Numeric using bd and 2 dimensionless ratios of tire variables [b/h and δ/d] which allows inclusion of b, d, h, and δ under the constraint of pressure units	79	0.064	90.2
6 [a]	Drawbar Numeric No. 4 (N_{D4}): Numeric using bd and 2 dimensionless ratios of tire variables [b/d and δ/d] which allows inclusion of b, d, and δ with optimal exponents under the constraint of pressure units	79	0.063	90.5
7	Drawbar Numeric No. 5 (N_{D5}): Numeric using bd and 1 dimensionless ratio of tire variables [b/d] which allows inclusion of b and d with optimal exponents under the constraint of pressure units	80	0.068	88.9
8	Drawbar Numeric No. 6 (N_{D6}): Numeric using d as the only tire variable with no constraint for pressure units	80	0.066	89.8
9	Drawbar Numeric No. 7 (N_{D7}): Numeric using d as the only tire variable under the constraint of pressure units	80	0.069	88.9
10 [a]	Drawbar Numeric No. 8 (N_{D8}): Numeric using d and L_δ [based on a consideration of Drawbar Model 6]	80	0.063	90.6
11	Drawbar Numeric No. 9 (N_{D9}): Numeric with RCI_x for soil strength and using d and L_δ	80	0.086	82.3
12	Drawbar Numeric No. 10 (N_{D10}): Numeric using L_δ as the only tire parameter	80	0.067	89.4
13	Drawbar Numeric No. 11 (N_{D11}): Numeric using d and a modified version of L_δ where an adjustment/correction is made using $c_1 d$ in the middle ordinate	79	0.063	90.5
14	Drawbar Numeric No. 12 (N_{D12}): Numeric using d and L_δ with TCF	79	0.063	90.5
15	Drawbar Numeric No. 13 (N_{D13}): Numeric using d and L_δ with aspect ratio for a width consideration	79	0.063	90.5
16	Drawbar Numeric No. 14 (N_{D14}): Numeric using d and L_δ with b/d for a width consideration	79	0.063	90.5

Table C1. (continued)

Model No.	Model Description	Degrees of Freedom	Standard Error (D/W)	Adjusted R-squared
17	Drawbar Numeric No. 15 (N_{D15}): Numeric using d and L_δ with $\sqrt{b/d}$ for a width consideration [based on Freitag's laboratory data]	79	0.076	86.4
18 [a]	Drawbar Numeric No. 16 (N_{D16}): Numeric using d and L_δ with $(h/d)^{0.6}$ [based on Freitag's laboratory data]	79	0.064	90.2

[a] - These models were discussed in the main text

Drawbar Model C1
Standard NRMM Model: Excess Rating Cone Index (RCI_x)

$$RCI_x = RCI - VCI_1$$

$$CPF \geq 4\,psi \quad \rightarrow \quad \frac{D^{RCI}}{W_{20}} = 0.621 - \frac{6.32}{RCI_x + 7.61}$$

$$CPF < 4\,psi \quad \Rightarrow \quad \frac{D^{RCI}}{W_{20}} = 0.678 - \frac{5.80}{RCI_x + 6.80}$$

Drawbar Model C2
Freitag's Clay Numeric ($N_{c(F)}$)

$$N_{c(F)} = \frac{RCI\,n\,b\,d}{w} \left(\frac{\delta}{h}\right)^{1/2}$$

$$\therefore N_{c(F)} = \frac{RCI}{w} \left(n\,b\,d\,\sqrt{\delta/h} \right)$$

$$\frac{D^{RCI}}{W_{20}} = 0.74 - \frac{3.6}{N_{c(F)} + 4.3}$$

Drawbar Model C3
Turnage's Clay Numeric ($N_{c(T)}$)

$$N_{c(T)} = \frac{RCI\, n\, b\, d}{w} \left(\frac{\delta}{h}\right)^{1/2} \left(\frac{2d}{2d+b}\right)$$

$$\therefore\; N_{c(T)} = \frac{RCI}{w} \left[n\, b\, d \sqrt{\delta/h} \left(\frac{2d}{2d+b}\right) \right]$$

$$\frac{D^{RCI}}{W_{20}} = 0.73 - \frac{2.5}{N_{c(T)} + 2.8}$$

Drawbar Model C4
Smith's Clay Numeric ($N_{c(S)}$)

$$N_{c(S)} = \frac{RCI\, n\, b\, d}{w} \left(1 - \frac{\delta}{h}\right)^{-3/2} \left(1 + \frac{b}{d}\right)^{-3/4}$$

$$\frac{D^{RCI}}{W_{20}} = 0.72 - \frac{7.1}{N_{c(S)} + 7.4}$$

Drawbar Model C5
Maclaurin's Drawbar Numeric (N_M)

$$N_M = \frac{RCI\, n\, b^{0.8}\, d^{0.8}\, \delta^{0.4}}{w}$$

$$\frac{D^{RCI}}{W_{20}} = 0.73 - \frac{2.7}{N_M + 3.2}$$

Drawbar Model P1
Bearing Ratio No. 1: Ratio of Soil Strength over Contact Pressure using RCI and $CP2_1'$

$$BR_1 = \frac{RCI}{CP2_1'}$$

$$\therefore BR_1 = \frac{RCI}{w}\left(2nb\sqrt{d(\delta + 0.026d) - (\delta + 0.026d)^2}\ (b/h)^{0.52}\right)$$

$$\frac{D^{RCI}}{W_{20}} = 0.76 - \frac{7.5}{BR_1 + 10.5}$$

Drawbar Model P2
Bearing Ratio No. 2: Ratio of Soil Strength over Contact Pressure using RCI and CPH

$$BR_2 = \frac{RCI}{CPH}$$

$$\therefore BR_2 = \frac{RCI}{w}\left(2nb\sqrt{d\delta - \delta^2}\right)$$

$$\frac{D^{RCI}}{W_{20}} = 0.74 - \frac{3.8}{BR_2 + 4.7}$$

Drawbar Model P3
Bearing Ratio No. 3: Ratio of Soil Strength over Contact Pressure using RCI and CPH_3'

$$BR_3 = \frac{RCI}{CPH_3'}$$

$$\therefore BR_3 = \frac{RCI}{w}\left(2nb\sqrt{d\delta - \delta^2}\ (b/h)^{0.6}\right)$$

$$\frac{D^{RCI}}{W_{20}} = 0.76 - \frac{6.2}{BR_3 + 8.9}$$

Drawbar Model P4
Excess Bearing Ratio No. 1: Ratio of Soil Strength over Contact Pressure using RCI_x and $CP2'_1$

$$BR_{x1} = \frac{RCI_x}{CP2'_1}$$

$$\therefore BR_{x1} = \frac{RCI - VCI_1}{w}\left(2\,n\,b\,\sqrt{d\,(\delta + 0.026\,d) - (\delta + 0.026\,d)^2}\,\,(b/h)^{0.52}\right)$$

$$\frac{D^{RCI}}{W}_{20} = 0.69 - \frac{2.83}{BR_{x1} + 4.10}$$

Drawbar Model P5
Excess Bearing Ratio No. 2: Ratio of Soil Strength over Contact Pressure using RCI_x and CPH

$$BR_{x2} = \frac{RCI_x}{CPH}$$

$$\therefore BR_{x2} = \frac{RCI - VCI_1}{w}\left(2\,n\,b\,\sqrt{d\,\delta - \delta^2}\right)$$

$$\frac{D^{RCI}}{W}_{20} = 0.69 - \frac{1.79}{BR_{x2} + 2.60}$$

Drawbar Model P6
Excess Bearing Ratio No. 3: Ratio of Soil Strength over Contact Pressure using RCI_x and CPH'_3

$$BR_{x3} = \frac{RCI_x}{CPH'_3}$$

$$\therefore BR_{x3} = \frac{RCI - VCI_1}{w}\left(2\,n\,b\,\sqrt{d\,\delta - \delta^2}\,\,(b/h)^{0.6}\right)$$

$$\frac{D^{RCI}}{W}_{20} = 0.69 - \frac{2.35}{BR_{x3} + 3.40}$$

Drawbar Model P7
Excess RCI Ratio No. 1: Ratio of RCI_x over VCI_1

$$RCIR_{x1} = \frac{RCI_x}{VCI_1}$$

$$\therefore RCIR_{x1} = \frac{RCI - VCI_1}{VCI_1}$$

$$\frac{D^{RCI}}{W_{20}} = 0.68 - \frac{0.82}{RCIR_{x1} + 1.20}$$

Drawbar Model P8
Excess RCI Ratio No. 2: Ratio of RCI_x over VCI_1 with aspect ratio (product)

$$RCIR_{x2} = \frac{RCI_x}{VCI_1}\left(\frac{h}{b}\right)$$

$$\therefore RCIR_{x2} = \frac{RCI - VCI_1}{VCI_1}\left(\frac{h}{b}\right)$$

$$\frac{D^{RCI}}{W_{20}} = 0.66 - \frac{0.40}{RCIR_{x2} + 0.60}$$

Drawbar Model 1a
Modified NRMM Model: Optimized Curve Fits to Database

$$CPF \geq 4\,psi \quad \rightarrow \quad \frac{D^{RCI}}{W_{20}} = 0.63 - \frac{5.14}{RCI_x + 8.16}$$

$$CPF < 4\,psi \quad \Rightarrow \quad \frac{D^{RCI}}{W_{20}} = 0.81 - \frac{17.8}{RCI_x + 22.0}$$

Drawbar Model 1b
Modified NRMM Model: Removed CPF Separation Criteria and Optimized Single Curve
Fit to Database

$$\frac{D^{RCI}}{W_{20}} = 0.65 - \frac{7.80}{RCI_x + 12.0}$$

Drawbar Model 2
Excess Bearing Ratio No. 4: Ratio of Soil Strength over Contact Pressure using RCI_x and $CP2'_3$

$$BR_{x4} = \frac{RCI_x}{CP2'_3}$$

where $CP2'_3 = \dfrac{w}{2\,n\,b\,\sqrt{d(\delta + c_1 d) - (\delta + c_1 d)^2}\,(b/h)^{P_1}}$

Numerical Optimization yields $c_1 = 0$ and $p_1 = -2$

$$\therefore BR_{x4} = \frac{RCI - VCI_1}{w}\left(2\,n\,b\,\sqrt{d\delta - \delta^2}\,(h/b)^2\right)$$

$$\frac{D^{RCI}}{W_{20}} = 0.65 - \frac{0.423}{BR_{x4} + 0.65}$$

Drawbar Model 3
Drawbar Numeric No. 1 (N_{DI}): Numeric using bd and 3 dimensionless ratios of tire variables [b/d, d/h, and δ/d] which allows inclusion of b, d, h, and δ with optimal exponents under the constraint of pressure units

$$N_{DI} = \frac{RCI}{w}\left(n\,b\,d\,(b/d)^{P_1}\,(d/h)^{P_2}\,(\delta/d)^{P_3}\right)$$

Numerical Optimization yields $p_1 = -0.90$, $p_2 = 0.82$, and $p_3 = 0.45$

$$\therefore N_{DI} = \frac{RCI}{w}\left(\frac{n\,b^{0.10}\,d^{2.27}\,\delta^{0.45}}{h^{0.82}}\right)$$

$$\frac{D^{RCI}}{W_{20}} = 0.695 - \frac{8.6}{N_{DI} + 7.5}$$

Drawbar Model 4

Drawbar Numeric No. 2 (N_{D2}): Numeric using bd and 3 dimensionless ratios of tire variables [b/h, d/b, and δ/d] which allows inclusion of b, d, h, and δ with optimal exponents under the constraint of pressure units (check model)

$$N_{D2} = \frac{RCI}{w}\left(n\,b\,d\,(b/h)^{p_1}\,(d/b)^{p_2}\,(\delta/d)^{p_3} \right)$$

Numerical Optimization yields $p_1 = 0.82$, $p_2 = 1.72$ *and* $p_3 = 0.45$

$$\therefore\ N_{D2} = \frac{RCI}{w}\left(\frac{n\,b^{\,0.10}\,d^{\,2.27}\,\delta^{\,0.45}}{h^{\,0.82}} \right)$$

$$\frac{D^{RCI}}{W_{20}} = 0.695 - \frac{8.6}{N_{D2} + 7.5}$$

Drawbar Model 5

Drawbar Numeric No. 3 (N_{D3}): Numeric using bd and 2 dimensionless ratios of tire variables [b/h and δ/d] which allows inclusion of b, d, h, and δ under the constraint of pressure units

$$N_{D3} = \frac{RCI}{w}\left(n\,b\,d\,(b/h)^{p_1}\,(\delta/d)^{p_2} \right)$$

Numerical Optimization yields $p_1 = -1.10$ *and* $p_2 = 0.60$

$$\therefore\ N_{D3} = \frac{RCI}{w}\left(\frac{n\,h^{\,1.10}\,d^{\,0.40}\,\delta^{\,0.60}}{b^{\,0.10}} \right)$$

$$\frac{D^{RCI}}{W_{20}} = 0.688 - \frac{0.456}{N_{D3} + 0.344}$$

Drawbar Model 6

Drawbar Numeric No. 4 (N_{D4}): Numeric using bd and 2 dimensionless ratios of tire variables [b/d and δ/d] which allows inclusion of b, d, and δ with optimal exponents under the constraint of pressure units

$$N_{D4} = \frac{RCI}{w}\left(n\,b\,d\,(b/d)^{p_1}\,(\delta/d)^{p_2}\right)$$

Numerical Optimization yields $p_1 = -1.0$ *and* $p_2 = 0.50$

$$\therefore N_{D4} = \frac{RCI}{w}\left(n\,d^{1.50}\,\delta^{0.50}\right)$$

$$N_{D4} = \frac{RCI}{w}\left(n\,d\,\sqrt{d\,\delta}\right)$$

$$\frac{D^{RCI}}{W_{20}} = 0.69 - \frac{2.55}{N_{D4} + 2.10}$$

Drawbar Model 7

Drawbar Numeric No. 5 (N_{D5}): Numeric using bd and 1 dimensionless ratio of tire variables [b/d] which allows inclusion of b and d with optimal exponents under the constraint of pressure units

$$N_{D5} = \frac{RCI}{w}\left(n\,b\,d\,(b/d)^{p_1}\right)$$

Numerical Optimization yields $p_1 = -1.05$

$$\therefore N_{D5} = \frac{RCI}{w}\left(\frac{n\,d^{2.05}}{b^{0.05}}\right)$$

$$\frac{D^{RCI}}{W_{20}} = 0.694 - \frac{12.3}{N_{D5} + 11.4}$$

Drawbar Model 8

Drawbar Numeric No. 6 (N_{D6}): Numeric using d as the only tire variable with no constraint for pressure units

$$N_{D6} = \frac{RCI}{w}\left(n\,d^{p_1}\right)$$

Numerical Optimization yields p_1 = 1.64

$$\therefore\ N_{D6} = \frac{RCI}{w}\left(n\,d^{1.64}\right)$$

$$\frac{D^{RCI}}{W_{20}} = 0.687 - \frac{2.71}{N_{D6} + 2.00}$$

Drawbar Model 9

Drawbar Numeric No. 7 (N_{D7}): Numeric using d as the only tire variable under the constraint of pressure units

$$N_{D7} = \frac{RCI}{w}\left(n\,d^2\right)$$

$$\frac{D^{RCI}}{W_{20}} = 0.695 - \frac{11.8}{N_{D7} + 10.9}$$

Drawbar Model 10

Drawbar Numeric No. 8 (N_{D8}): Numeric using d and L_δ [based on a consideration of Drawbar Model 6]

$$N_{D8} = \frac{RCI}{w}\left(n\,d\,L_\delta\right)$$

where $L_\delta = 2\sqrt{d\delta - \delta^2}$

$$\therefore\ N_{D8} = \frac{RCI}{w}\left(2n\sqrt{d^3\delta - d^2\delta^2}\right)$$

$$\frac{D^{RCI}}{W_{20}} = 0.692 - \frac{5.0}{N_{D8} + 4.1}$$

Drawbar Model 11

Drawbar Numeric No. 9 (N_{D9}): Numeric with RCI_x for soil strength and using d and L_δ

$$N_{D9} = \frac{RCI_x}{w}\left(n\,d\,L_\delta\right)$$

$$\therefore N_{D9} = \frac{RCI - VCI_1}{w}\left(2n\sqrt{d^3\delta - d^2\delta^2}\right)$$

$$\frac{D^{RCI}}{W_{20}} = 0.672 - \frac{3.41}{N_{D9} + 5.08}$$

Drawbar Model 12

Drawbar Numeric No. 10 (N_{D10}): Numeric using L_δ as the only tire parameter

$$N_{D10} = \frac{RCI}{w}\left(n\,L_\delta^2\right)$$

$$\therefore N_{D10} = \frac{RCI}{w}\left[4\,n\left(d\delta - \delta^2\right)\right]$$

$$\frac{D^{RCI}}{W_{20}} = 0.698 - \frac{2.50}{N_{D10} + 2.30}$$

Drawbar Model 13

Drawbar Numeric No. 11 (N_{D11}): Numeric using d and a modified version of L_δ where an adjustment/correction is made using $c_1 d$ in the middle ordinate

$$N_{D11} = \frac{RCI}{w}\left(n\,d\,L_\delta'\right)$$

where $L_\delta' = 2\sqrt{d(\delta + c_1 d) - (\delta + c_1 d)^2}$

Numerical Optimization yields $c_1 = -0.003$

$$\therefore N_{D11} = \frac{RCI}{w}\left(2\,n\,d\sqrt{d(\delta - 0.003d) - (\delta - 0.003d)^2}\right)$$

$$\frac{D^{RCI}}{W_{20}} = 0.692 - \frac{4.86}{N_{D11} + 4.00}$$

Drawbar Model 14
Drawbar Numeric No. 12 (N_{D12}): Numeric using d and L_δ with TCF

$$N_{D12} = \frac{RCI}{w}\left[n\,d\,L_\delta\,(1 + c_1\,TCF)\right]$$

Numerical Optimization yields $c_1 = -0.015$

$$\therefore N_{D12} = \frac{RCI}{w}\left[2n\sqrt{d^3\delta - d^2\delta^2}\,(1 - 0.015\,TCF)\right]$$

$$\frac{D^{RCI}}{W_{20}} = 0.691 - \frac{4.9}{N_{D12} + 4.0}$$

Drawbar Model 15
Drawbar Numeric No. 13 (N_{D13}): Numeric using d and L_δ with aspect ratio for a width consideration

$$N_{D13} = \frac{RCI}{w}\left(n\,d\,L_\delta\right)\left(\frac{h}{b}\right)^{p_1}$$

Numerical Optimization yields $p_1 = -0.005$

$$\therefore N_{D13} = \frac{RCI}{w}\left(2n\sqrt{d^3\delta - d^2\delta^2}\right)\left(\frac{b}{h}\right)^{0.005}$$

$$\frac{D^{RCI}}{W_{20}} = 0.692 - \frac{5.0}{N_{D13} + 4.1}$$

Drawbar Model 16

Drawbar Numeric No. 14 (N_{D14}): Numeric using d and L_δ with b/d for a width consideration

$$N_{D14} = \frac{RCI}{w}\left(n\, d\, L_\delta\right)\left(\frac{b}{d}\right)^{p_1}$$

Numerical Optimization yields p_1 = 0.0014

$$\therefore N_{D14} = \frac{RCI}{w}\left(2n\sqrt{d^3\delta - d^2\delta^2}\right)\left(\frac{b}{d}\right)^{0.0014}$$

$$\frac{D^{RCI}}{W_{20}} = 0.692 - \frac{5.0}{N_{D14} + 4.1}$$

Drawbar Model 17

Drawbar Numeric No. 15 (N_{D15}): Numeric using d and L_δ with $\sqrt{b/d}$ for a width consideration [based on Freitag's laboratory data]

$$N_{D15} = \frac{RCI}{w}\left(n\, d\, L_\delta\right)\left(\frac{b}{d}\right)^{0.5}$$

$$\therefore N_{D15} = \frac{RCI}{w}\left(2n\sqrt{bd^2\delta - bd\delta^2}\right)$$

$$\frac{D^{RCI}}{W_{20}} = 0.714 - \frac{4.11}{N_{D15} + 4.06}$$

Drawbar Model 18

Drawbar Numeric No. 16 (N_{D16}): Numeric using d and L_δ with $(h/d)^{0.6}$ [based on Freitag's laboratory data]

$$N_{D16} = \frac{RCI}{w}\left(n\, d\, L_\delta\right)\left(\frac{h}{d}\right)^{0.6}$$

$$\therefore N_{D16} = \frac{RCI}{w}\left(2n\sqrt{d^3\delta - d^2\delta^2}\right)\left(\frac{h}{d}\right)^{0.6}$$

$$\frac{D^{RCI}}{W_{20}} = 0.690 - \frac{2.18}{N_{D16} + 1.70}$$

APPENDIX D

TYPICAL PROCEDURES FOR MEASURING

VCI$_1$ AND DRAWBAR PERFORMANCE

Multi-Pass Experiments

VCI_1 is not directly measurable. Rather it is interpreted from the results of multi-pass experiments. In a typical multi-pass experiment, a level, straight-line, homogeneous (as much as possible) test lane is marked off, and cone index measurements are taken throughout the lane. Then the vehicle makes passes through the test lane at a slow, steady-state speed (approximately 2 mph) in its lowest gear. The experiment is usually conducted with the vehicle first traversing forward through the test lane for pass number one and then traversing backward (i.e., in reverse gear) through the test lane for pass number two. The vehicle will continue to make passes until immobilization occurs. When immobilization is reached, the immobilization pass number is recorded, and other supporting soil consistency data (e.g., remold index, moisture content, density, etc.) are measured in a spot adjacent to the immobilization but out of the zone of disturbance. The measured soil consistency data are intended to represent the soil characteristics with the greatest influence on the immobilization for the particular vehicle and terrain conditions.

To establish the VCI_1 measurement for a particular vehicle configuration, several multi-pass experiments are conducted on ranging soil strengths in order to acquire several observations for passes-made-good versus soil strength in the critical layer. The critical layer is the layer of soil (typically 3-9" or 6-12") that contributes most significantly to the performance of the vehicle. The soil strength value at which the vehicle is capable of consistently making one pass is then interpreted from a x-y plot of the collected multi-pass observations, and this inferred soil strength represents the VCI_1 performance measurement. Figure D1

provides a sample x-y plot of multi-pass observations that were used to determine the VCI_1

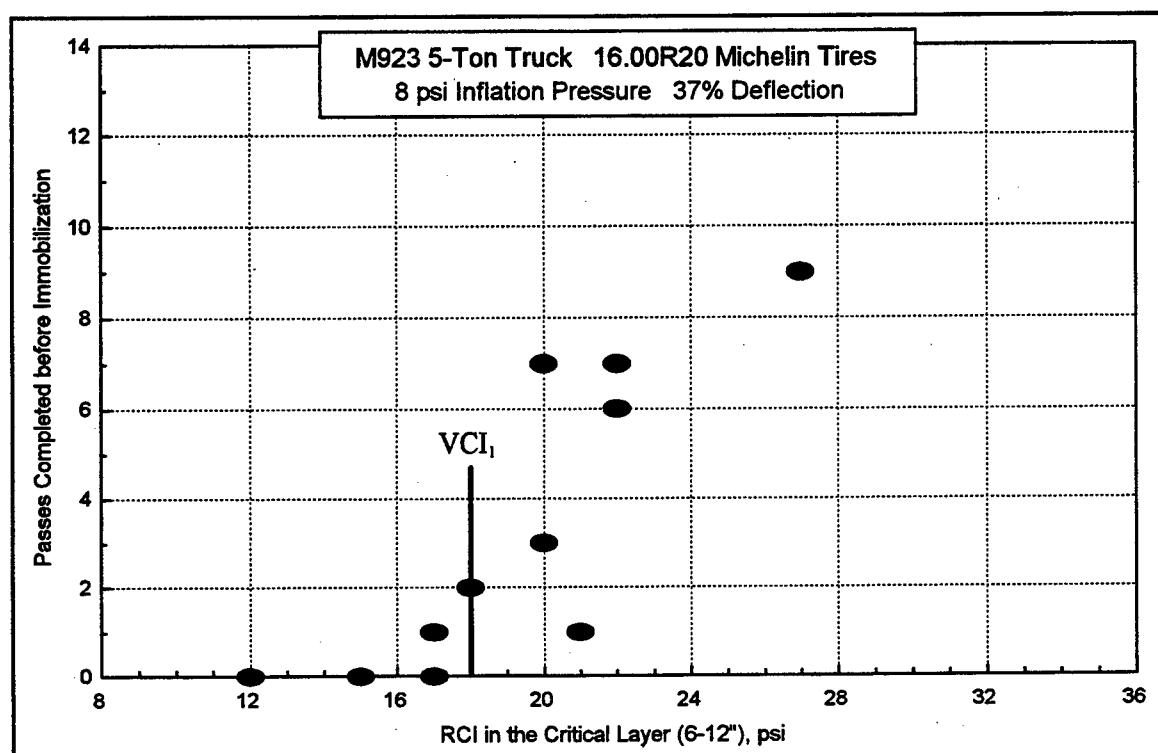measurement for one of the vehicle configurations used during this research.

Figure D1. Sample multi-pass observations used for determining VCI_1

Drawbar Experiments

A drawbar experiment is conducted to determine the drawbar performance as a

function of slip for a particular vehicle configuration and soil condition (i.e., type, strength,

surface wetness, etc.). In the typical drawbar experiment, a level, straight-line, homogeneous

(as much as possible) test lane is marked off, the lane is prepared with simulated rainfall (i.e.,

surface wetness) or left dry (i.e., normal) depending on the desired test condition, and then

soil consistency data are measured in the lane, out of the zone of passage for the traction

elements. The test vehicle is connected to a load vehicle with a tension member (e.g., steel

cable, nylon strap, etc.), and a force load cell is connected between the vehicles within the tension member. The test vehicle is also instrumented so that the actual horizontal distance traveled and the apparent horizontal distance traveled, as indicated by the rotational velocity of the traction elements, can be measured.

The test vehicle enters the lane followed by the load vehicle at a slow, steady-state speed (approximately 2 mph). The load vehicle controls the experiment by controlling the force in the connection load cell (i.e., drawbar force). It applies braking force in stepwise increments so that the test vehicle undergoes a stepwise transition from a zero pull, zero slip condition to a high pull, high slip condition. The test vehicle simply attempts to maintain constant motion by applying more horsepower as necessary. The measured data resulting from a drawbar experiment are principally drawbar force, slip, and soil consistency.

In order to reduce the measured data from a drawbar experiment into a single drawbar performance quantity, a x-y plot of drawbar coefficient versus slip is generated for the particular vehicle configuration and soil condition. Then a best-fit curve (and possibly an accompanying equation) is established to describe the trend using visual or statistical methods. This best-fit curve is used to determine the expected drawbar coefficient at a single slip magnitude. The slip magnitude typically used is either 20% or the true optimum slip which normally occurs between 10% and 30% for fine-grained soils. If optimum slip is used, it is determined by evaluating the work index versus slip trend in addition to the drawbar versus slip trend, and the optimum slip is that occurring at the maximum work index. The inferred drawbar coefficient at 20% or optimum slip represents the drawbar performance measurement. Figure D2 provides a sample x-y plot of data that were used to determine a

drawbar measurement for one of the vehicle configurations used during this research. Note that there can be several drawbar measurements for a single vehicle configuration since drawbar experiments can (and often should) be conducted on several different soil strengths and/or surface conditions depending on the goals of the particular study.
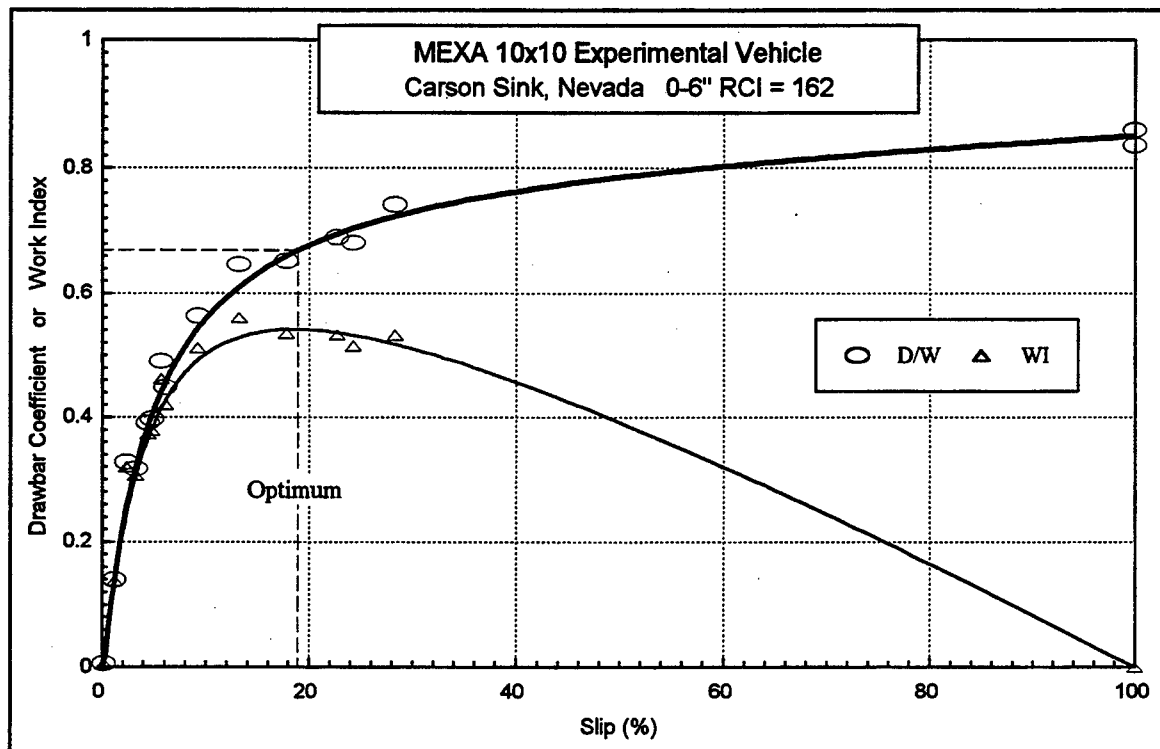

Figure D2. Sample drawbar data

REPORT DOCUMENTATION PAGE

Public reporting burden for this collection of information is estimated to average 1 hour per response, including the time for reviewing instructions, searching existing data sources, gathering and maintaining the data needed, and completing and reviewing the collection of information. Send comments regarding this burden estimate or any other aspect of this collection of information, including suggestions for reducing this burden, to Washington Headquarters Services, Directorate for Information Operations and Reports, 1215 Jefferson Davis Highway, Suite 1204, Arlington, VA 22202-4302, and to the Office of Management and Budget, Paperwork Reduction Project (0704-0188), Washington, DC 20503.

1. AGENCY USE ONLY *(Leave blank)*	2. REPORT DATE August 1999	3. REPORT TYPE AND DATES COVERED Final report

4. TITLE AND SUBTITLE
Improving the Traction Prediction Capabilities in the NATO Reference Mobility Model (NRMM)

5. FUNDING NUMBERS

6. AUTHOR(S)
Jody D. Priddy

7. PERFORMING ORGANIZATION NAME(S) AND ADDRESS(ES)
U.S. Army Engineer Waterways Experiment Station
3909 Halls Ferry Road, Vicksburg, MS 39180-6199

8. PERFORMING ORGANIZATION REPORT NUMBER
Technical Report GL-99-8

9. SPONSORING/MONITORING AGENCY NAME(S) AND ADDRESS(ES)
U.S. Army Corps of Engineers
Washington, DC 20314-1000

10. SPONSORING/MONITORING AGENCY REPORT NUMBER

11. SUPPLEMENTARY NOTES
Available from National Technical Information Service, 5285 Port Royal Road, Springfield, VA 22161.

12a. DISTRIBUTION/AVAILABILITY STATEMENT
Approved for public release; distribution is unlimited.

12b. DISTRIBUTION CODE

13. ABSTRACT *(Maximum 200 words)*

The NATO Reference Mobility Model (NRMM) has traction relationships that describe the performance of vehicles in naturally occurring soils reasonably well, but they have weaknesses stemming primarily from an inadequate consideration of the influence of vehicle characteristics on traction. This research sought to demonstrate the feasibility of developing better traction relationships for NRMM through exploitation of existing data. In order to demonstrate the feasibility, a statistical modeling effort was conducted for developing new traction relationships. The research involved a systematic and extensive exploration of new and old traction modeling concepts that rely on relatively simple characterizations of the vehicle and the soil. The effort concentrated on one-pass vehicle cone index (VCI1) and drawbar performance of pneumatic-tired vehicles on nonslippery, highly plastic clay soils (CH classification). The results demonstrated that better traction relationships can be developed for NRMM and provided new insight into the controlling mechanisms in VCI1 and drawbar performance.

14. SUBJECT TERMS

Drawbar pull	Mobility modeling	NRMM
Pneumatic tire	Traction	Vehicle Cone Index
Wheeled vehicle		

15. NUMBER OF PAGES
215

16. PRICE CODE

17. SECURITY CLASSIFICATION OF REPORT UNCLASSIFIED	18. SECURITY CLASSIFICATION OF THIS PAGE UNCLASSIFIED	19. SECURITY CLASSIFICATION OF ABSTRACT	20. LIMITATION OF ABSTRACT